

**THE DISCRETE LINEAR CHIRP TRANSFORM
AND ITS APPLICATIONS**

by

Osama A. S. Alkishriwo

B. S. in Electrical and Electronic Engineering, Al-Zawiya
University, Libya, 2002

M. S. in Electrical and Electronic Engineering, Tripoli University,
Libya, 2006

Submitted to the Graduate Faculty of
the Swanson School of Engineering in partial fulfillment
of the requirements for the degree of

Doctor of Philosophy

University of Pittsburgh

2013

UNIVERSITY OF PITTSBURGH
SWANSON SCHOOL OF ENGINEERING

This dissertation was presented

by

Osama A. S. Alkishriwo

It was defended on

March 7, 2013

and approved by

Luis F. Chaparro, PhD, Professor, Department of Electrical and Computer Engineering

Amro El-Jaroudi, PhD, Professor, Department of Electrical and Computer Engineering

Zhi-Hong Mao, PhD, Professor, Department of Electrical and Computer Engineering

Ervin Sejdic, PhD, Professor, Department of Electrical and Computer Engineering

Mingui Sun, PhD, Professor, Department of Electrical and Computer Engineering

Juan Manfredi, PhD, Professor, Department of Mathematics

Dissertation Director: Luis F. Chaparro, PhD, Professor, Department of Electrical and

Computer Engineering

Copyright © by Osama A. S. Alkishriwo
2013

THE DISCRETE LINEAR CHIRP TRANSFORM AND ITS APPLICATIONS

Osama A. S. Alkishriwo, PhD

University of Pittsburgh, 2013

In many applications in signal processing, the discrete Fourier transform (DFT) plays a significant role in analyzing characteristics of stationary signals in the frequency domain. The DFT can be implemented in a very efficient way using the fast Fourier transform (FFT) algorithm. However, many actual signals by their nature are non-stationary signals which make the choice of the DFT to deal with such signals not appropriate. Alternative tools for analyzing non-stationary signals come with the development of time-frequency distributions (TFD). The Wigner-Ville distribution is a time-frequency distribution that represents linear chirps in an ideal way, but it has the problem of cross-terms which makes the analysis of such tools unacceptable for multi-component signals. In this dissertation, we develop three definitions of linear chirp transforms which are: the continuous linear chirp transform (CLCT), the discrete linear chirp transform (DLCT), and the discrete cosine chirp transform (DCCT). Most of this work focuses on the discrete linear chirp transform (DLCT) which can be considered a generalization of the DFT to analyze non-stationary signals. The DLCT is a joint frequency chirp-rate transformation, capable of locally representing signals in terms of linear chirps. Important properties of this transform are discussed and explored. The efficient implementation of the DLCT is given by taking advantage of the FFT algorithm. Since this novel transform can be implemented in a fast and efficient way, this would make the proposed transform a candidate to be used for many applications, including chirp rate estimation, signal compression, filtering, signal separation, elimination of the cross-terms in the Wigner-Ville distribution, and in communication systems. In this dissertation, we will explore some of these applications.

TABLE OF CONTENTS

1.0 INTRODUCTION	1
1.1 OVERVIEW	1
1.1.1 Fractional Fourier transform	2
1.1.2 Discrete chirp–Fourier transform	5
1.2 DISSERTATION CONTRIBUTIONS	6
1.3 ORGANIZATION OF THE DISSERTATION	8
2.0 DISCRETE LINEAR CHIRP TRANSFORM	10
2.1 LINEAR CHIRP BASES	10
2.1.1 Continuous linear chirps	10
2.1.2 Complex discrete linear chirps	14
2.1.3 Cosine discrete linear chirps	22
2.2 COMPARING THE DLCT WITH THE DFrFT	27
2.3 ESTIMATION OF LINEAR CHIRP PARAMETERS	34
3.0 SIGNAL COMPRESSION	37
3.1 COMPRESSIVE SENSING USING DCCT	37
3.1.1 Compressive sensing	38
3.1.2 Using the DCCT to obtain sparse signals	39
3.1.3 Compression mechanism	42
3.1.4 Real and complex chirp bases in CS application	44
3.2 PARAMETER COMPRESSION METHOD	46
3.2.1 The proposed compression algorithm	46
3.2.2 Data Structure	47

3.2.3	Experimental results	48
4.0	DECOMPOSITION OF NON-STATIONARY SIGNALS AND TIME-FREQUENCY ANALYSIS	50
4.1	EMPIRICAL MODE DECOMPOSITION	50
4.2	INTRINSIC MODE FUNCTIONS USING LINEAR CHIRPS	52
4.3	Comparison of EMD and DLCT	53
4.3.1	Instantaneous frequency estimation	53
4.3.2	Decomposition of speech signals.	55
4.4	TIME-FREQUENCY ANALYSIS USING DLCT	56
5.0	HIGH DATA RATE AND HIGH CAPACITY COMMUNICATION SYSTEMS	66
5.1	DIGITAL COMMUNICATIONS BASED ON LINEAR CHIRP CARRIERS	67
5.1.1	Bit error rate calculation	67
5.1.2	Digital modulation schemes	70
5.2	COUPLED OFDM COMMUNICATION SYSTEM	77
5.2.1	Coupled OFDM system (C-OFDM)	78
5.2.2	Simulation and numerical analysis	83
5.2.3	Implementation scenarios	84
6.0	CONCLUSIONS AND FUTURE WORK	86
6.1	SUMMARY	86
6.2	FUTURE WORK	89
	BIBLIOGRAPHY	91

LIST OF TABLES

1	Comparison of mean square error (MSE) for different time–frequency distributions with four different SNRs.	60
2	Comparison of mean square error (MSE) for different time–frequency distributions with four different SNRs.	64
3	Comparison of different digital modulation schemes in terms of power and channel bandwidth with $P_e = 10^{-4}$	77

LIST OF FIGURES

1	Relation between the fractional order α and the chirp rate β	5
2	The CLCT of $x_1(t)$ with $\Omega_0 = 50.27/T_b$ and $\gamma_0 = 35.19/T_b^2$: (a) The CLCT in two-dimensions; (b) The CLCT in three-dimensions; (c) The bandwidth of the signal $x_1(t)$ in the γ_0 domain and in Fourier domain.	12
3	Comparison of the DLCT and the DCFT: (a) Wigner–Ville distribution of signal $x_1(n)$; (b) Magnitude of the DLCT; (c) Magnitude of the DCFT. . . .	20
4	Comparison of the DLCT and the DCFT: (a) Wigner–Ville distribution of signal $x_2(n)$; (b) Magnitude of the DLCT; (c) Magnitude of the DCFT. . . .	21
5	(a) The signal $x_1(n)$; (b) The magnitude of the DCCT of $x_1(n)$; (c) The reconstructed signal; (d) The reconstruction error.	25
6	(a) Signal $x_1(n)$ in time domain; (b) Wigner–Ville distribution of $x_1(n)$; (c) The $ \text{DFrFT}\{x_1(n)\} $ with $\alpha = -0.44\pi$; (d) The DLCT of $x_1(n)$ with $\beta = 0.1$	30
7	Comparing the computation time between the DLCT and the DFrFT	31
8	Resolution: (a) Signal $x_2(n)$ in time domain; (b) Wigner–Ville distribution of $x_2(n)$; (c) The $ \text{DFrFT}\{x_2(n)\} $ in three-dimension space; (d) The $ \text{DFrFT}\{x_2(n)\} $ at $\alpha = -0.44\pi$; (e) The DLCT of $x_2(n)$ in three-dimension space; (f) The DLCT of $x_2(n)$ at $\beta = 0.1$	33
9	Peak detection: (a) $ \text{DFrFT}\{x_3(n)\} $ in two-dimension space; (b) $ \text{DFrFT}\{x_3(n)\} $ in three-dimension space; (c) The DLCT of $x_3(n)$ in two-dimension space; (d) The DLCT of $x_3(n)$ in three-dimension space.	34

10	Parameters of chirp and reconstruction: (a) $ X(k, m) $ in two–dimensions; (b) $ X(k, m) $ in three–dimensions; (c) Original, estimated and error; (d) Mean square error (MSE) of $x(n)$	36
11	Sparseness of $x_w(n)$: (a) using the DCT; (b) using the DCCT.	40
12	Sparseness of bird signal: (a) Bird signal in the time domain; (b) Sparseness using the DCT; (c) Sparseness using the DCCT.	41
13	Sparseness of bat signal: (a) Bat signal in the time domain; (b) Sparseness using the DCT; (c) Sparseness using the DCCT.	42
14	Compression sampling frame.	43
15	Compression using compressive sensing: (a) Experiment 1: two windowed chirps; (b) Experiment 2: bird signal; (c) Experiment 3: bat signal.	44
16	(a) The sparseness of the bat signal using the DLCT; (b) Comparison between CS with the DCCT and CS with the DLCT.	45
17	Compression algorithm.	47
18	Data structure.	47
19	Experiment 1: (a) Segment of speech; (b) $ X(k, \beta) $ in two–dimensions; (c) The Wigner–Ville distribution of the signal showing time and frequency marginals; (d) Compression ratio vs SNR for different methods.	48
20	Experiment 2: (a) Bird chirping; (b) $ X(n, \beta_d) $ in two–dimensions; (c) The Wigner–Ville distribution of the signal showing time and frequency marginals; (d) Compression ratio vs SNR for different methods.	49
21	Experiment 1: (a) Signal $x_1(n)$; (b) Actual IFs of $x_1(n)$ components; (c) Estimated IF of $x_1(n)$ using DLCT; (d) Estimated IF of $x_1(n)$ using EMD.	54
22	Experiment 2, $x_2(n)$ with additive noise (SNR=5dB): (a) Noiseless signal $x_2(n)$; (b) Actual IFs of noiseless $x_2(n)$; (c) Estimated IFs of $x_2(n)$ using DLCT; (d) Estimated IFs of $x_2(n)$ using EMD.	55
23	(a) Decomposition of the speech segment and their corresponding spectra using DLCT; (b) The synthesized IMFs of the speech segment using EMD; (c) Original and reconstructed speech segments, and error signal $e(t)$; (d) Original speech signal, reconstructed signal, and error signal $r(t)$	57

24	Time–frequency representation algorithm and instantaneous frequency estimator.	58
25	Joint chirp–rate frequency filtering in chirp–rate frequency plane and in time–frequency plane.	60
26	Example 1, $x_1(n)$ with SNR = –5 dB: (a) Wigner–Ville distribution of $x_1(n)$; (b) STFT with Hamming window of length 64; (c) Synthesized Wigner–Ville distribution; (d) Original IF; (e) Estimated IF; (f) Mean square error.	61
27	Example 2, $x_2(n)$ with SNR = 0 dB: (a) Wigner–Ville distribution of $x_2(n)$; (b) STFT with Hamming window of length 64; (c) Synthesized Wigner–Ville distribution; (d) Original IF; (e) Estimated IF; (f) Mean square error.	63
28	Example 3: (a) The bat signal in the time domain; (b) Wigner–Ville distribution of the bat signal; (c) STFT with Hamming window of length 64; (d) Synthesized Wigner–Ville distribution; (e) Estimated IF.	65
29	Coherent detection of C-OOK or C-PSK schemes.	70
30	(a) BER of C-OOK and OOK; (b) Effect of bit rate on λ_{max} and λ_{min}	71
31	(a) BER of C-PSK and PSK; (b) Effect of bit rate on λ_{max} and λ_{min}	72
32	Coherent detection of C-FSK, CRSK, and CRFSK digital modulation schemes.	73
33	(a) BER of C-FSK and FSK; (b) Effect of bit rate on λ_{max} and λ_{min}	73
34	(a) BER of CRSK for $T_b/T_s = 32$; (b) Effect of bit rate on λ_{max} and λ_{min}	74
35	(a) BER of CRFSK for $T_b/T_s = 32$; (b) Effect of bit rate on λ_{max} and λ_{min}	75
36	Comparison of proposed binary digital modulation schemes performance.	76
37	The proposed coupled OFDM communication system.	79
38	The cross–correlation as a function of $\Delta\gamma$	82
39	(a) Performance comparison of OFDM and C-OFDM with different values of M ; (b) Impact of increasing parallel paths M on BER for different values of SNRs.	83
40	Capacity (in bps/Hz) as a function of E_b/N_0 for various values of M where $E_b/N_0 = E/\sigma_w^2$	84
41	Implementation scenarios: (a) scenario I; (b) scenario II; (c) scenario III.	85

ACKNOWLEDGEMENTS

I would like to thank my advisor Prof. Luis F. Chaparro for his guidance and constant support during my Ph.D. studies. I would also like to express my appreciation for my committee members for serving in my committee and for their invaluable comments and discussions.

I am grateful to my family and especially my parents Ahmed and Salma who always been there for me and for their support and encouragement. Finally, I wish to express my love to my wife Hajer and daughter Marine for their understanding and endurance through these many years.

Osama A. S. Alkishriwo

March 7, 2013

1.0 INTRODUCTION

Stationary signals are well analyzed using the discrete Fourier transform (DFT). The DFT is a widely used transform since it can be implemented in a very efficient way using the fast Fourier transform (FFT) algorithm. However, many actual signals are non-stationary by nature. In some of these signals, we could assume the signal might be stationary, if we choose short segments, for instance, human speech. In general, analyzing non-stationary signals using the DFT is not a good choice.

To study non-stationary signals, many time-frequency distributions (TFD) have been developed to address and characterize signal properties in the joint time-frequency domain [1, 2]. Wigner-Ville distribution is one of these distributions that can give an ideal representation for chirps, but it has the problem of cross-terms which are undesirable terms that appear in the TFD of multi-component signals. This issue of cross-terms or interference has limited the ability of using the Wigner-Ville distribution in many applications. Although some techniques have been introduced to suppress cross-terms, such a process is computationally expensive [3, 4].

1.1 OVERVIEW

To capture the variability of the non-stationary signal parameters it is necessary to consider extensions of the Fourier-based representations that provide instantaneous-frequency information for multi-component signals. The fractional Fourier transform (FrFT) is a generalization of the conventional Fourier transform. It was introduced by Namias [5] in 1980, and since then it has been applied to different problems in signal processing including signal

separation, denoising, image watermarking, and communications [6, 7, 48, 9, 10, 11]. The FrFT provides a continuous representation of a signal from the time to the frequency domain at intermediate domains by means of the fractional order of the transform that changes from $-\pi/2$ to $\pi/2$. Although it has been introduced by many researchers as a tool for analyzing ideal chirp signals in radar, the ability of the FrFT to deal with real-life signals is limited for many reasons which will be discussed in chapter 2. Another chirp based transform can be achieved by considering polynomial-phase transforms [12]. However, second-order polynomial transforms [13, 14] are preferable due to computational viability. Furthermore, a parametric characterization of the instantaneous frequency of each of the components [15] provides a realistic view of the evolving nature of the signal. Although procedures based on the chirplet transform [16, 17, 18, 40, 20, 21, 22], and polynomial chirplet transform (PCT) [23] have been proposed, their numerical implementation are difficult because of no straightforward way to solve a non-convex optimization problem with multi-extremes.

1.1.1 Fractional Fourier transform

The fractional Fourier transform (FrFT) is defined as [48]

$$X_\alpha(u) = \int_{-\infty}^{\infty} x(t) K_\alpha(t, u) dt \quad (1.1)$$

where $-\pi/2 < \alpha < \pi/2$ is called the fractional order and $K_\alpha(t, u)$ is the kernel of the transformation which is defined as

$$K_\alpha(t, u) = \sqrt{\frac{1 - j \cot \alpha}{2\pi}} \exp\left(j \frac{t^2 + u^2}{2} \cot \alpha - jut \csc \alpha\right)$$

When $\alpha = 0$, the FrFT of the signal $x(t)$ is the signal itself, while if $\alpha = \pm\pi/2$, the FrFT becomes the Fourier transform of the signal. That is why it is considered a generalization of the Fourier transform. The signal $x(t)$ can be obtained by the inverse fractional Fourier transform as

$$x(t) = \int_{-\infty}^{\infty} X_\alpha(u) K_\alpha^*(t, u) du \quad (1.2)$$

where “ * ” stands for complex conjugate.

Unfortunately, (1.1) and (1.2) are continuous transformations. Several authors have proposed a discrete FrFT [24, 25, 26, 27].

The discrete fractional Fourier transform (DFrFT) is defined in terms of a particular set of eigenvectors

$$X_\alpha(\rho) = \sum_{n=0}^{N-1} \hat{K}_\alpha(n, \rho) x(n) \quad (1.3)$$

where the kernel $\hat{K}_\alpha(n, \rho)$ of the transformation has the following spectral expression

$$\hat{K}_\alpha(n, \rho) = \sum_{k \in \mathcal{M}} \nu_k(\rho) e^{-j\alpha k} \nu_k(n)$$

where $\nu_k(n)$ is the k th discrete Hermite–Gaussian function as defined in [25] and $\mathcal{M} = \{0, \dots, N-2, N-N \bmod 2\}$. The signal $x(n)$ can be reconstructed using the inverse DFrFT as

$$x(n) = \sum_{\rho=0}^{N-1} \hat{K}_\alpha^*(n, \rho) X_\alpha(\rho) \quad (1.4)$$

The FrFT has an important property which is the rotation property [28, 29]. It can be used to rotate a linear chirp in the time–frequency plane to become a sinusoid or an impulse by setting the fractional order (α) to an appropriate value— which is the fractional order that corresponds to the chirp rate of the signal. Now, we would like to find the connection between the chirp–rate γ and the fractional order α of the FrFT.

For a discrete signal $x(n)$, we can define the connection between the fractional order (α) and the chirp rate (γ) as

$$\alpha = -\tan^{-1} \left(\frac{1}{2\gamma} \right) \quad (1.5)$$

Indeed, if $x(t)$ is a continuous linear chirp given by

$$x(t) = \exp(j(\gamma t^2 + \Omega t))$$

Substitute $x(t)$ into (1.1) as

$$\begin{aligned} X_\alpha(u) &= \sqrt{\frac{1-j\cot\alpha}{2\pi}} e^{j\frac{u^2}{2}\cot\alpha} \int_{-\infty}^{\infty} e^{j(\cot\alpha+2\gamma)\frac{t^2}{2}} \times e^{-j(u\csc\alpha-\Omega)t} dt \\ &= \sqrt{\frac{1-j\cot\alpha}{a}} \exp\left(j\frac{u^2}{2}\cot\alpha\right) \exp\left(\frac{b^2}{2a}\right) \end{aligned}$$

where $a = -j\cot\alpha - j2\gamma$ and $b = ju\csc\alpha - j\Omega$. $|X_\alpha(u)| \rightarrow \infty$, when

$$\cot(\alpha) + 2\gamma = 0 \tag{1.6}$$

From the condition given in (1.6), we can write the relation between α and γ as

$$\alpha = -\tan^{-1}\left(\frac{1}{2\gamma}\right) \tag{1.7}$$

In the discrete form, the signal $x(t)$ can be defined as

$$x(n) = \exp\left(j\frac{2\pi}{N}(\beta n^2 + kn)\right)$$

Therefore, we can write the relation between the discrete chirp rate β and the fractional order α as

$$\alpha = -\tan^{-1}\left(\frac{1}{2\beta}\right) \tag{1.8}$$

The connection between α and γ was shown geometrically in [30, 31]. Figure 1 illustrates the plot of (1.8).

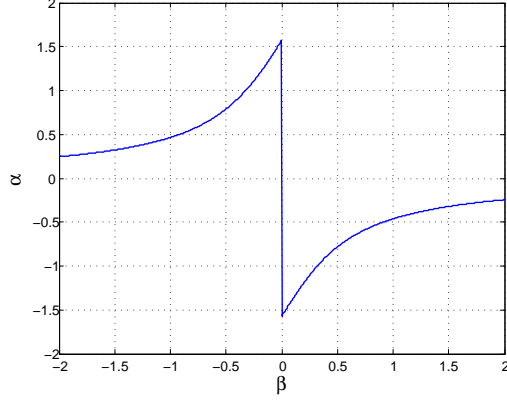


Figure 1: Relation between the fractional order α and the chirp rate β

1.1.2 Discrete chirp–Fourier transform

In [14] the discrete chirp–Fourier transform (DCFT) was defined. Given a signal $x(n)$ of length N , the discrete chirp–Fourier transform (DCFT) is

$$X_c(k, r) = \frac{1}{\sqrt{N}} \sum_{n=0}^{N-1} x(n) \exp\left(-j \frac{2\pi}{N} (rn^2 + kn)\right), \quad 0 \leq r, k \leq N-1 \quad (1.9)$$

where k represents the frequencies and r is an arbitrarily fixed integer that represents the chirp rates. The DCFT is the same as the DFT when $r = 0$. The inverse discrete chirp transform (IDCFT) is given as

$$x(n) = \exp\left(j \frac{2\pi}{N} rn^2\right) \frac{1}{\sqrt{N}} \sum_{k=0}^{N-1} X_c(k, r) \exp\left(j \frac{2\pi}{N} kn\right), \quad 0 \leq n \leq N-1 \quad (1.10)$$

The DCFT approximates the chirp rate by integer numbers r . Therefore, when using the DCFT to detect a chirp signal, the discrete chirp rate r_0 of the signal should be an integer to guarantee that the parameter can be matched and that the peak will not be lost. This restriction affects the practical applications of the DCFT.

1.2 DISSERTATION CONTRIBUTIONS

Non-stationarity relates to the time-dependence of the statistics of a random process. As such, non-stationary signals display either time-varying mean, variance or evolving spectra, or a combination of some or all of these. That is why it is necessary to consider extensions of the Fourier-based representations that provide instantaneous-frequency information for multi-component signals. The work presented in this dissertation contributes to the literature of non-stationary signal representation and analysis in the following aspects.

- We develop pairs of direct and inverse transforms in terms of linear chirps bases. The continuous linear chirp transform is introduced to deal with continuous signals. The discrete linear chirp transform (DLCT) is proposed. The DLCT uses discrete complex linear chirp bases. It is not a time-frequency but rather a frequency chirp-rate transformation, implementable using fast Fourier transform (FFT). The discrete Fourier transform or the DFT is a special case of the DLCT which has the properties of modulation and duality in time and frequency. We use the DLCT to estimate chirp parameters. The estimation of chirp parameters is a complicated problem when dealing with multi-component signals embedded in noise.

Some applications require real transforms to give better performance. Hence, we introduce the discrete cosine chirp transform (DCCT) and its inverse which are based on orthogonal real linear chirps. The proposed transform can be implemented using the fast Fourier transform algorithm (FFT).

- The DLCT can be considered an extension of the discrete Fourier transform. Likewise, the fractional Fourier transform can be considered a generalization of the Fourier transform. Thus, we explore the connection and differences between the DLCT and the DFrFT.
- Signal compression aims to decrease transmission rate (increase storage capacity) by reducing the amount of data necessary to be transmitted. We propose a new algorithm for signal compression based on the direct and the dual DLCT, depending on the sparsity of the signal in either time or in frequency. Furthermore, we develop a data structure for the extracted coefficients of compressed signals. In the data structure, the extracted

parameters are arranged in certain way that are predetermined for the compress and decompress processes.

- In compressive sensing (CS), a transformation is used to obtain a sparse representation of a signal in order to assure the reconstruction of the original signal by ℓ -minimization process. To obtain sparse signals, joint time–frequency is needed. Thus, the potential of the DCCT in compressive sensing has been presented, illustrated, and compared with the results of using the DCT with compressive sensing. In addition, we present the advantage of using the DCCT, which uses real bases (real linear chirps) instead of the DLCT which represents signals in terms of complex bases (complex linear chirps).
- The empirical mode decomposition (EMD) has gained a great deal of interest for its simplicity and for its connection with the Hilbert spectrum. The EMD is a decomposition into intrinsic mode functions (IMFs) satisfying a symmetry condition on their envelopes and a matching of their number of extrema and zero-crossings. Generalized chirp functions can be made to satisfy the IMF conditions. By decreasing the support locally, linear chirps are used for representing discrete non–stationary signals.
- Time–frequency distributions (TFDs) are widely used for IF estimation based on peak detection techniques. The most frequently TFD used for linear chirps is the Wigner–Ville distribution (WVD) due to its ideal representation for such signals. However, in the case of multi–component signals, Wigner–Ville distribution does not perform well because of the presence of extraneous cross–terms. Hence, we propose an algorithm for time–frequency analysis based on the DLCT. The developed approach takes advantage of the separation of linear chirps given by the DLCT, and that for each of them, the Wigner–Ville distribution (WVD) provides an optimal representation. Combining the WVD of linear chirp components, we obtain a time–frequency representation free of cross terms. It is observed that the DLCT decomposition and the related TFD provides more compact representation compared with the commonly used time–frequency distributions.
- The design of signal carrier waveforms in digital communication systems has great impact on system performance. This work is motivated by looking for carrier waveforms that can maximize the transmitted difference signal energy. We propose five different digital communication schemes which are: chirp on-off keying (C-OOK), chirp phase shift keying

(C-PSK), chirp frequency shift keying (C-FSK), chirp rate shift keying (CRSK), and chirp rate frequency shift keying (CRFSK) where all based on linear chirp carriers. The performance in terms of bit error rate (BER) and spectrum usage of the proposed schemes is evaluated for coherent detection receivers.

- Wireless communications suffer from increasing demand on capacity and transmission speed to support services such as multimedia with high quality. In this section, we propose a coupled OFDM (C-OFDM) system that connects M OFDM systems, each of them having N channels, via linear chirps. The coupled OFDM can be operated on three different scenarios based on the application and user satisfaction. The performance of the coupled OFDM is investigated and analytical expression for the capacity of the system is derived.

1.3 ORGANIZATION OF THE DISSERTATION

The rest of the dissertation is organized as follows. In chapter 2, we introduce definitions of continuous, discrete, and cosine linear chirp transforms. Reconstruction of signals is also discussed. Fast implementation algorithms for calculating the discrete linear chirp transforms using fast Fourier transform algorithm are presented. Properties such as duality, modulation, and linearity are illustrated. Furthermore, we compare the discrete FrFT with the DLCT. In particular, we consider which of these two transforms is more efficient to transform a non-sparse signal into a sparse-signal in time or frequency, the resolution at which the transforms do it and the computational time required. The generality of our transform in estimating the parameters of chirp signals is illustrated by comparing our results with those using the discrete chirp-Fourier transform proposed in [14].

Chapter 3 focuses on using the discrete linear chirp transform in signal compression. We give a brief introduction to the concept of compressive sensing. The discrete cosine chirp transform is used to transform signals into sparse signals so that compressive sensing can be applied. Moreover, we illustrate fundamentals of the proposed parameter estimation method.

In chapter 4, we use the DLCT for decomposition of non-stationary signals and time-frequency analysis applications. Starting with the theory of empirical mode decomposition, we define the concept of using linear chirps as intrinsic mode functions which forms the platform of empirical mode decomposition theory. Furthermore, we employ the DLCT as a time-varying filter to separate multi-component non-stationary signals locally into a superposition of linear chirps. Thus, by combining the Wigner-Ville distribution of the linear chirp components, we obtain a time-frequency representation free of cross-terms that clearly displays the instantaneous frequency. Applying this procedure locally, we obtain an instantaneous frequency estimate of a non-stationary multi-component signal.

Chapter 5 discusses the possibility of using linear chirp carriers in communication systems. Different digital modulation schemes are developed and their performance for Gaussian channel is evaluated. Moreover, We present the coupled OFDM system and its performance and capacity have been studied and analyzed.

Finally, chapter 6 summarizes dissertation results and directions for future research are outlined.

2.0 DISCRETE LINEAR CHIRP TRANSFORM

2.1 LINEAR CHIRP BASES

The term “chirp” comes from the bird chirp or cricket sounds— a short pulse, high-pitched sound. This pulse is called a chirped pulse. Scientifically, the term chirp means a wave whose instantaneous frequency varies over time. Chirps come in many frequency sweep forms: linear chirp, quadratic chirp, logarithmic-chirp, etc.

A linear chirp is a function whose frequency changes linearly with time. For example, while a wave function of the form $\exp(j\Omega_0 t)$ has constant frequency Ω_0 , the chirp $\exp(j(\Omega_0 t + \gamma_0 t^2))$ has an instantaneous frequency $\Omega_0 + 2\gamma_0 t$ at time $t \in \mathbb{R}$. Chirps often arise in nature as a consequence of the Doppler effect, the phenomenon by which the perceived frequency of a wave is altered whenever the wave is emanating from or reflecting off a moving body. As such, chirps have historically been of great interest in applications such as radar and sonar. Thus, we need to use linear chirp bases instead of the classical Fourier bases because they are more suitable for representing the frequency changes of non-stationary signals.

2.1.1 Continuous linear chirps

Let the space $\mathbb{L}^2(\mathbb{R})$ be a Hilbert space of complex functions such that

$$\|x\| = \int_{-\infty}^{+\infty} |x(t)|^2 dt < +\infty$$

The inner product of $\langle x, y \rangle \in \mathbb{L}^2(\mathbb{R})$ is defined by

$$\langle x, y \rangle = \int_{-\infty}^{+\infty} x(t) y^*(t) dt$$

where $y^*(t)$ is the complex conjugate of $y(t)$. The continuous linear chirp transform (CLCT) of $x(t) \in \mathbb{L}^2(\mathbb{R})$ is defined as

$$X(\Omega, \gamma) = \int_{-\infty}^{+\infty} x(t) e^{-j(\Omega t + \gamma t^2)} dt \quad (2.1)$$

The inverse continuous linear chirp transform (ICLCT) is given by

$$x(t) = \int_{-\infty}^{+\infty} X(\Omega, \gamma) e^{j(\Omega t + \gamma t^2)} d\Omega \quad (2.2)$$

where $-\infty < \gamma < +\infty$. We can show that $x(t)$ is the inverse continuous linear chirp transform (ICLCT) of $X(\Omega, \gamma)$ as follows. We have,

$$x(t) = \int_{-\infty}^{+\infty} X(\Omega, \gamma) e^{j(\Omega t + \gamma t^2)} d\Omega$$

Replace $X(\Omega, \gamma)$ by its integral expression yields

$$\int_{-\infty}^{+\infty} \int_{-\infty}^{+\infty} x(\tau) e^{j\Omega(t-\tau)} e^{j\gamma(t^2-\tau^2)} d\Omega d\tau$$

using the following integral

$$\int_{-\infty}^{+\infty} e^{j\Omega(t-\tau)} d\Omega = \delta(t - \tau)$$

we have that

$$\int_{-\infty}^{+\infty} x(\tau) e^{j\gamma(t^2-\tau^2)} \delta(t - \tau) d\tau = x(t)$$

The CLCT is the generalization of the conventional Fourier transform. If the Fourier transform of the signal $x(t)$ is represented by $\hat{X}_F(\Omega)$, then we can write $X(\Omega, 0) = \hat{X}_F(\Omega)$.

We also can illustrate the continuous linear chirp transform (CLCT) in the framework of time-varying filtering for continuous time signals. The CLCT can provide us with the same bandwidth of sinusoid signals if we intent to filter linear chirps in the frequency chirp-rate space. Thus, the CLCT can eliminate the effect of the chirp rate on the channel bandwidth of chirp communication systems (chapter 6) if we filter the signal at the corresponding chirp rate. Thus, we present the CLCT to overcome the broadness of the channel bandwidth.

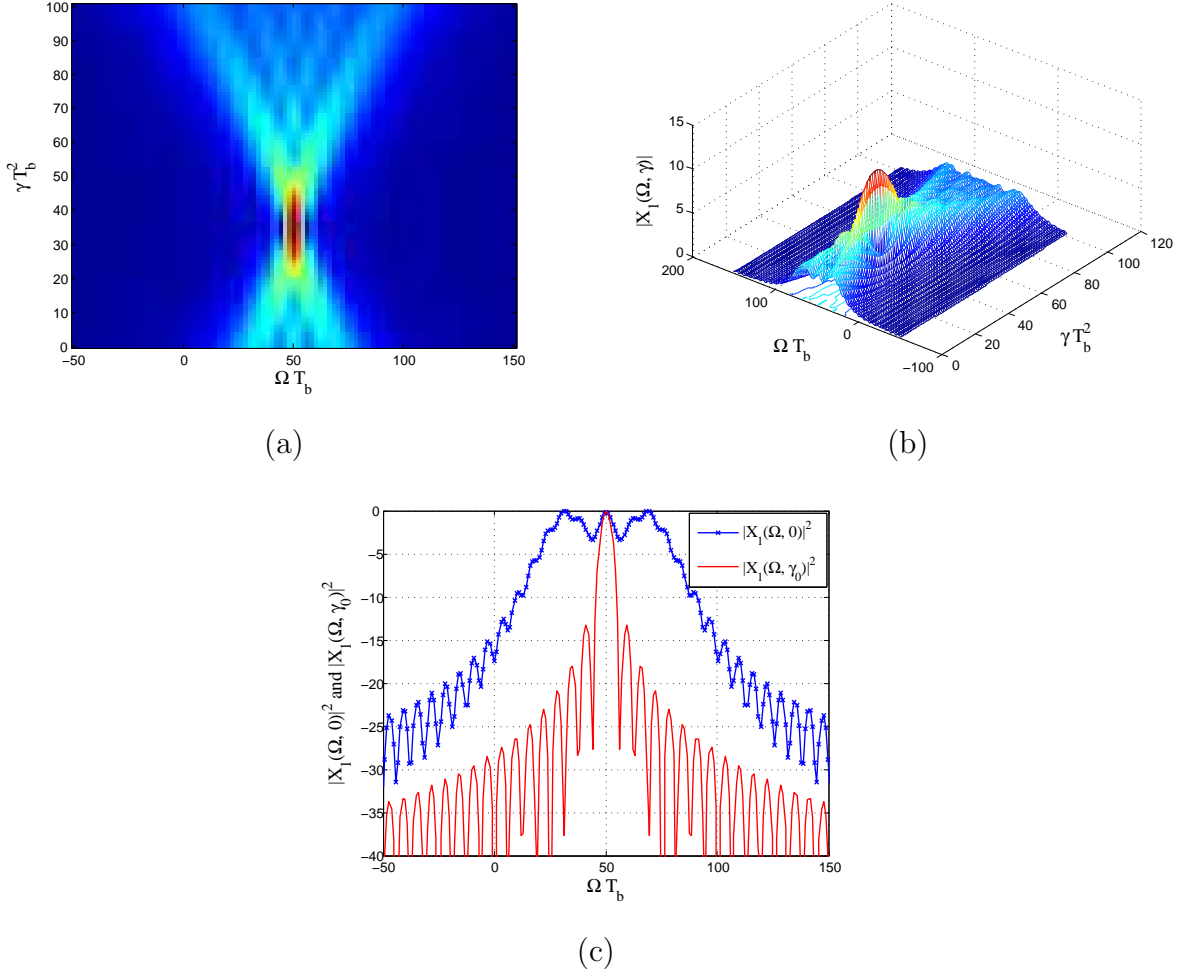


Figure 2: The CLCT of $x_1(t)$ with $\Omega_0 = 50.27/T_b$ and $\gamma_0 = 35.19/T_b^2$: (a) The CLCT in two-dimensions; (b) The CLCT in three-dimensions; (c) The bandwidth of the signal $x_1(t)$ in the γ_0 domain and in Fourier domain.

Example 1. Let the signal $x_1(t)$ be a complex linear chirp as

$$x_1(t) = \exp(j(\Omega_0 t + \gamma_0 t^2)), \quad -T_b/2 \leq t \leq T_b/2$$

Given,

$$\begin{aligned} \int_0^{T_b} \cos(a t + b t^2) dt &= \sqrt{\frac{\pi}{2b}} \times [\cos(\theta_1^2) \left\{ C_F(\theta_2) - C_F\left(\sqrt{\frac{2}{\pi}}\theta_1\right) \right\} \\ &+ \sin(\theta_1^2) \left\{ S_F(\theta_2) - S_F\left(\sqrt{\frac{2}{\pi}}\theta_1\right) \right\}] \end{aligned}$$

where $C_F(u)$ and $S_F(u)$ are Fresnel functions defined as

$$C_F(u) = \int_0^u \cos\left(\frac{\pi}{2}z^2\right) dz,$$

$$S_F(u) = \int_0^u \sin\left(\frac{\pi}{2}z^2\right) dz$$

$$\theta_1 = \frac{a}{2\sqrt{b}}, \quad \text{and} \quad \theta_2 = \sqrt{\left(\frac{2b}{\pi}\right)} \left(T_b + \frac{a}{2b}\right)$$

then, the magnitude of the CLCT for $x_1(t)$ is given by

$$|X_1(\Omega, \gamma)| = \sqrt{\frac{\pi}{2(\gamma - \gamma_0)}} \times \sqrt{[C_F(z_2) - C_F(z_1)]^2 + [S_F(z_2) - S_F(z_1)]^2}$$

where

$$z_2 = T_b \sqrt{\frac{(\gamma - \gamma_0)}{2\pi}} + \frac{(\Omega - \Omega_0)}{\sqrt{2\pi(\gamma - \gamma_0)}}$$

and

$$z_1 = -T_b \sqrt{\frac{(\gamma - \gamma_0)}{2\pi}} + \frac{(\Omega - \Omega_0)}{\sqrt{2\pi(\gamma - \gamma_0)}}$$

Figures 2(a) and (b) show the CLCT of the signal $x_1(t)$ for the case of $\Omega_0 = 50.27/T_b$ and $\gamma_0 = 35.19/T_b^2$ in two and three dimensions. The bandwidth of the signal $x_1(t)$ in the γ_0 space is presented in Fig. 2(c) which shows the bandwidth width of the signal $x_1(t)$ in the γ_0 domain is much smaller than its width in the Fourier domain which corresponds to $\gamma = 0$.

2.1.2 Complex discrete linear chirps

In this section, we develop an orthogonal representation using linear chirps for a discrete signal $x(n)$ of finite support $0 \leq n \leq N - 1$. A discrete-time linear chirp

$$\phi_{\beta,k}(n) = \exp\left(j\frac{2\pi}{N}(\beta n^2 + kn)\right) \quad (2.3)$$

is characterized by the discrete frequency $2\pi k/N$ and by its chirp rate β , a continuous variable connected with the instantaneous frequency of the chirp

$$IF(n, k) = \frac{2\pi}{N}(2\beta n + k),$$

Assuming a finite support for β , i.e., $-\Lambda \leq \beta < \Lambda$, we can construct an orthonormal basis $\{\phi_{\beta,k}(n)\}$ with respect to k in the supports of β and n as

$$\begin{aligned} \int_{-\Lambda}^{\Lambda} \sum_{n=0}^{N-1} \phi_{\beta,k}(n) \phi_{\beta,\ell}^*(n) d\beta &= \int_{-\Lambda}^{\Lambda} N\delta(k - m) d\beta \\ &= 2\Lambda N\delta(k - \ell) \end{aligned} \quad (2.4)$$

Thus, we have the linear-chirp representation for a discrete signal $x(n)$, $0 \leq n \leq N - 1$, to be

$$x(n) = \int_{-\Lambda}^{\Lambda} \sum_{k=0}^{N-1} \frac{X(k, \beta)}{N} \exp\left(j\frac{2\pi}{N}((\beta n + k)n)\right) d\beta \quad (2.5)$$

where the coefficients $X(k, \beta)$ are obtained by using the orthogonality of the basis as

$$X(k, \beta) = \sum_{n=0}^{N-1} x(n) \exp\left(-j\frac{2\pi}{N}(\beta n^2 + kn)\right) \quad (2.6)$$

To obtain a discrete transformation, we approximate the chirp rate as

$$\begin{aligned} \beta &= Cm, \quad \text{where } C = \frac{2\Lambda}{L} \text{ so that} \\ -\frac{L}{2} &\leq m \leq \frac{L}{2} - 1 \text{ integer} \end{aligned}$$

we thus have the discrete linear-chirp transform (DLCT)

$$X(k, m) = \sum_{n=0}^{N-1} x(n) \exp\left(-j\frac{2\pi}{N}(Cmn^2 + kn)\right)$$

$$0 \leq k \leq N-1, \quad -L/2 \leq m \leq (L/2) - 1 \quad (2.7)$$

$$x(n) = \sum_{m=-L/2}^{L/2-1} \sum_{k=0}^{N-1} \frac{X(k, m)}{LN} \exp\left(j\frac{2\pi}{N}(Cmn^2 + kn)\right)$$

$$0 \leq n \leq N-1, \quad C = \frac{2\Lambda}{L} \quad (2.8)$$

Remarks

1. The DLCT is not a time–frequency transformation, but rather a frequency chirp–rate transformation.
2. One could think of the DLCT as a generalization of the discrete Fourier transform (DFT). Indeed,

$$X(k, m) = \frac{1}{N} X(k) \odot \text{DFT} \left\{ \exp\left(-j\frac{2\pi}{N} Cm\right) \right\}$$

where “ \odot ” is the circular convolution. If $m = 0$, then $X(k, 0)$ is the DFT of $x(n)$ or the representation using chirp bases with zero chirp rates (or sinusoids.)

3. It is important to notice that in a discrete chirp, obtained by sampling a continuous chirp satisfying the Nyquist criteria, the chirp rate β cannot be exclusively an integer as proposed in [14]. Indeed, if a finite support continuous chirp

$$x(t) = e^{j\gamma t^2} \quad \gamma = \frac{\zeta_\Omega \Omega_{max}}{2\zeta_t T}, \quad 0 \leq t \leq T$$

where $|\zeta_\Omega|$ and $|\zeta_t| \leq 1$, and using a sampling frequency $\Omega_s = 2\pi/T_s = M\Omega_{max}$, $M \geq 2$, as determined by the Nyquist criteria, the obtained discrete signal is

$$x(nT_s) = e^{j[\gamma T_s^2]n^2}, \quad \text{where}$$

$$\gamma T_s^2 = \left(\frac{\zeta_\Omega \Omega_{max}}{2\zeta_t T}\right) T_s^2 = \frac{\pi/M}{N-1} \frac{\zeta_\Omega}{\zeta_t}$$

after replacing $\Omega_{max} = 2\pi/(MT_s)$ and $T = (N - 1)T_s$. Comparing then the discretized linear chirp and equation (2.3) we have that

$$\frac{2\pi}{N}\beta = \gamma T_s^2 \Rightarrow \beta = \frac{N}{2M(N - 1)} \frac{\zeta_\Omega}{\zeta_t}$$

which in general is not an integer. For N large, $M = 2$, and $\zeta_t = \zeta_\Omega = 1$, the normalized chirp rate is 0.25.

4. For each value of m it can be shown that

$$x_m(n) = \sum_{k=0}^{N-1} \frac{X(k, m)}{N} \exp\left(j \frac{2\pi}{N} (Cmn^2 + kn)\right) \quad (2.9)$$

equals $x(n)$ so that the inverse DLCT is the average over all values of m . Indeed this can be shown by replacing $X(k, m)$ in equation (2.9) which yields

$$\begin{aligned} x_m(n) &= \sum_{\ell=0}^{N-1} \frac{x(\ell)}{N} \exp\left(j \frac{2\pi}{N} Cm(n^2 - \ell^2)\right) \\ &\times \underbrace{\sum_{k=0}^{N-1} \exp\left(j \frac{2\pi}{N} k(n - \ell)\right)}_{N\delta(n-\ell)} = x(n). \end{aligned}$$

• Properties of the DLCT

Properties of the DLCT are similar to those of the DFT. We are particularly interested in the modulation and the duality properties which will be useful in time–frequency shifts and in representing time–impulses and functions of them which cannot be represented when the chirp rate is assumed to be finite.

1. Modulation Property: If $X(k, m)$ is the DLCT of $x(n)$ then the linear-chirp modulated signal

$$y(n) = x(n) \exp \left(j \frac{2\pi}{N} (C_0 m_0 n^2 + k_0 n) \right)$$

where $C_0 = \zeta C$, has a DLCT

$$Y(k, m) = X(k - k_0, m - \zeta m_0)$$

where ζ should be an integer to preserve the discrete nature of the transform. This shifting property allows the transformation of one chirp representation into another, and in particular, the transformation of chirp representations into sinusoidal representations.

2. Duality Property: Although the finite chirp rate assumption made before allows a large range of values for the chirp rate it cannot be used to represent signals that are impulses and functions of impulses in time. To include them we consider a duality property for the DLCT. Interchanging the time and frequency variables and using equation (2.7) and (2.8)

$$\begin{aligned} X(n, -\tilde{m}) &= \sum_{k=0}^{N-1} x(-k) \exp \left(j \frac{2\pi}{N} (C\tilde{m}k^2 + nk) \right) \\ 0 \leq n \leq N-1, \quad -L/2 \leq m \leq (L/2) - 1 \end{aligned} \quad (2.10)$$

we then have that

$$\begin{aligned} x(-k) &= \sum_{\tilde{m}=-L/2}^{L/2-1} \sum_{n=0}^{N-1} \frac{X(n, -\tilde{m})}{LN} \exp \left(-j \frac{2\pi}{N} (C\tilde{m}k^2 + nk) \right) \\ 0 \leq k \leq N-1, \quad C &= \frac{2\Lambda}{L} \end{aligned} \quad (2.11)$$

Following the same procedure in (2.9), it can be shown that

$$x_{\tilde{m}}(-k) = \sum_{n=0}^{N-1} \frac{X(n, -\tilde{m})}{N} \exp \left(-j \frac{2\pi}{N} (C\tilde{m}k^2 + nk) \right) \quad (2.12)$$

is, also, equal to $x(-k)$. Thus, if $x(n)$ is an impulse or a function of impulses, then its DFT would be a constant or a sinusoid of zero frequency, and its DLCT can be calculated.

The proof of the dual pair can be illustrated as follows. Since,

$$x(-k) = x_{\tilde{m}}(-k) = \sum_{n=0}^{N-1} \frac{X(n, -\tilde{m})}{N} \exp\left(-j \frac{2\pi}{N} (C\tilde{m}k^2 + nk)\right)$$

Replacing this equation into (2.11), we obtain

$$\begin{aligned} & \sum_{r=0}^{N-1} \frac{X(r, -\tilde{m})}{N} \sum_{k=0}^{N-1} \exp\left(j \frac{2\pi}{N} k(n-r)\right) \\ &= X(n, -\tilde{m}) \end{aligned}$$

We can find the connection between m and \tilde{m} or (β and $\tilde{\beta}$) from the time–frequency distribution of a linear chirp. The IF of a linear chirp has a slope of 2β from the time axis and a slope of $2\tilde{\beta}$ from the frequency axis. Given a linear chirp $h(t) = \exp(-j\gamma t^2)$ for $-\infty < t < \infty$, its Fourier transform is

$$H(\Omega) = \frac{1}{2\sqrt{\pi\gamma}} e^{-j\frac{\pi}{4}} \exp\left(j \frac{\Omega^2}{4\gamma}\right)$$

If we calculate the dual of $H(\Omega)$, we obtain

$$H(t) = \frac{1}{2\sqrt{\pi\tilde{\gamma}}} e^{-j\frac{3\pi}{4}} \exp\left(-j \frac{t^2}{4\tilde{\gamma}}\right)$$

Since,

$$IF_{h(t)}(t) = IF_{H(t)}(t) = -2\gamma t = -\frac{2}{4\tilde{\gamma}} t$$

Hence,

$$\tilde{\gamma} = \frac{1}{4\gamma}$$

In the discrete form, we have

$$C\tilde{m} = \frac{1}{4Cm} \quad \text{or} \quad \tilde{\beta} = \frac{1}{4\beta}$$

If $\tilde{\beta} = \beta = 0.5$, then the slope of the IF is equal to 45° which separates the time–frequency space into two symmetric halves.

- **Implementation with the FFT**

The DLCT can be implemented using the fast Fourier transform (FFT). Rewriting $X(k, m)$ as

$$X(k, m) = \sum_{n=0}^{N-1} \underbrace{\left[x(n) e^{-j2\pi Cmn^2/N} \right]}_{h(n, m)} e^{-j2\pi kn/N}$$

then for each $-L/2 \leq m_0 \leq L/2 - 1$ the $X(k, m_0)$ is the DFT of $h(n, m_0)$ which can be obtained by the FFT algorithm.

The inverse DLCT can also be implemented with the inverse FFT. Rewriting the expression for $x(n)$ as

$$x(n) = \frac{1}{L} \sum_{m=-L/2}^{L/2-1} \underbrace{\left[\sum_{k=0}^{N-1} \frac{X(k, m)}{N} e^{j2\pi kn/N} \right]}_{g(n, m)} e^{j2\pi Cmn^2/N}$$

where $g(n, m)$ is the inverse DFT for each $-L/2 \leq m_0 \leq L/2 - 1$. Then

$$x(n) = \frac{1}{L} \sum_{m=-L/2}^{L/2-1} g(n, m) e^{j2\pi Cmn^2/N}$$

If a vector $\mathbf{x} = [x(0) \cdots x(N-1)]^T$ then

$$\mathbf{x} = \frac{1}{L} \text{diag}[\mathbf{G} \mathbf{E}]$$

or the diagonal of the product of an $N \times L$ matrix

$\mathbf{G} = \{g(n, m)\}$ with an $L \times N$ matrix $\mathbf{E} = \{e(m, n) = e^{j2\pi Cmn^2/N}\}$.

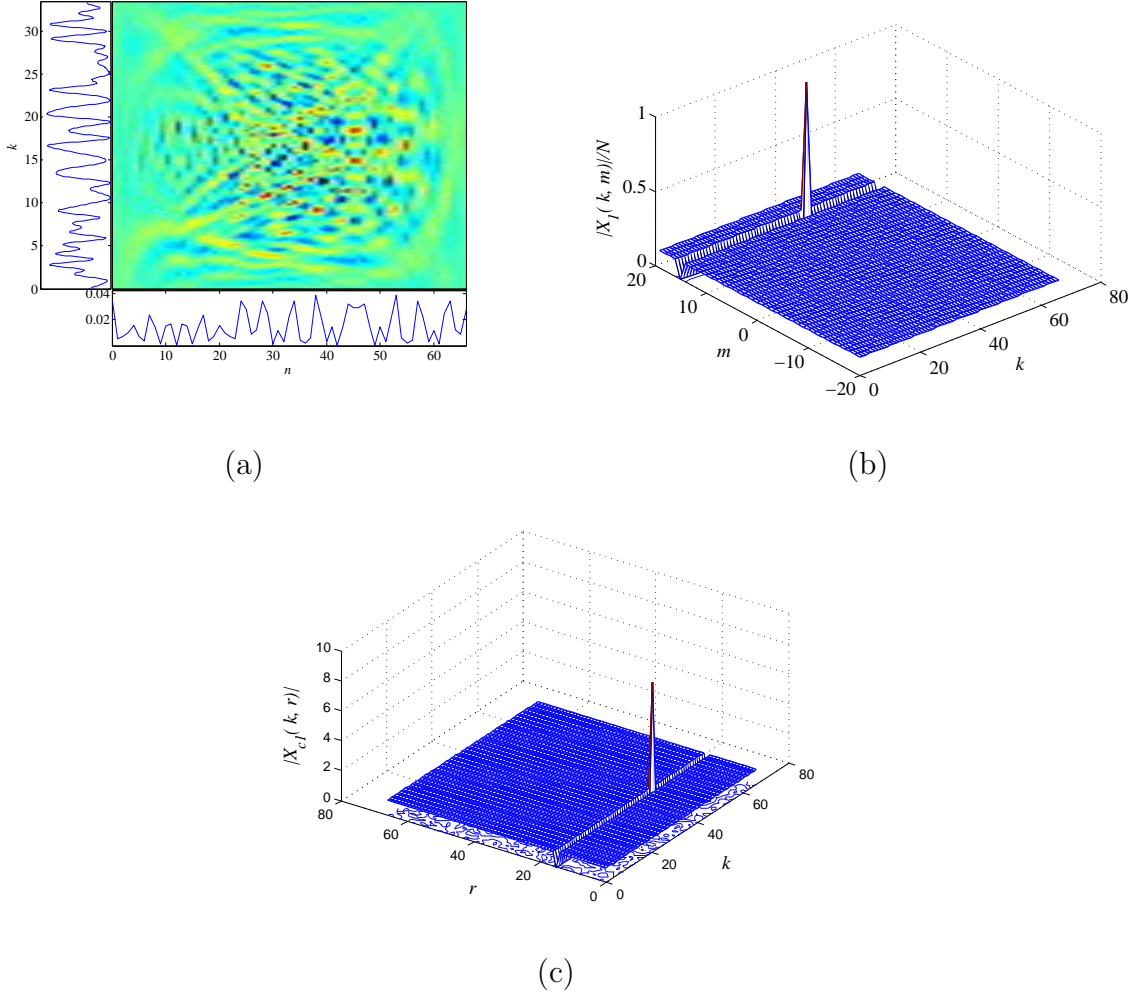


Figure 3: Comparison of the DLCT and the DCFT: (a) Wigner–Ville distribution of signal $x_1(n)$; (b) Magnitude of the DLCT; (c) Magnitude of the DCFT.

- **Comparison with the Discrete Chirp–Fourier transform**

Although similar to the DLCT presented above, the discrete chirp–Fourier transform has a significant drawback. It considers only chirp rates which are integers, which as indicated before are aliased if they are obtained by sampling continuous chirps without windowing or filtering. To illustrate this, consider the signal given in [14]

$$x_1(n) = \exp\left(j\frac{2\pi}{67}(15n^2 + 42n)\right)$$

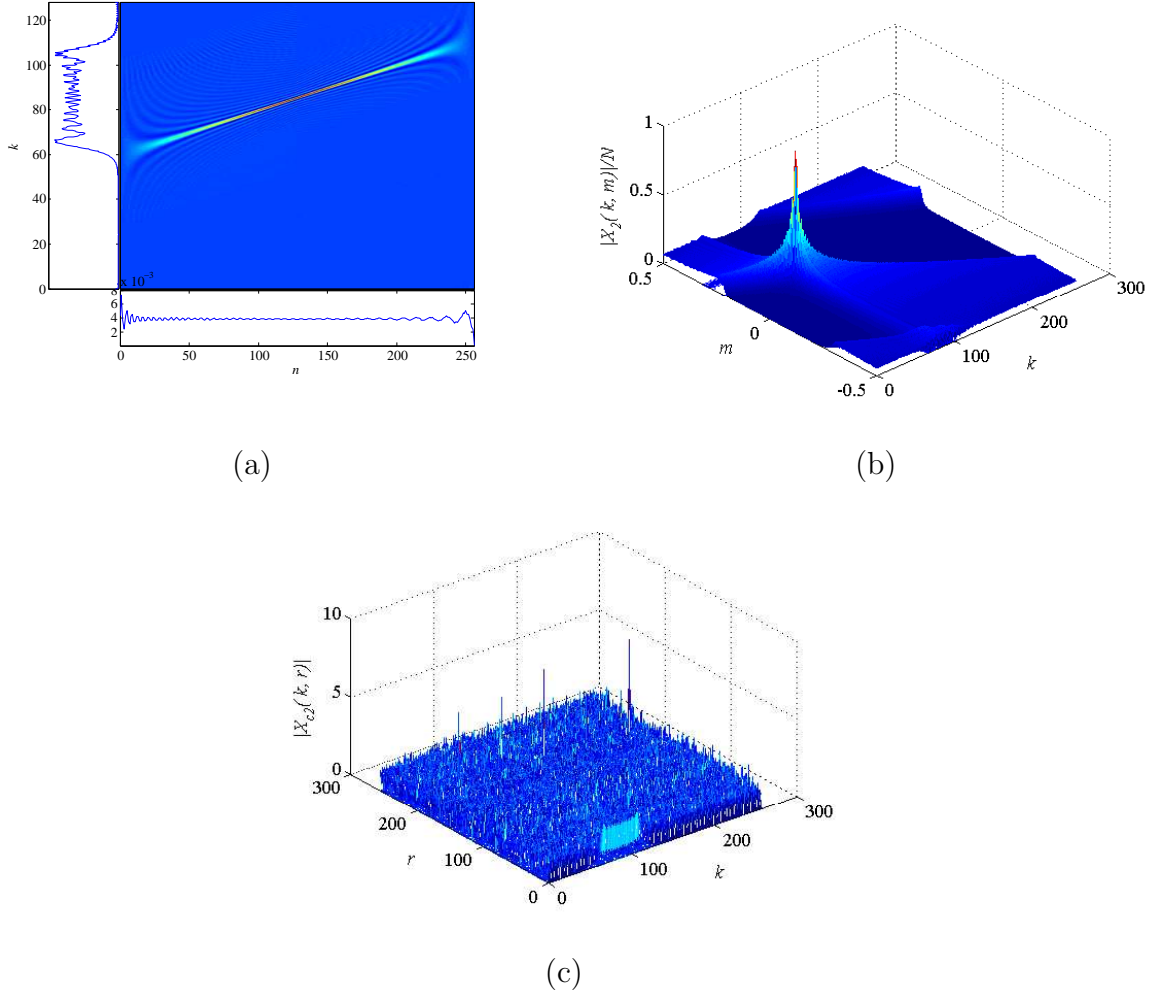


Figure 4: Comparison of the DLCT and the DCFT: (a) Wigner–Ville distribution of signal $x_2(n)$; (b) Magnitude of the DLCT; (c) Magnitude of the DCFT.

The Wigner distribution corresponding to $x_1(n)$ is shown in Fig. 3(a), which does not display the instantaneous frequency of the linear chirp due to the aliasing caused by the integer β . Figure 3(b) displays the magnitudes of the DLCT and Fig. 3(c) the magnitude of the discrete chirp–Fourier transform proposed by [14]. In this case the results coincide. If we then test the two procedures for a chirp signal

$$x_2(n) = \exp\left(j \frac{2\pi}{257} (0.1n^2 + 60n)\right)$$

with chirp rate $\beta = 0.1$, the results are very different. The Wigner distribution clearly shows the alias-free chirp (Fig. 4(a)). In this case, when the β is not an integer, our algorithm provides the correct parameters (Fig. 4(b)) while the discrete chirp-Fourier transform proposed by [14] does not as shown in Fig. 4(c).

2.1.3 Cosine discrete linear chirps

In the previous section we consider the local representation of signals in terms of complex linear chirps, and thus develop the discrete linear chirp transform (DLCT). This is a joint chirp-rate frequency transform, that generalizes the discrete Fourier transform (DFT). We will next develop the discrete cosine chirp transform (DCCT): definition, implementation, and linearity property. The presented transform is more applicable to signal compression application.

- **Definition**

For a discrete real-valued signal $x(n)$ of finite support $0 \leq n \leq N - 1$ we define its DCCT as

$$X(k, m) = \sum_{n=0}^{N-1} x(n) \cos \left(\frac{Cm\pi n^2 + k\pi(2n+1)}{2N} \right) \\ 0 \leq k \leq N - 1, -L/2 \leq m \leq L/2 - 1 \quad (2.13)$$

or a representation in terms of cosines with instantaneous frequency

$$IF(n, k) = \beta\pi n/N + k\pi/N.$$

The assumptions made for the DLCT related to the chirp rate β are still valid for the DCCT. That is, we consider its support finite, $-\Lambda \leq \beta < \Lambda$, and that $\beta = mC$, and $C = 2\Lambda/L$, or that is not exclusively an integer. We can think of the DCCT as a generalization of the discrete cosine transform as $X(k, 0)$ is equal to the DCT of $x(n)$. The DCCT decomposes a signal using real linear chirps as

$$\psi_{\beta,k}(n) = \cos \left(\frac{\beta\pi n^2}{2N} + \frac{k\pi(2n+1)}{2N} \right).$$

The signal is reconstructed by the inverse discrete cosine chirp transform (IDCCT), which has the form

$$x(n) = \sum_{m=-\frac{L}{2}}^{\frac{L}{2}-1} \sum_{k=0}^{N-1} \frac{2X(k, m)}{LN} \cos\left(\frac{Cm\pi n^2 + k\pi(2n+1)}{2N}\right) \quad 0 \leq n \leq N-1 \quad (2.14)$$

We can prove that (2.13) and (2.14) forms a pair as follows. Substitute (2.13) into (2.14)

$$\sum_{m=-\frac{L}{2}}^{\frac{L}{2}-1} \sum_{k=0}^{N-1} \sum_{\ell=0}^{N-1} \frac{2x(m)}{LN} \cos\left(\frac{Cm\pi\ell^2 + k\pi(2\ell+1)}{2N}\right) \times \cos\left(\frac{Cm\pi n^2 + k\pi(2n+1)}{2N}\right) \quad (2.15)$$

Assume that $\theta_1 = Cm\pi n^2/(2N)$, $\phi_1^k = k\pi(2n+1)/(2N)$, $\theta_2 = Cm\pi\ell^2/(2N)$, and $\phi_2^k = k\pi(2\ell+1)/(2N)$ and first evaluate the summation with respect to k as follows

$$\sum_{k=0}^{N-1} \cos(\theta_1 + \phi_1^k) \cos(\theta_2 + \phi_2^k) = \frac{N \cos(\theta_1 - \theta_2)}{2} \delta(n - \ell) \quad (2.16)$$

where the following identities are used for the evaluation of (2.15)

$$\begin{aligned} \sum_k \cos \phi_1^k \sin \phi_2^k &= 0, \\ \sum_k \cos \phi_2^k \sin \phi_1^k &= 0, \\ \sum_k \cos \phi_1^k \cos \phi_2^k &= \frac{N}{2} \delta(n - \ell), \text{ and} \\ \sum_k \sin \phi_1^k \sin \phi_2^k &= \frac{N}{2} \delta(n - \ell) \end{aligned}$$

Also, for $n = \ell$, we have

$$\cos(\theta_1 - \theta_2) = 1$$

Thus,

$$\sum_{k=0}^{N-1} \cos(\theta_1 + \phi_1^k) \cos(\theta_2 + \phi_2^k) = \frac{N}{2} \delta(n - \ell)$$

After we calculate the summation with respect to k , equation (2.15) becomes,

$$\sum_{m=-\frac{L}{2}}^{\frac{L}{2}-1} \sum_{\ell=0}^{N-1} \frac{2x(\ell)N}{LN} \frac{N}{2} \delta(n - \ell) = \begin{cases} x(n) & \text{if } n = \ell \\ 0 & \text{if } n \neq \ell \end{cases}$$

or

$$x(n) = \sum_{m=-\frac{L}{2}}^{\frac{L}{2}-1} \sum_{k=0}^{N-1} \frac{2X(k, m)}{LN} \cos\left(\frac{Cm\pi n^2 + k\pi(2n + 1)}{2N}\right) \quad 0 \leq n \leq N - 1 \quad (2.17)$$

In Fig. 5 we show an example of calculating the DCCT of $x_1(n)$ given below. The signal $x_1(n)$ and its DCCT transform are presented in Figs. 5(a) and (b) whereas the reconstructed signal using (2.14) is given in Fig. 5(c). Figure 5(d) depicts reconstruction error.

$$x_1(n) = \cos\left(\frac{\pi}{1024} (0.25n^2 + 100n)\right) + \cos\left(\frac{\pi}{1024} (-0.1n^2 + 400n)\right)$$

• Implementation

The implementation of the DCCT is very efficient, since it depends on the fast Fourier transform (FFT) algorithm. Equation (2.13) can be rewritten as follows

$$\begin{aligned} X(k, m) &= \mathcal{R}e \left\{ e^{-j\frac{\pi k}{2N}} \sum_{n=0}^{2N-1} \underbrace{\left[x(n) e^{-j\frac{Cm\pi n^2}{2N}} \right]}_{h(n, m)} e^{-j\frac{2\pi kn}{2N}} \right\} \\ &= \mathcal{R}e \left\{ e^{-j\frac{\pi k}{2N}} H(k, m) \right\} \end{aligned}$$

where

$$H(k, m) = FFT \{h(n, m)\}$$

and $h(n, m) = 0$ for all m and $n = N, N + 1, \dots, 2N - 1$, and $\mathcal{R}e[\cdot]$ stands for the real part. Also, we can use the inverse FFT algorithm to compute the inverse DCCT.

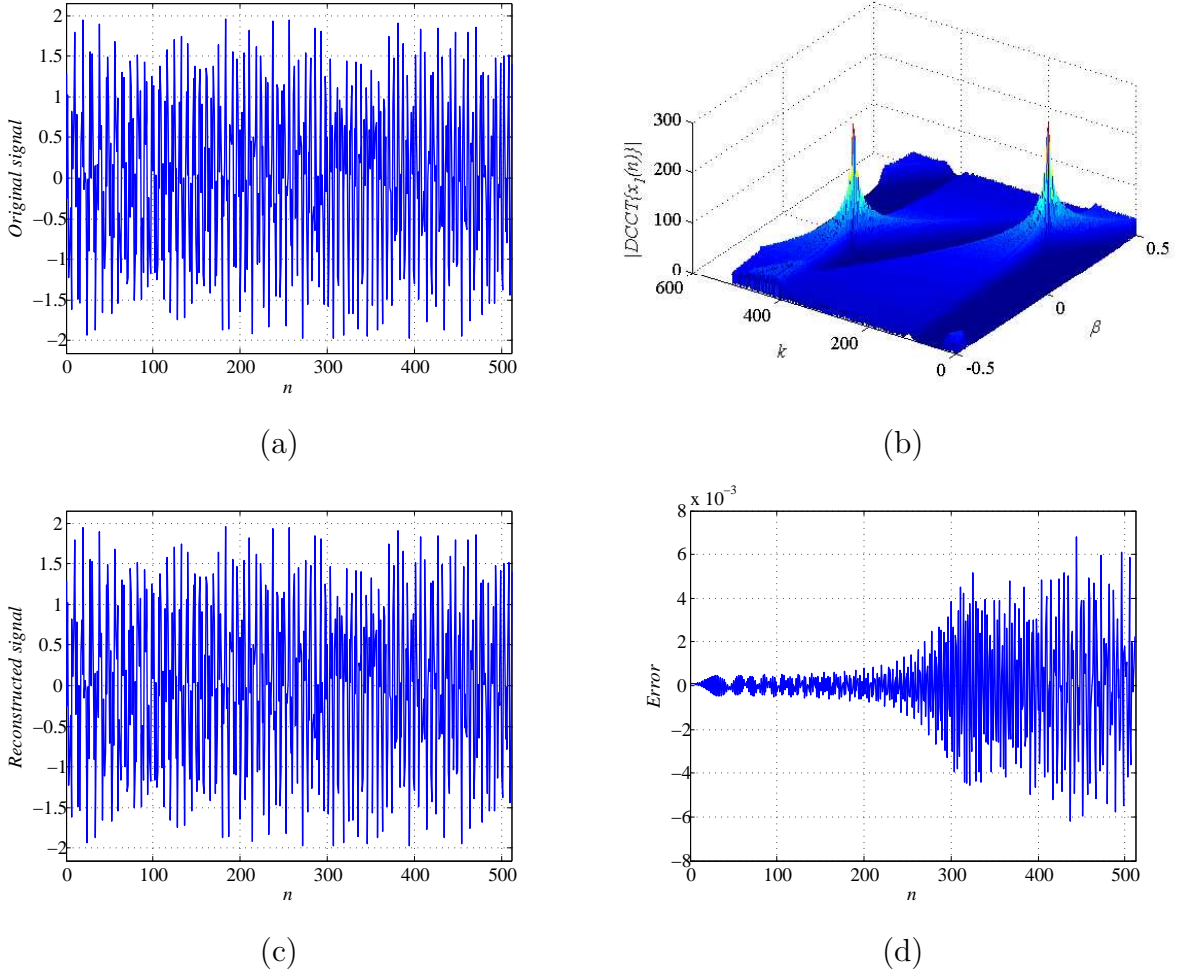


Figure 5: (a) The signal $x_1(n)$; (b) The magnitude of the DCCT of $x_1(n)$; (c) The reconstructed signal; (d) The reconstruction error.

Defining $F(k, m) = 2X(k, m)/N \times \exp(j\pi k/(2N))$ where $F(k, m) = 0$ when $k \geq N$ and $\forall m$, we can express (2.14) as

$$\begin{aligned}
 x(n) &= \mathcal{R}e \left\{ \frac{1}{L} \sum_{m=-L/2}^{L/2-1} \underbrace{\left[\sum_{k=0}^{2N-1} F(k, m) e^{j\frac{2\pi kn}{2N}} \right]}_{f(n, m)} e^{j\frac{Cm\pi n^2}{2N}} \right\} \\
 &= \mathcal{R}e \left\{ \frac{1}{L} \sum_{m=-L/2}^{L/2-1} f(n, m) e^{j\frac{Cm\pi n^2}{2N}} \right\}
 \end{aligned}$$

where

$$f(n, m) = \text{IFFT} \{F(k, m)\}$$

• **Linearity property**

The DCCT is a linear transformation, since for any $x_1(n)$ and $x_2(n)$ with a DCCT transform $X_1(k, m)$ and $X_2(k, m)$, respectively, then the signal $x(n) = a x_1(n) + b x_2(n)$ has the DCCT transform given as

$$X(k, m) = a X_1(k, m) + b X_2(k, m) \quad (2.18)$$

where a and b are constants. The linearity property can be easily proved because the summation is a linear operator as shown below.

If $x_1(n)$ and $x_2(n)$ are real finite signals in the time support $n = 0, \dots, N - 1$ and their discrete cosine chirp transforms are

$$X_1(k, m) = \sum_{n=0}^{N-1} x_1(n) \cos \left(\frac{Cm\pi n^2 + k\pi(2n+1)}{2N} \right)$$

and

$$X_2(k, m) = \sum_{n=0}^{N-1} x_2(n) \cos \left(\frac{Cm\pi n^2 + k\pi(2n+1)}{2N} \right)$$

that is

$$x_1(n) \iff X_1(k, m)$$

$$x_2(n) \iff X_2(k, m)$$

then for $x(n) = a x_1(n) + b x_2(n)$, its DCCT can be written as

$$\begin{aligned} X(k, m) &= \sum_{n=0}^{N-1} x(n) \cos \left(\frac{Cm\pi n^2 + k\pi(2n+1)}{2N} \right) \\ &= a \sum_{n=0}^{N-1} x_1(n) \cos \left(\frac{Cm\pi n^2 + k\pi(2n+1)}{2N} \right) \\ &\quad + b \sum_{n=0}^{N-1} x_2(n) \cos \left(\frac{Cm\pi n^2 + k\pi(2n+1)}{2N} \right) \end{aligned}$$

which yields,

$$X(k, m) = a X_1(k, m) + b X_2(k, m)$$

Linearity is very important property for the DCCT since it can be used in many applications such as signal separation, signal modeling, compressive sensing, and other applications. Thus, we can decompose a real signal $x(n)$ in terms of real chirps as

$$x(n) = \sum_{i=1}^P d_i \cos\left(\frac{\beta_i n^2 + k_i(2n + 1)}{2N}\right)$$

where d_i , β_i , and k_i are amplitudes, chirp rates, and frequencies of P real linear chirps.

2.2 COMPARING THE DLCT WITH THE DFRFT

The DLCT just like the FrFT can be used to convert non-sparse signals into sparse signals in time or frequency. In the following, we consider the performance in this respect of the two methods and also consider the resolution, peak location, and computational time for the two methods.

- **Sparsity**

Sparsity or compressibility reflects the fact that information carried by certain signal is much smaller than their bandwidth. Most signals are not sparse in the time domain, so linear transformation are used to make them sparse in either time or frequency using certain basis [47, 32]. Stationary signals, such as sinusoids or quasi-periodic speech segments, are well represented by the discrete cosine transform (DCT) [33]. The DCT can be used to obtain a sparse representation in frequency for such signals. However, non-stationary signals, such as chirps may not be sparse in either time or frequency, but rather in an intermediate domain.

Sparseness is an essential signal characteristic in many applications such as compressive sensing, compression, and denoising. It can be defined as a concentration of a signal energy on a few coefficients and the rest of them have low energy so that they can be

neglected. Therefore, the transform that can give higher sparsity (few coefficients) is considered better than the one that gives low sparsity (too many coefficients).

For mono-component signals, we can measure the sparsity of a signal analytically by measuring the broadness of its support in the transformed domain (could be time or frequency). The frequency spread (B) can be defined in the discrete form as [34]

$$B = \sqrt{\frac{\sum_k (\omega_k - \langle \omega_k \rangle)^2 |X(e^{j\omega_k})|^2}{\sum_k |X(e^{j\omega_k})|^2}} \quad (2.19)$$

where $\omega_k = 2\pi k/N$ for $k = 0, 1, \dots, N-1$ and $\langle \omega_k \rangle$ is the expected value given by

$$\langle \omega_k \rangle = \frac{\sum_k \omega_k |X(e^{j\omega_k})|^2}{\sum_k |X(e^{j\omega_k})|^2}$$

Similarly, we can define the time spread (T) as

$$T = \sqrt{\frac{\sum_n (n - \langle n \rangle)^2 |x(n)|^2}{\sum_n |x(n)|^2}} \quad (2.20)$$

given that $\langle n \rangle$ is the expected value defined as

$$\langle n \rangle = \frac{\sum_n n |x(n)|^2}{\sum_n |x(n)|^2}$$

In (2.19) and (2.20), for finite energy signals and without loss of generality we can assume the energy of the signal is normalized

$$\sum_n |x(n)|^2 = \frac{1}{N} \sum_k |X(e^{j\omega_k})|^2 = 1$$

The idea of measuring the sparsity by determining the broadness of the time spread or the frequency spread for mono-component signals can be generalized to multi-component signals. Since the DLCT can separate the components of the signal, we can define the sparsity measure in the frequency domain for multi-component signals as

$$B = \sum_{i=1}^P B_i \quad (2.21)$$

and the time spread as

$$T = \sum_{i=1}^P T_i \quad (2.22)$$

where T_i and B_i are the time and frequency spread for each component of a signal which has P components. We can also define the sparsity metric for multi-component signals in the form of time-bandwidth product (TB) as

$$\text{TB} = \sum_{i=1}^P T_i B_i \quad (2.23)$$

To evaluate the sparsity of the DLCT and the DFrFT, we use a synthetic signal $x_1(n)$ which is generated as follows

$$x_1(n) = \exp\left(j \frac{\pi}{256} (0.1n^2 + 10n)\right)$$

The signal $x_1(n)$ is shown in Fig. 6(a) and its Wigner-Ville distribution is illustrated in Fig. 6(b). The discrete fractional Fourier transform of $x_1(n)$ for $\alpha = -0.44\pi$ ($\beta \approx 0.1$) is given in Fig. 6(c) while Fig. 6(d) depicts the discrete linear chirp transform of $x_1(n)$ with $\beta = 0.1$. It is clear that, the DLCT gives a transformed signal that is sparser than the transformed signal that we obtain using the DFrFT.

Applying the sparsity metric to the signal $x_1(n)$, we find the frequency spread of the signal in Fig. 6(c) is $B_{DFrFT} = 0.063$ rad while it is equal to $B_{DLCT} = 5.1 \times 10^{-14}$ rad for the signal given in Fig. 6(d). Since $B_{DLCT} \ll B_{DFrFT}$, this implies that the transformed signal that we obtain using the DLCT is much sparser than the transformed signal using the DFrFT.

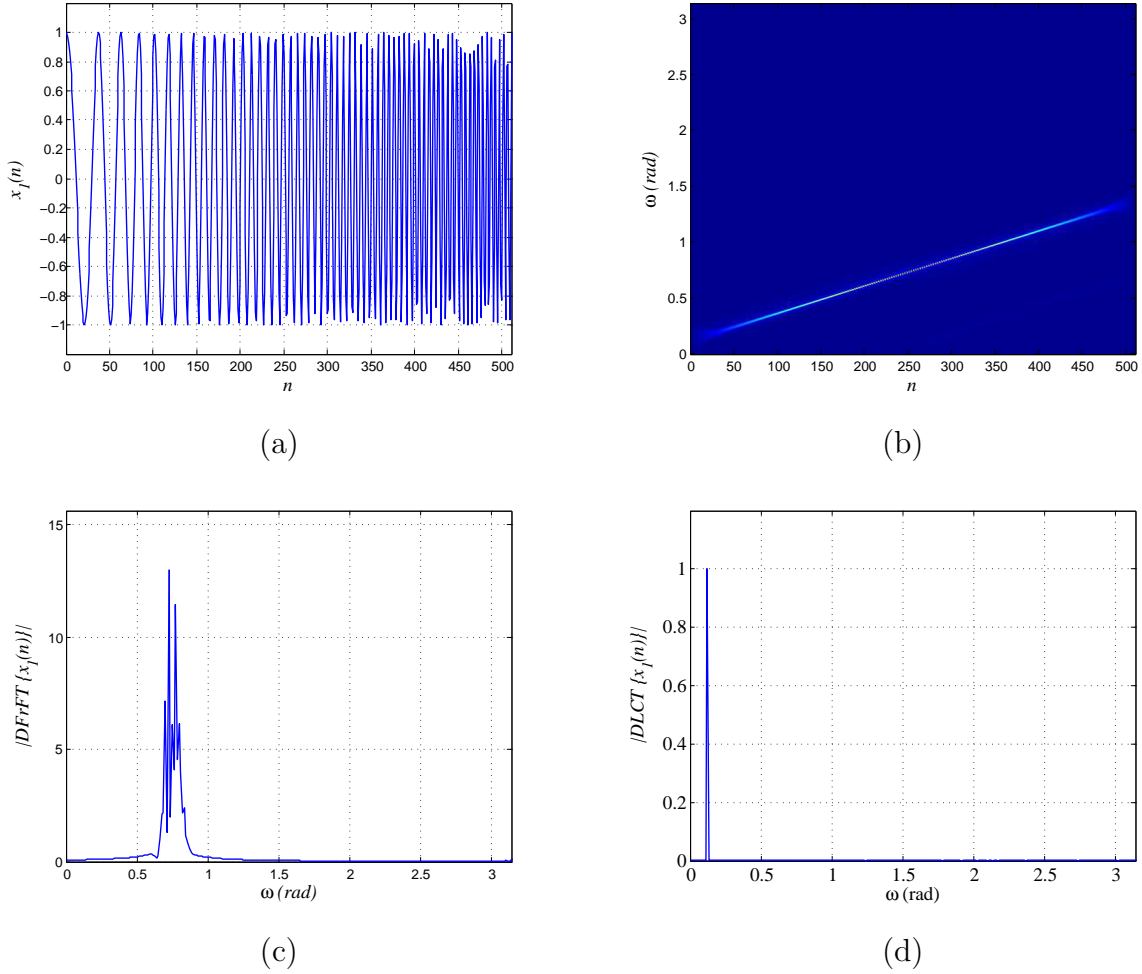


Figure 6: (a) Signal $x_1(n)$ in time domain; (b) Wigner–Ville distribution of $x_1(n)$; (c) The $|DFrFT\{x_1(n)\}|$ with $\alpha = -0.44\pi$; (d) The DLCT of $x_1(n)$ with $\beta = 0.1$.

• Computation time

Most of applications in signal processing that uses the DLCT or the DFrFT require to analyze the signal in three dimension space which are frequency, chirp–rate (fractional order), and magnitude. Computation time is very important factor that we should consider. Figure 7 explains the computation time load for the DLCT and the DFrFT. The experiment was executed in a HP machine that has an Intel(R) Core(TM) *i7 – 2670QM* CPU which is running at 2.2 GHz and installed memory RAM= 8.0 GB. As can be seen from Fig. 7 the DLCT consumes less time than the DFrFT. For instance, if we have

2048 Samples, the DLCT can do the task in 0.06 sec whereas the DFrFT needs about 6.13 sec to make the same role. So, we can save a lot of time if we consider using the DLCT instead of the DFrFT.

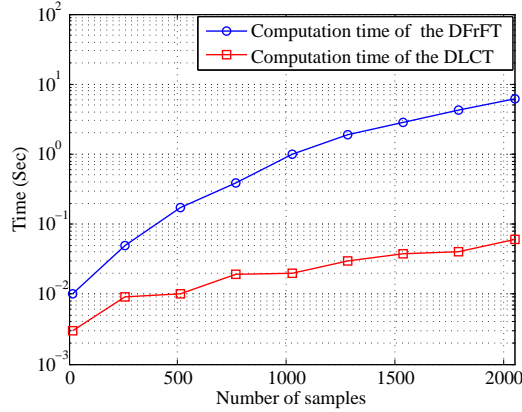


Figure 7: Comparing the computation time between the DLCT and the DFrFT

- **Resolution of the transform**

A critical point of the time–frequency analysis and signal separation is the resolution of the transform. The DLCT and the DFrFT have been used to separate linear chirps in the time–frequency plane by projecting (rotating) them and then followed by a filtering or a windowing procedure. If the resolution of the transform is good, even very close harmonics can be separated easily and viceversa. To explain the impact of the resolution of the DLCT and the DFrFT in signal separation application, a synthetic signal $x_2(n)$ is used.

$$x_2(n) = \exp\left(j\frac{\pi}{256}(0.1n^2 + 20n)\right) + \exp\left(j\frac{\pi}{256}(0.1n^2 + 30n)\right)$$

Figure 8(a) depicts the signal $x_2(n)$ whereas Fig. 8(b) shows its Wigner–Ville distribution. The signal $x_1(n)$ consists of two linear chirps with the same chirp rate but different frequencies which are close to each other. The magnitude of the DFrFT of $x_2(n)$ in three dimensions is given in Fig. 8(c) while Fig. 8(d) shows the magnitude of the DFrFT $\{x_2(n)\}$ at the fractional order $\alpha = -0.44\pi$. The three dimension space for the DLCT of $x_2(n)$ is given in Fig. 8(e) and Fig. 8(f) presents the DLCT of $x_2(n)$ when

$\beta = 0.1$. We can observe from Figs. 8(d) and (f) that the DLCT has higher resolution than the DFrFT since we can separate the two chirps using the DLCT easily while it is difficult to do so by using the DFrFT.

In general for any combination of ideal linear chirps, the resolution of the DLCT is finer than the resolution of the DFrFT. From examples we observe, the DLCT can separate two frequency components if they are $2\pi/N$ far apart while the DFrFT can separate them if they are close to each other by $19(2\pi/N)$.

- **Peak location**

All the algorithms that use the DLCT or the DFrFT for parametric characterization of chirps depend on searching for peaks for all possible chirp rates or fractional orders to obtain the optimal chirp rate or the optimal fractional order that maximizes the $|\text{DLCT}\{x(n)\}|$ or equivalently $|\text{DFrFT}\{x(n)\}|$. Therefore, it is obvious that the peaks should occur at the corresponding chirp rates and frequencies. For instance, if we consider a signal $x_3(n)$ which is given as

$$x_3(n) = \exp\left(j\frac{\pi}{256}(0.15n^2 + 80n)\right)$$

and its Wigner–Ville distribution is shown in Fig. 9(a), the peak should show up at $\beta = 0.15$ ($\alpha = -0.4\pi$). Unfortunately, that is not the case when we use the DFrFT as shown in Figs. 9(b) and (c) because the peak occurs at $\alpha = -0.28\pi$ ($\beta \approx 0.41$). On the other hand, if we use the DLCT to estimate the chirp rate, the peak shows up exactly at $\beta = 0.15$ as presented in Figs. 9(d) and (e).

It should be clarified that the DLCT can be used to estimate the chirp rate (β) and the frequency (k) as illustrated in example 1 (Fig. 6(d)), but the DFrFT can not be used to estimate the frequency (k) because the fractional Fourier transform rotates the signal around its center frequency as shown in Fig. 6(c).

Finally, when the chirp rate of the DLCT matches the optimal chirp rate or (the fractional order of the DFrFT matches the optimal fractional order), then the transformed signal at the optimal chirp rate (optimal fractional order) will be sparser than for any other chirp rate or fractional order because the time–bandwidth product will be minimum.

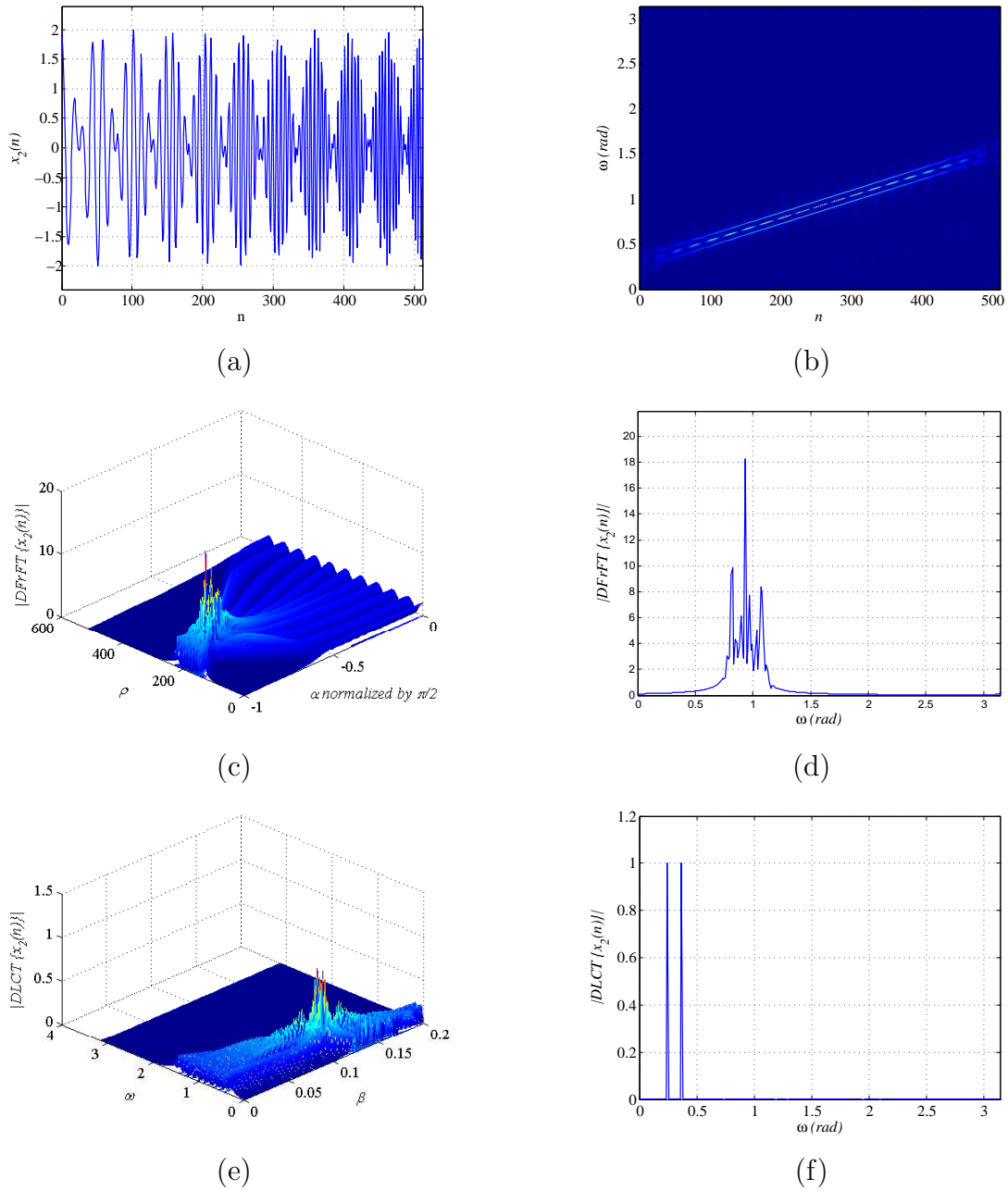


Figure 8: Resolution: (a) Signal $x_2(n)$ in time domain; (b) Wigner–Ville distribution of $x_2(n)$; (c) The $|\text{DFrFT}\{x_2(n)\}|$ in three–dimension space; (d) The $|\text{DFrFT}\{x_2(n)\}|$ at $\alpha = -0.44\pi$; (e) The DLCT of $x_2(n)$ in three–dimension space; (f) The DLCT of $x_2(n)$ at $\beta = 0.1$.

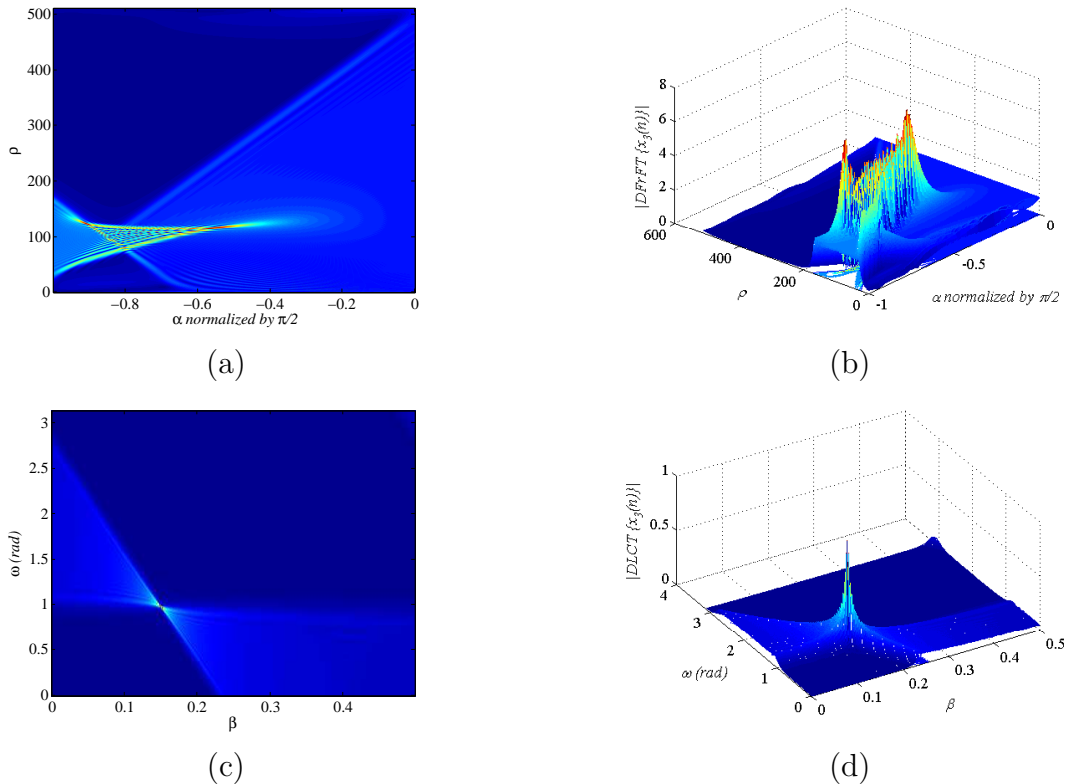


Figure 9: Peak detection: (a) $|DFrFT\{x_3(n)\}|$ in two–dimension space; (b) $|DFrFT\{x_3(n)\}|$ in three–dimension space; (c) The DLCT of $x_3(n)$ in two–dimension space; (d) The DLCT of $x_3(n)$ in three–dimension space.

2.3 ESTIMATION OF LINEAR CHIRP PARAMETERS

Chirp signals are frequently encountered in many signal processing applications such as radar, sonar, and telecommunications. The estimation of chirp parameters is a complicated problem when dealing with multi–component signals embedded in noise. Many methods have been proposed, but they have problems with initialization. In [35, 36], Kalman filtering is used to estimate parameters of chirps. A minimum mean square error method (MMSE) to estimate the parameters of the chirps was explained by [37]. It is an extension to the MMSE estimation method of sinusoidal parameters proposed in [38]. The maximum likelihood estimation method offers the optimal solution to this problem, but it is very difficult to

implement because it involves the numerical optimization of nonlinear cost function with many local minima [39]. Therefore, many approaches were developed to look for suboptimal solution, for instance, the chirplet decomposition [40, 41].

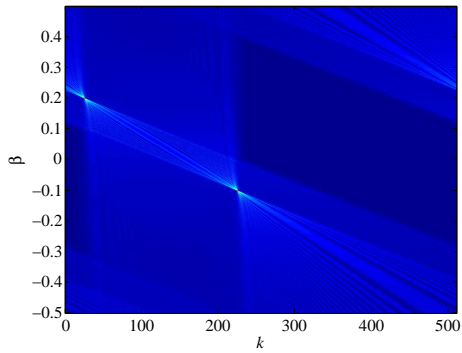
Consider a signal representation using complex linear chirps as

$$x(n) = \sum_{i=1}^P a_i \exp \left(j \frac{2\pi}{N} (\beta_i n^2 + k_i n) + j \phi_i \right) \quad (2.24)$$

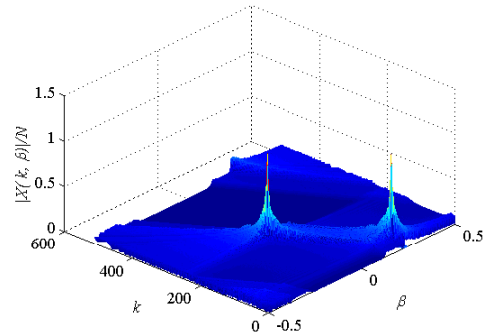
where a_i , β_i , k_i , and ϕ_i are amplitude, chirp rate, frequency, and phase of the i th linear chirp, respectively. Each chirp can be described by a set of parameters $\{a_i, \beta_i, k_i, \text{ and } \phi_i\}$. In this section, we use the DLCT to estimate these parameters. Given the signal

$$x(n) = e^{j\pi/2} \exp \left(j \frac{2\pi}{512} (0.2n^2 + 25n) \right) + e^{j\pi/4} \exp \left(j \frac{2\pi}{512} (-0.1n^2 + 225n) \right)$$

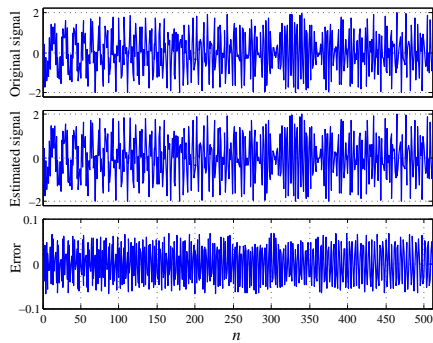
Figures 10(a) and (b) display the two and three-dimensional plots of $|X(k, m)|$. At the locations $(k, \beta) = (25, 0.2)$ and $(k, \beta) = (225, -0.1)$ the transformation displays peaks corresponding to the two chirps with the given frequencies and chirp rates. In Fig. 10(c), we display the reconstruction of the signal using $(k, \beta) = (25, 0.2)$ and $(225, -0.1)$ and the magnitude and phase of the peaks. In the case when noise is added, the parameters of the two chirps are not estimated that accurately. However, as shown in Fig. 10(d) measuring the reconstruction mean square error for different noise levels, it decreases as expected and levels off at -27.68 dB for SNRs higher than about 45 dBs. At these levels the parameters of the signal are estimated exactly.



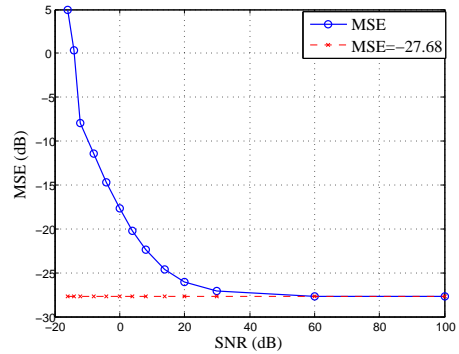
(a)



(b)



(c)



(d)

Figure 10: Parameters of chirp and reconstruction: (a) $|X(k, m)|$ in two-dimensions; (b) $|X(k, m)|$ in three-dimensions; (c) Original, estimated and error; (d) Mean square error (MSE) of $x(n)$.

3.0 SIGNAL COMPRESSION

Signal compression transforms a signal into an efficient compact form, for transmission or storage, that can be decompressed back to produce the original or a close approximation of the original signal. The goal of signal compression is to minimize data rate and to conserve bandwidth, while keeping the quality and intelligibility of the original signal. Unfortunately, the compression ratio is inversely proportional to the quality of the signal. Hence, there is always a tradeoff between compression ratio and quality [42, 43].

The performance of compression algorithms is measured by the signal to noise ratio SNR and the compression ratio Cr:

$$\text{SNR} = 10 \log (\sigma_x^2 / \sigma_e^2)$$

$$\text{Cr} = \frac{\text{length of original signal}}{\text{length of compressed signal}}$$

where σ_x^2 is the variance of the original signal and σ_e^2 is the variance of the difference between original and reconstructed signals. Another factor that plays an important role in compression is the threshold value. After calculating the DLCT or the DCCT of a signal, many of the coefficients of the resulted signal are close to or equal to zero. Thus, we can modify those coefficients to produce more zeros by zeroing them out using certain threshold.

3.1 COMPRESSIVE SENSING USING DCCT

Compressive sensing (CS) [44] aims to take advantage of the signal's sparser representation dictated by the uncertainty principle. For instance, in [45] the signal to be compressed is

represented in the sparser domain using the discrete cosine transform (DCT) and taking random measurements from the new sparse signal so that the length of the measurement is smaller than the length of the original signal. The original signal can be reconstructed from the measurements using ℓ_1 -minimization. Although CS provides very good results for signals that are sparse in either time or frequency, it does not for signals that are not sparse in either time or frequency such as the case of chirp signals [46, 47]. Time–frequency analysis is needed to obtain an intermediate domain where the signal is sparser than in time or in frequency. The Fractional Fourier Transform [48, 49] can be used for that, here we propose the DCCT to obtain a sparse representation of a signal that is not sparse in time or frequency domains.

3.1.1 Compressive sensing

The conventional paradigm in digital signal processing for reconstructing signals from measured data follows Shannon sampling theorem. This approach guarantees the preservation of the information that is in the signal being sampled, but the cost is reflected in the number of samples that are needed to represent the signal. Recently, the new theory of compressive sensing— also known as compressive sampling or sparse recovery — has emerged [50, 51] as an alternative to the traditional sampling theory. Compressive sensing asserts that we can reconstruct certain signals using fewer samples than those required by the sampling theory if we satisfy two conditions: sparsity and incoherence which means the sensing vectors are as different as possible from the sparsity basis. If we satisfy those conditions, signal reconstruction can be achieved from cardinally smaller measurements by using ℓ_1 -minimization [45], [44].

Consider a finite support real signal with values given by a vector $\mathbf{x} \in \mathbb{R}^n$, and that is expressed in terms of the basis $\psi = [\psi_1 \dots \psi_N]$ [44] as

$$\mathbf{x} = \sum_{i=1}^N s_i \psi_i \quad \text{or} \quad \mathbf{x} = \psi \mathbf{s} \quad (3.1)$$

where ψ is an $N \times N$ matrix, and \mathbf{s} is a vector of size $N \times 1$. The basis that transforms \mathbf{x} into a sparse signal \mathbf{s} can be, for instance, the one for the discrete cosine transform for a certain class of signals.

When the signal \mathbf{x} is sparse it can be represented with $K \ll N$ nonzero coefficients. Compressive sensing assumes that the K nonzero coefficients are not extracted directly, but we project the vector \mathbf{x} onto a matrix ϕ of size $M \times N$ where $M < N$. The matrix ϕ is called the measurement matrix and it satisfies the condition that the columns of the sparsity basis ψ cannot sparsely represent the rows of the measurement matrix ϕ (incoherence condition). We can represent the measurement signal \mathbf{y} as follows

$$\mathbf{y} = \phi \mathbf{x} = \underbrace{\phi \psi}_{\theta} \mathbf{s}$$

where \mathbf{y} is a vector of size $M \times 1$. Reconstruction of the signal is a convex optimization aimed at recovering the signal via ℓ_1 -minimization as shown in [45]

$$\hat{\mathbf{s}} = \underset{\mathbf{s}}{\operatorname{argmin}} \|\mathbf{s}\|_1 \quad \text{subject to} \quad \mathbf{y} = \theta \mathbf{s} \quad (3.2)$$

from which we can recover \mathbf{s} , and then we use the inverse basis to obtain the original signal \mathbf{x} .

3.1.2 Using the DCCT to obtain sparse signals

Just like the DCT that is used to convert stationary signals into sparse signals in either time or frequency, the real chirp basis (DCCT) can be used to obtain sparse non-stationary signals. To illustrate how the DCCT can be used to give sparse signals, several experiments are conducted.

In the first experiment, the signal is a combination of two real linear chirps, windowed by a Hamming window $w(n)$

$$\begin{aligned} x_w(n) &= x_1(n) w(n) \quad \text{where} \\ x_1(n) &= \cos\left(\frac{0.1\pi n^2 + 25\pi(2n+1)}{512}\right) + 2 \cos\left(\frac{0.1\pi n^2 + 300\pi(2n+1)}{1024}\right) \end{aligned}$$

This signal is clearly not sparse in time, so we consider if it is sparse in frequency or in other domain. The plot in Fig. 11(a) shows the DCT of $x_w(n)$ whereas Fig. 11(b) presents the frequency sparse signal $Y(k, 0)$ obtained from the DCCT of the signal $x_w(n)$ after projecting the two chirps on the time domain by $\beta_1 = 0.4$ and $\beta_2 = 0.2$, obtained from the DCCT

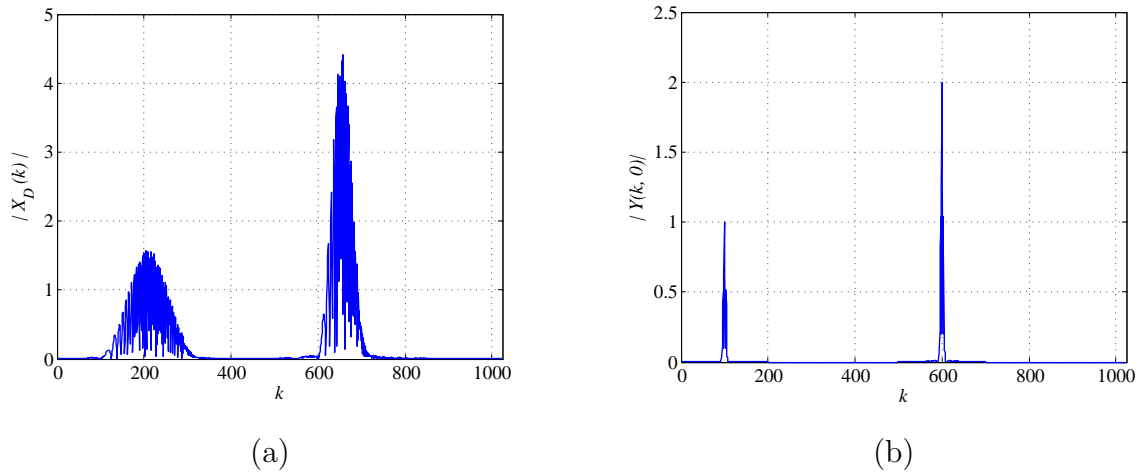


Figure 11: Sparseness of $x_w(n)$: (a) using the DCT; (b) using the DCCT.

of $x_w(n)$. The projection in the DCCT is different from the DLCT modulation property. The projection in the DCCT is to reallocate the peaks from their locations $\{(k_i, \beta_i)\}$ to new locations $\{(k_i, 0)\}$ or sinusoids.

We can measure the resulted sparsity using (2.21), (2.22), or (2.23). The frequency spread, and the time-bandwidth product metric of $X_w(k)$ are $B= 0.29$ rad and $TB= 22.71$ rad while they are $B= 0.027$ rad and $TB= 2.14$ rad for $Y(k, 0)$ where the original signal can be reconstructed (see (2.14)) from these sparse signals with $SNR= 32$ dB. Comparing the time-bandwidth product of both signals, the DCCT signal is much sparser than the DCT signal where $TB_{DCCT} \ll TB_{DCT}$.

In the second experiment, we use an actual bird song signal $x_b(n)$ (see Fig. 12(a)) to show that for such signals, the DCCT can give sparser representations than the DCT. Figure 12(b) gives the DCT of the bird signal showing this signal is not sparse in either time or frequency. Figure 12(c) gives the transformed signal obtained via the DCCT of the bird signal after being rotated with $\beta = -0.48$. The DCCT of the rotated signal $y_b(n)$ at $\beta = 0$ yields $Y_b(k, 0)$.

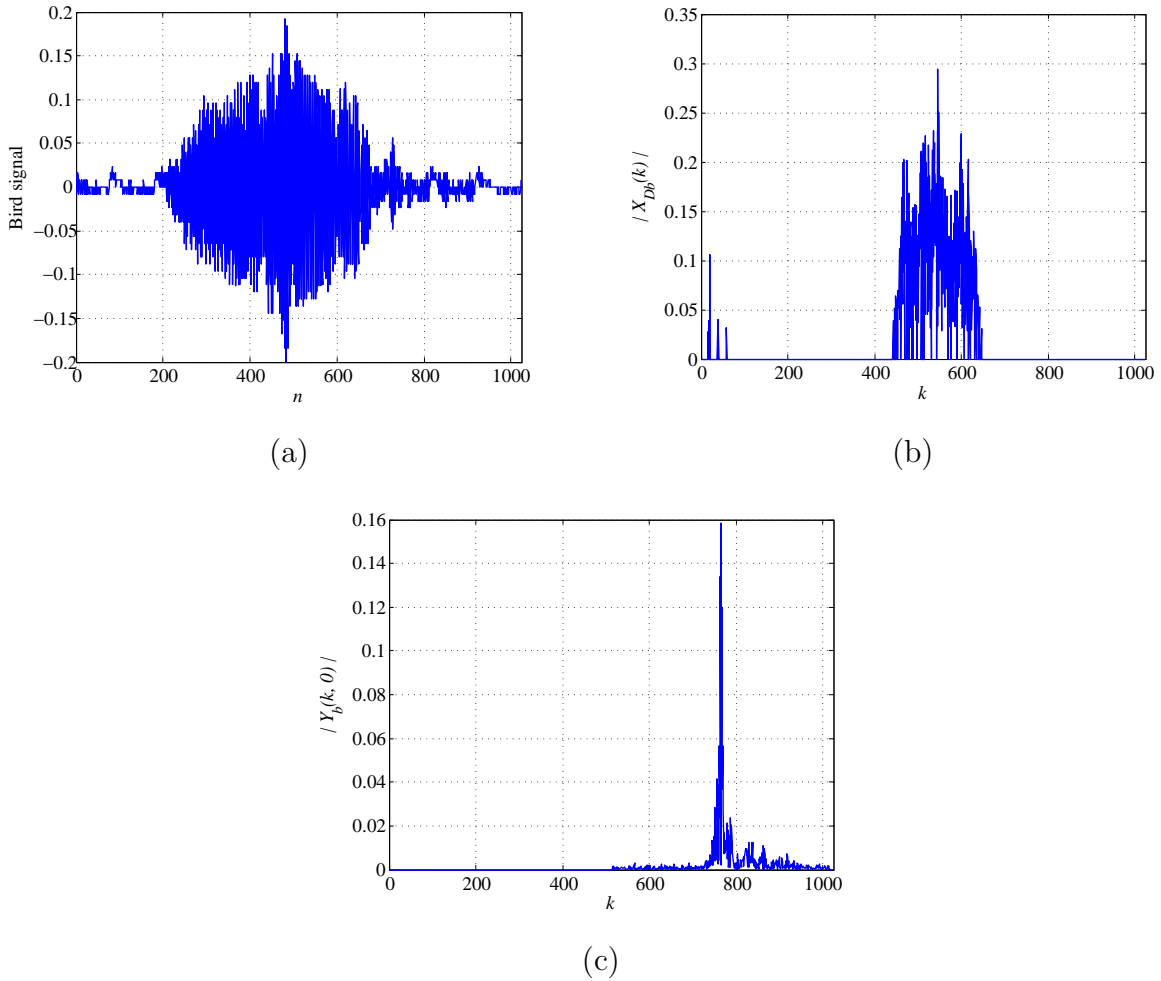


Figure 12: Sparseness of bird signal: (a) Bird signal in the time domain; (b) Sparseness using the DCT; (c) Sparseness using the DCCT.

In the third experiment, we use the bat echolocation signal shown in Fig. 13(a). Its DCT is depicted in Fig. 13(b). Figure 13(c) presents a sparse signal, which is obtained from the DCCT of the bat signal. It can be seen from these plots, the DCCT gives a sparser signal than the DCT.

The signal given in Fig. 13(c) is sparser than the signal shown in Fig. 13(b). The frequency spread or the time–bandwidth product of each signal with a reconstruction SNR=15 dB is given as, $B=0.904$ rad or $TB=66.52$ rad for the DCT and $B=0.246$ rad or $TB=13.97$ rad for the DCCT.

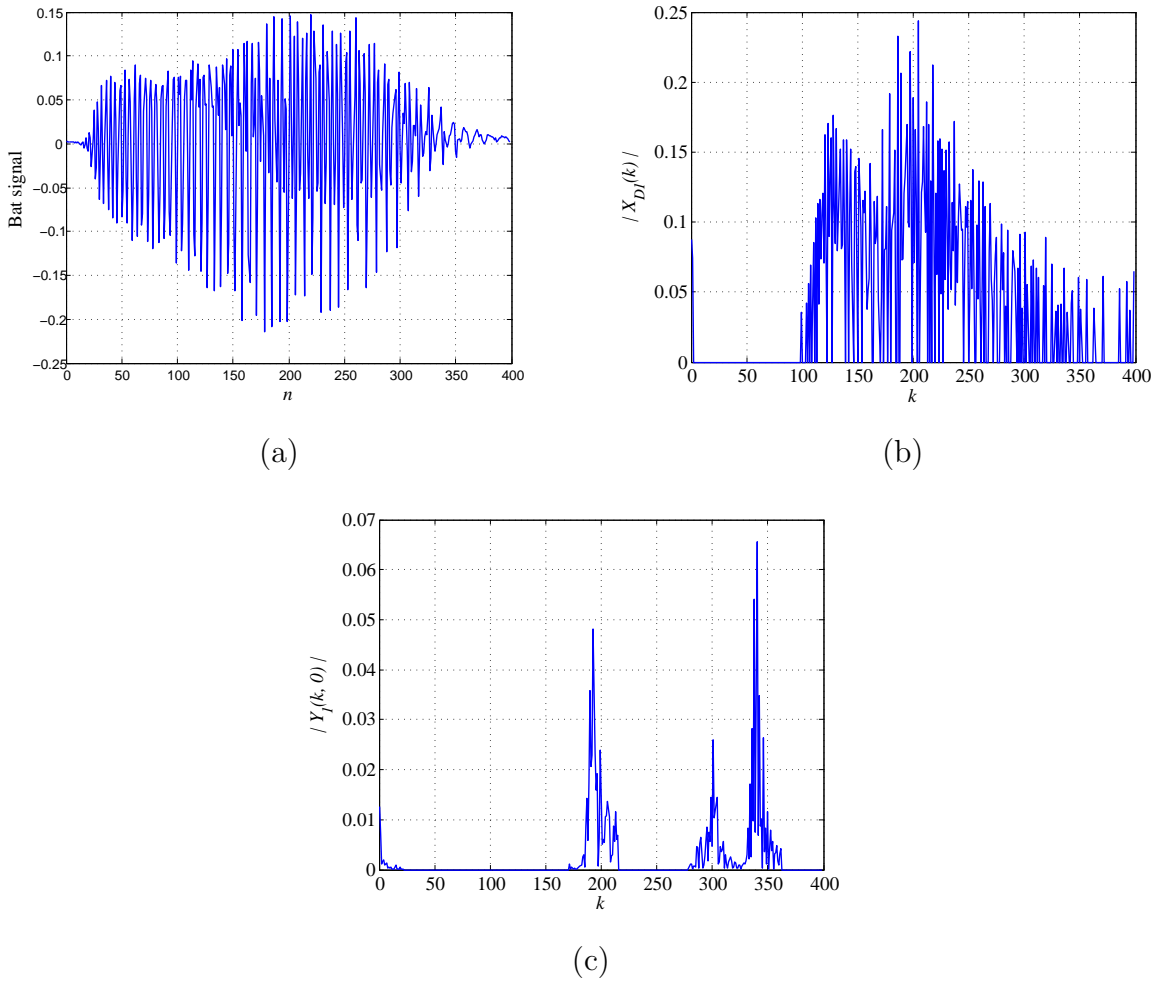


Figure 13: Sparseness of bat signal: (a) Bat signal in the time domain; (b) Sparseness using the DCT; (c) Sparseness using the DCCT.

3.1.3 Compression mechanism

Compression with compressive sensing using DCCT is different from the one that uses DCT in that we need to know the chirp rates that we use for obtaining a sparse representation of the original signal. Thus, the frame sample is given in Fig. 14. The first part of the frame contains the measurement signal \mathbf{y} which is obtained from CS and the second part of the frame has the chirp rates which decomposes the original signal into a combination of real linear chirps.

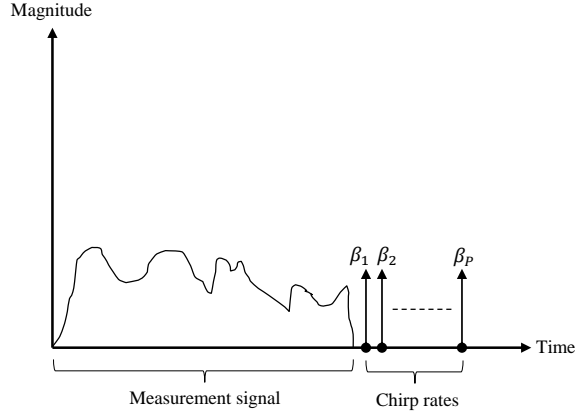
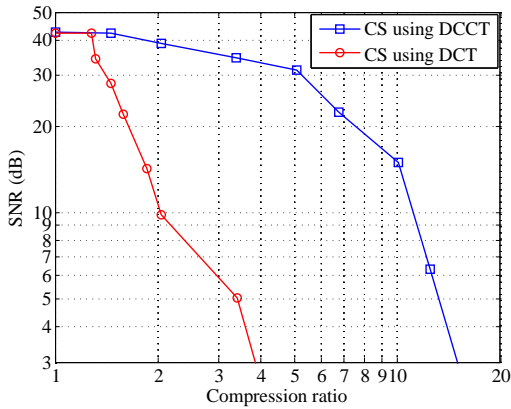
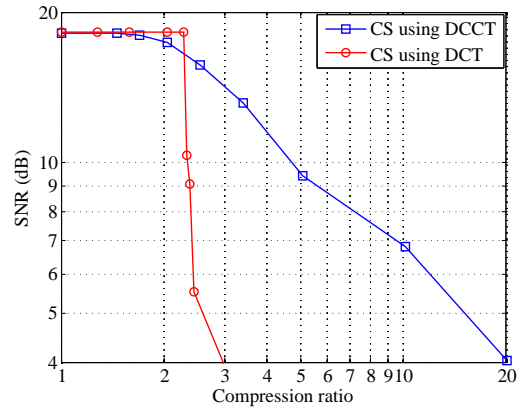


Figure 14: Compression sampling frame.

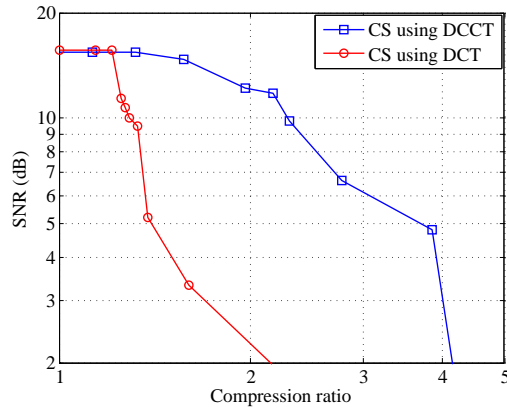
To illustrate how the DCCT improves compressive sensing performance, we consider the three experiments from the previous section. Figure 15(a) shows the results of the first experiment. Since our goal is to achieve high SNR with high compression ratio, it is obvious compressive sensing using the DCCT gives better results than compressive sensing using the DCT. In this case, the sample frame has two chirps ($\beta_1 = 0.2$ and $\beta_2 = 0.4$) with the measurement signal. Another example of interest is the bird signal given in Fig. 12(a). The compressed signal (sample frame) in this experiment consists of the measurement signal and the chirp rate ($\beta = -0.48$). The compression ratio versus the SNR is shown in Fig. 15(b) which explains the improvement that can be achieved using the DCCT. Also, the results of compression the bat signal using compressive sensing with the DCCT and the DCT are given in Fig. 15(c). It is shown that the performance of compressive sensing with the DCCT is fabulous compared with it with the DCT. In this case, the sample frame has four chirp rates $\{-0.58 \ -0.426 \ 0.829 \ 0\}$ along with the measurement signal.



(a)



(b)



(c)

Figure 15: Compression using compressive sensing: (a) Experiment 1: two windowed chirps; (b) Experiment 2: bird signal; (c) Experiment 3: bat signal.

In the theory of CS, the most important condition that we have to satisfy is the signal sparsity. Hence, the DCCT achieves better results than the DCT as shown in Figs. 11, 12, and 13 where clearly the DCCT is more applicable for analyzing such signals than the DCT.

3.1.4 Real and complex chirp bases in CS application

In this section, we want to justify considering real chirp bases in compressive sensing application by comparing them with the complex chirp bases. The discrete linear chirp transform

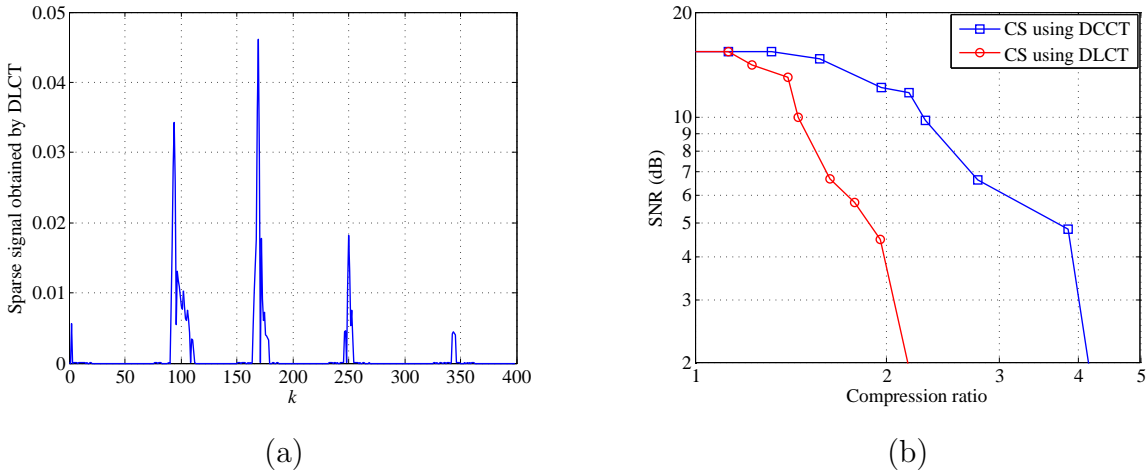


Figure 16: (a) The sparseness of the bat signal using the DLCT; (b) Comparison between CS with the DCCT and CS with the DLCT.

(DLCT), which uses complex chirp bases, will be used for this purpose instead of the other transforms that based on complex chirp bases because it is more efficient. The bat signal is considered since it is multi-component. The sparse signal that we obtain using the DLCT is shown in Fig. 16(a) where its frequency spread $B = 0.118$ rad and its time-bandwidth $TB = 6.1$ rad. Comparing the frequency spread of the DCCT signal which is shown in Fig. 13(c) with the signal given in Fig. 16(a), we observe the DLCT provides sparser signal than the DCCT where $B_{DLCT} = 0.118 \ll B_{DCCT} = 0.246$. Figure 16 provides the compression using compressive sensing with the DCCT (real chirp bases) and the DLCT (complex chirp bases). Although the DLCT gives sparser signals than the DCCT, it does not achieve good results in terms of compression. The reason for that stands for the fact that the DLCT is combined the signal in terms of complex chirps.

3.2 PARAMETER COMPRESSION METHOD

The direct and the dual DLCT are used to represent signals that can be better represented by one of them locally. Considering that a sinusoid has a chirp rate $\beta = 0$, while an impulse has as chirp rate $\beta \rightarrow \infty$, we separate signals into two groups: one having $|\beta| \leq 0.5$, corresponding to a linear chirp with a slope with an angle in $[-45^\circ, 45^\circ]$, and the other for $0.5 < |\beta| < \infty$ corresponding to a linear chirp with a slope with an angle in $[45^\circ, 90^\circ]$ or $[-45^\circ, -90^\circ]$. The value of $\beta = 0.5$ is not arbitrarily chosen since it relates to the slope of the instantaneous frequency such that

$$\text{Slope} = \tan(\theta) = 2\beta$$

If $\beta = 0.5$, then $\theta = \pi/4$ which is the angle that separates the time-frequency space into two symmetric halves.

3.2.1 The proposed compression algorithm

In this section, we present a new algorithm for signal compression using DLCT. Figure 17 shows the block diagram of the proposed method.

Consider the local representation of a signal $x(n)$, $0 \leq n \leq N - 1$, as a superposition of P linear chirps

$$\begin{aligned} x(n) &= \sum_{i=0}^{P-1} a_i \exp \left(j \frac{2\pi}{N} (\beta_i n^2 + k_i n) + j \varphi_i \right) \\ &= \sum_{i=0}^{P-1} x_{\{|\beta_i| \leq 0.5\}}(n) + x_{\{|\beta_i| > 0.5\}}(n) \end{aligned}$$

where $\{a_i, \varphi_i, k_i, \beta_i\}$ are the amplitude, phase, frequency, and chirp rate of the i^{th} linear chirp. The algorithm has two paths for the signal, the upper which is the dual path and the lower which is the direct path. Depending on the minimum value of the extracted β s for certain segment of the signal, we can do the compression either by the dual path or by the direct path. The coefficients $\{a_i, \varphi_i, k_i, \beta_i\}$ are extracted and from these coefficients

we can reconstruct an approximation for the signal $x(n)$ — where the arrangement of these coefficients is done according to the proposed data structure shown in Fig. 18.

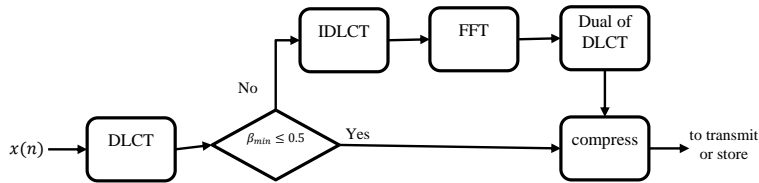


Figure 17: Compression algorithm.

3.2.2 Data Structure

The proposed data structure for sending or storing the extracted parameters is shown in Fig. 18, we choose P chirp rates that correspond to the peaks of chirps from the DLCT of the signal and P is the order of the chirp model. Then, from each vector which corresponds to the chosen chirp rates from the chirp transform $X(k, \beta)$ or $X(n, -\tilde{\beta})$ matrix, we select M_j amplitudes, phases, and frequencies or samples that have more energy of the signal concentrated upon them.

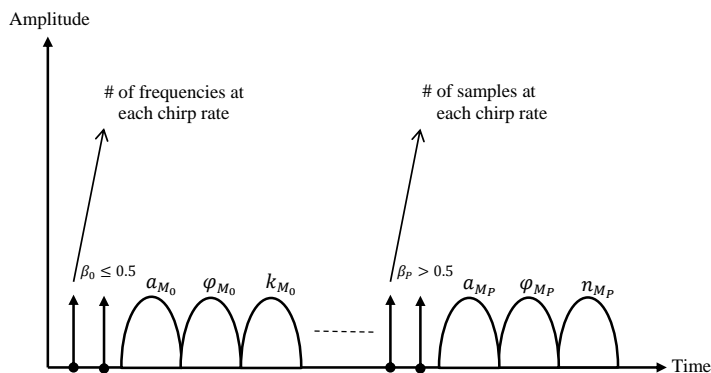


Figure 18: Data structure.

3.2.3 Experimental results

In this section, we present three experiment to illustrate the performance of the proposed method and compare the results with the compressive sensing method.

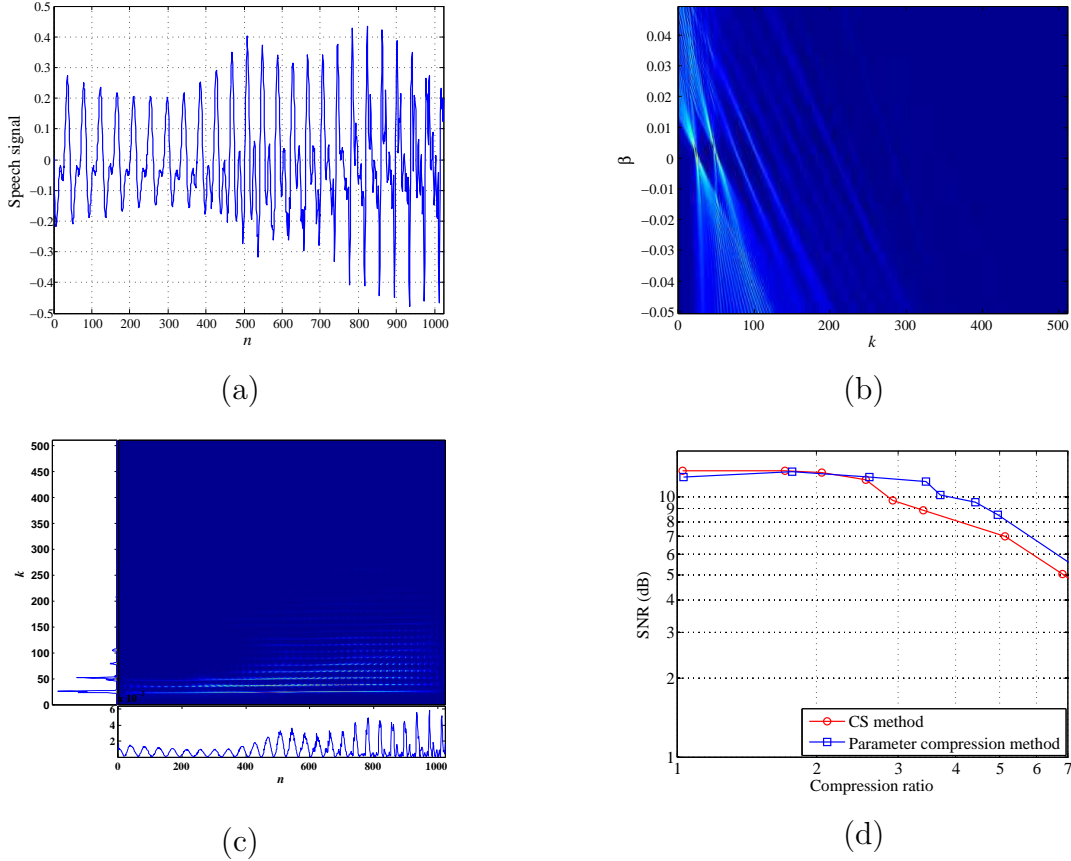


Figure 19: Experiment 1: (a) Segment of speech; (b) $|X(k, \beta)|$ in two-dimensions; (c) The Wigner-Ville distribution of the signal showing time and frequency marginals; (d) Compression ratio vs SNR for different methods.

In the first experiment, we use a segment of speech (1024 samples, sampling rate $f_s = 8kHz$) as shown in Fig. 19(a). Figure 19(b) and (c) give the magnitude of the DLCT and the Wigner-Ville distribution for this segment of speech. The compression ratio versus the SNR plot is shown in Fig. 19(d). Our goal is to obtain high SNR with high compression ratio as shown in Fig. 19(d), the proposed method gives more compression ratio than compressive sensing method, for an acceptable SNR. This segment of speech has very small chirp rates at high frequency components, with low concentrated energy, and sinusoids at low frequency

components with high concentrated energy. Since the minimum value β is less than 0.5, the compression is obtained by the direct path. Even though, this segment of speech can be considered a sparse signal in the frequency domain, the proposed algorithm outperforms the compressive sensing method.

In the second experiment, a bird song signal (2048 samples and sampling rate $f_s = 7,350\text{Hz}$) with $\beta = 0.88$ is considered; see Fig. 20(a). This signal is sparser in the time domain than in the frequency domain. Its dual DLCT and its Wigner distribution are shown in Figs. 20(b) and (c). Figure 20(d) displays SNR versus compression ratio. In this experiment, the minimum value of β is greater than 0.5. Thus, the dual path is used for the compression. The proposed method performs better than CS method.

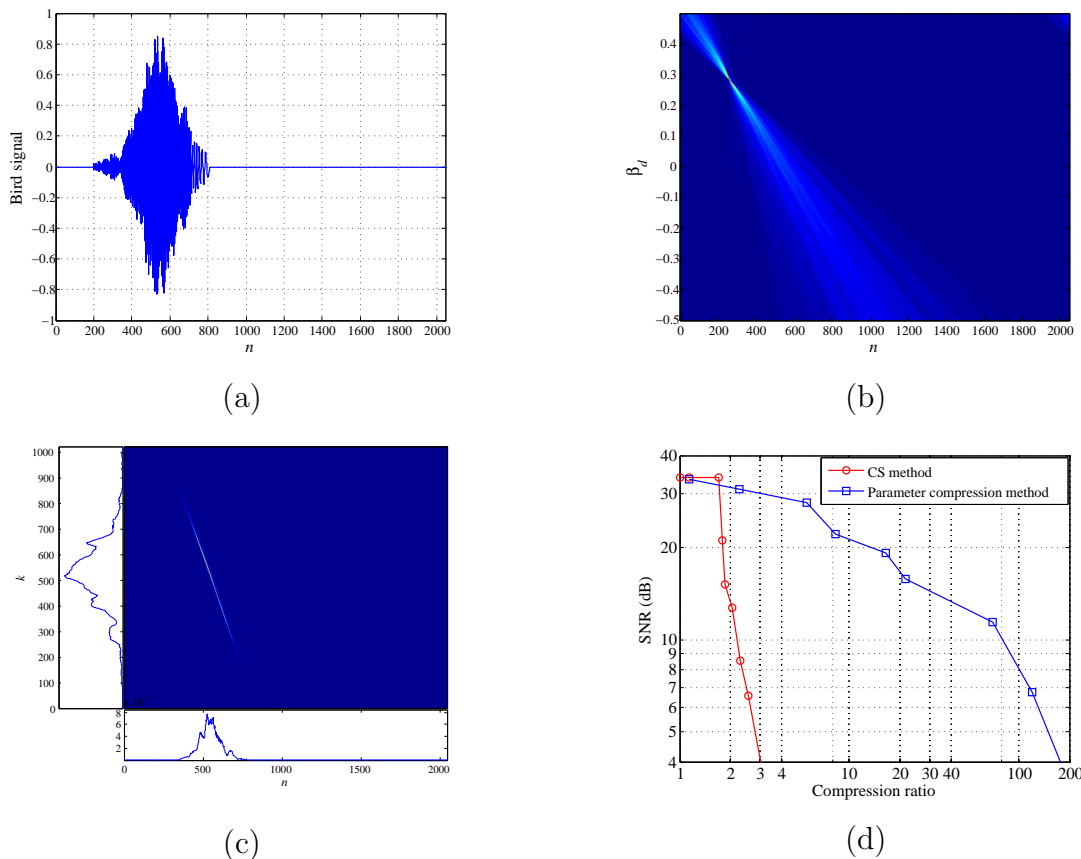


Figure 20: Experiment 2: (a) Bird chirping; (b) $|X(n, \beta_d)|$ in two-dimensions; (c) The Wigner-Ville distribution of the signal showing time and frequency marginals; (d) Compression ratio vs SNR for different methods.

4.0 DECOMPOSITION OF NON-STATIONARY SIGNALS AND TIME-FREQUENCY ANALYSIS

The processing of non-stationary signals in applications is complicated by the continuous variation of local signal characteristics. Over the years, many approaches have been proposed to represent such signals from wavelets to time-frequency distributions to the more recent empirical mode decomposition and Hilbert spectrum.

4.1 EMPIRICAL MODE DECOMPOSITION

The Hilbert-Huang transform (HHT) method was developed to represent non-stationary signals in the time-frequency plane without assistance of window functions. It is a combined approach of Hilbert transformation (HT) and the empirical mode decomposition (EMD) [52]. The EMD is used to decompose the signal into a set of functions called Intrinsic Mode Functions (IMFs). It does not have priori defined basis function, unlike the Fourier and Wavelet transform, the whole decomposition is adaptive and depends on the local oscillation of the data. The decomposition is based on the local characteristic time scale of the data and, therefore, it is applicable to nonlinear and non-stationary processes. Hilbert transform is applied to each intrinsic mode function for the purpose of providing the global time-frequency distribution of the underlying signal to estimate its instantaneous frequency (IF) [53]. The application of the HHT method to audio and speech signals have already been done [54, 55, 56]. In [57, 58, 59] the HHT is used to estimate the IF of biomedical signals such as EEG data and heart signals.

The empirical mode decomposition is an approach that we can use to separate a multi-component signal into its basic component. Thus, a non-stationary signal can be decomposed into a finite set of functions that have meaningful instantaneous frequencies. These functions are called intrinsic mode functions (IMFs) in which each mode should be independent of the others and must satisfy the following two conditions: First, the number of extrema and the number of zero crossings must either equal or differ at most by one. Second, the mean value of the envelope defined by the maxima and the envelope given by the minima is zero. The IMFs can be computed according to the following algorithm [52]

1. Let $\hat{x}(t) = x(t)$ where $x(t)$ is the original signal.
2. Identify all local maxima and minima of $\hat{x}(t)$.
3. Find a lower envelope $e_l(t)$ that interpolates all local minima.
4. Generate an upper envelope $e_u(t)$ that interpolates all local maxima.
5. Evaluate the local mean value,

$$m(t) = \frac{e_l(t) + e_u(t)}{2}$$

6. Subtract the local mean value from $\hat{x}(t)$,

$$d(t) = \hat{x}(t) - m(t)$$

7. Let $\hat{x}(t) = d(t)$ and go to step 2.
8. Repeat until $d(t)$ becomes an IMF.

The decomposition of the signal $x(t)$ can be written as

$$x(t) = \sum_{i=1}^M f_i(t) + r(t) \tag{4.1}$$

where M is the number of IMFs, $f_i(t)$ is the set of IMFs, and $r(t)$ is the final residue.

4.2 INTRINSIC MODE FUNCTIONS USING LINEAR CHIRPS

A chirp function

$$c(t) = Ae^{j\phi(t)} \quad 0 \leq t \leq T \quad (4.2)$$

where $\phi(t)$ is a polynomial in t

$$\phi(t) = \Omega_0 t + \sum_{k=0}^{\infty} \beta_k t^{k+2}$$

can be considered an IMF. Indeed, its envelope is symmetric so that its instantaneous mean is zero, and by adjusting the value of T the number of extrema and of zero crossings are made to match.

Given the complexity of using higher order chirps, we consider linear chirps with an appropriate support so that they are IMFs.

The signal $x(n)$ can be expressed in terms of the extracted IMFs or sources $s_i(n)$ as

$$x(n) = \sum_{i=1}^M s_i(n) + e(n) \quad (4.3)$$

where $e(n) \approx 0$ since most of signal energy is decomposed inside $s_i(n)$.

4.3 COMPARISON OF EMD AND DLCT

4.3.1 Instantaneous frequency estimation

The Hilbert transform is used to compute the IF of each of the signal components. Given one of the IMFs $x_i(t)$ of $x(t)$ we obtain its Hilbert transform

$$y_i(t) = \frac{1}{\pi} \int_{-\infty}^{\infty} \frac{x_i(\tau)}{t - \tau} d\tau$$

to get the analytic signal $z_i(t)$ from which we find its phase function to obtain the IF of $x_i(t)$:

$$\begin{aligned} z_i(t) &= x_i(t) + jy_i(t) = a_i(t)e^{j\psi_i(t)} \\ IF_{x_i}(t) &= \frac{d\psi_i(t)}{dt} \end{aligned}$$

For the DLCT, the peaks of the $|X(k, m)|^2$ provide the parameters $\{k, Cm\}$ of the linear chirps of the signal (See (2.7)). Using these parameters we obtain for each component an IF by computing the derivative of the phase of each component.

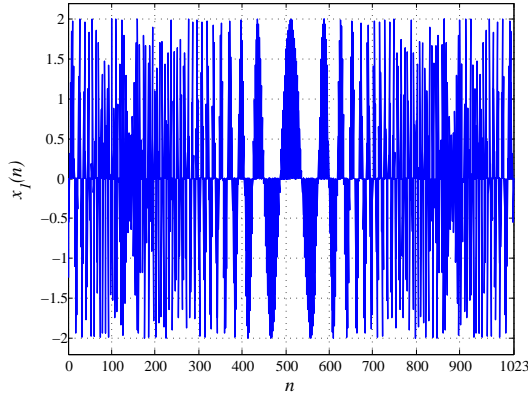
Consider the sum of two crossed quadratic chirps

$$x_1(n) = \exp\left(j\frac{\pi}{512}(10n + \xi(n - 512)^3)\right) + \exp\left(j\frac{\pi}{256}(-502n + \xi(n - 512)^3)\right)$$

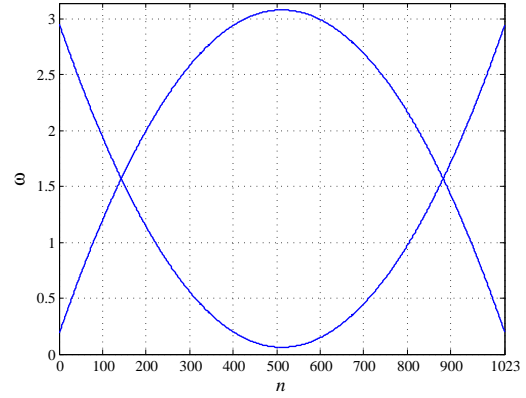
where $\xi = 6 \times 10^{-4}$. The signal is shown in Fig. 21(a) while the actual IFs of the two linear chirps are given in Fig. 21(b). The estimated IFs using the DLCT are depicted in Fig. 21(c). Figure 21(d) illustrates the results of applying the EMD algorithm for estimating the IFs. The performance of the IF estimation using the EMD is degraded at the crossing of the chirps due to the closeness of the frequencies. The parametric estimation provided by the DLCT does not suffer from this condition.

As a second example to test the IF estimation, consider the addition of two sinusoidal chirps corrupted by Gaussian noise $\eta(n)$ with a signal to noise ratio SNR=5 dB:

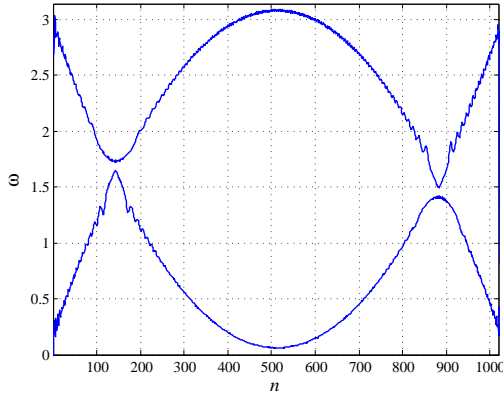
$$x_2(n) = \cos\left(\frac{\pi}{10}n + \frac{\pi}{6400}n^2 + 8 \sin\left(\frac{\pi}{200}n\right)\right) + \cos\left(\frac{2\pi}{5}n + \frac{0.18\pi}{1024}n^2 + 8 \sin\left(\frac{\pi}{50}n\right)\right) + \eta(n)$$



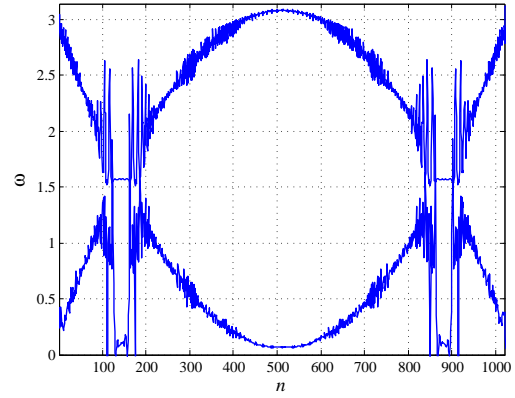
(a)



(b)



(c)

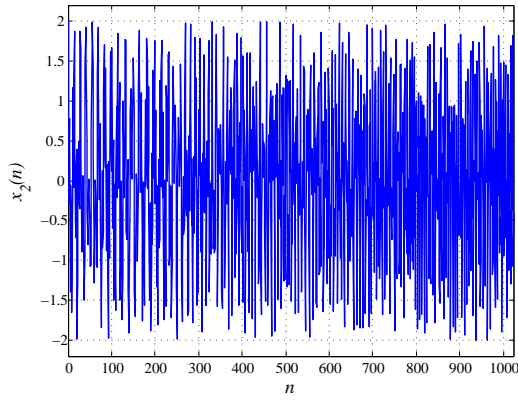


(d)

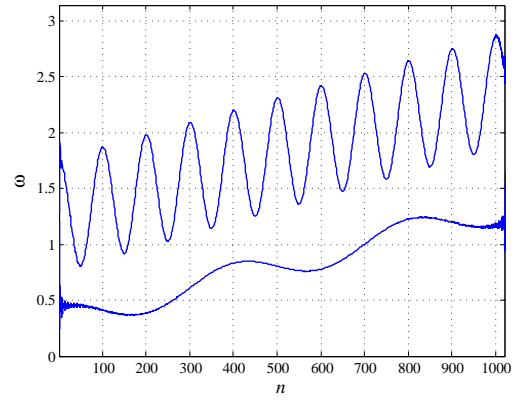
Figure 21: Experiment 1: (a) Signal $x_1(n)$; (b) Actual IFs of $x_1(n)$ components; (c) Estimated IF of $x_1(n)$ using DLCT; (d) Estimated IF of $x_1(n)$ using EMD.

Figure 22(a) depicts the signal $x_2(n)$, while the actual IFs of the two individual components are shown in Fig. 22(b). Figures 22(c) and (d) give the estimated IFs of $x_2(n)$ using the DLCT and the EMD decomposition algorithms, respectively. The performance of the EMD as an IF estimator is very much affected by the presence of the noise.

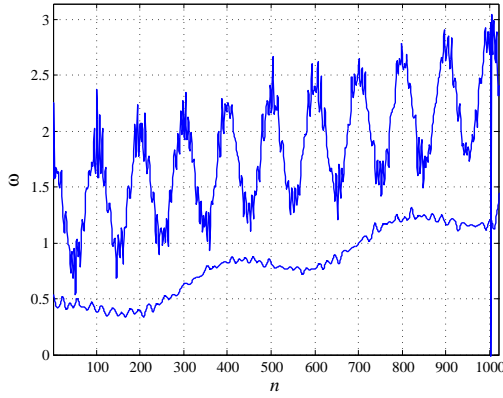
Comparing the estimated IFs based on the DLCT and the EMD of both experiments with the actual IFs, we conclude the DLCT decomposition attains better results than the EMD.



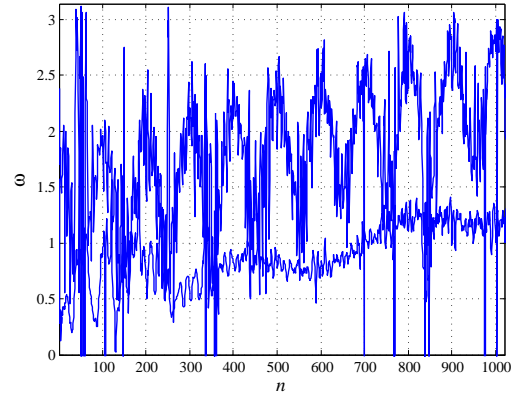
(a)



(b)



(c)



(d)

Figure 22: Experiment 2, $x_2(n)$ with additive noise (SNR=5dB): (a) Noiseless signal $x_2(n)$; (b) Actual IFs of noiseless $x_2(n)$; (c) Estimated IFs of $x_2(n)$ using DLCT; (d) Estimated IFs of $x_2(n)$ using EMD.

4.3.2 Decomposition of speech signals.

The performance of decomposition and representation of speech signals using the EMD and the DLCT is explored. Our experiment is conducted using a speech segment corresponding to “*among them are canvases by a young artist*” sampled at 8 kHz. The speech signal is divided into blocks of 437 msec to capture its local characteristics.

The DLCT decomposes the speech segment into 5 components $s_i(t)$ as shown in Fig. 23(a) along with their spectra. Notice these five components display the characteristics of IMFs. Using these five components a reconstruction of the signal and its error are shown in Fig. 23(c) with a SNR=25.69 dB.

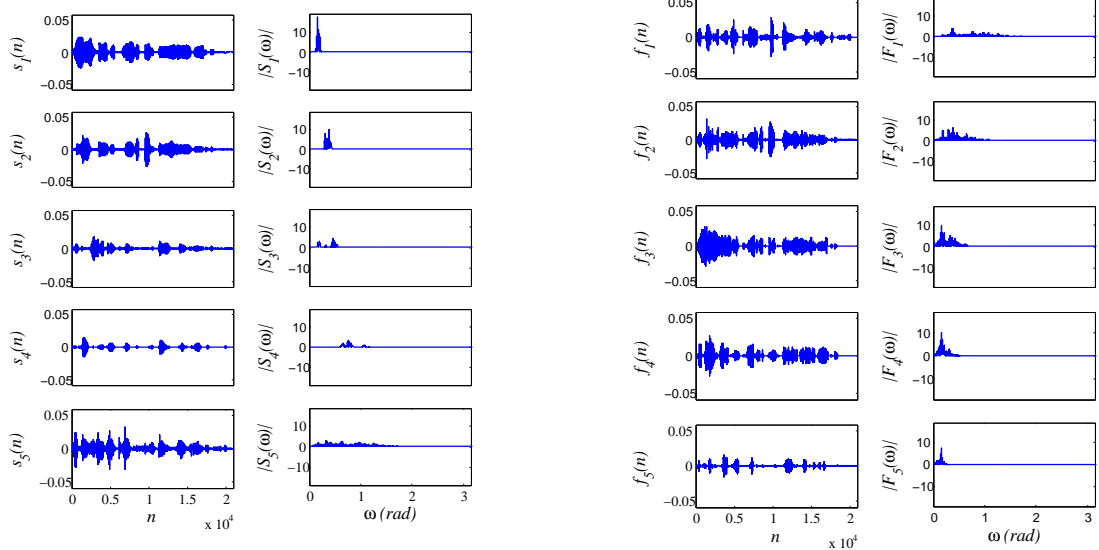
For comparison, we decompose the same speech signal using the EMD. The speech segment is windowed into blocks of the same width as before. The EMD decomposes the speech signal also into 5 IMFs as shown on the left in Fig. 23(b). However, the reconstructed signal gives a SNR=20.8 dB not as good as the reconstructed signal from the DLCT method. Also the frequency representation of each of the five components has overlapping bandwidths (see Fig. 23(b) on the right) while the frequency representation for each of the components obtained with the DLCT (see Fig. 23(a) on the right) appear in slightly different bands.

4.4 TIME–FREQUENCY ANALYSIS USING DLCT

In many applications in biomedicine, speech processing, communications, radar, underwater acoustics, where non–stationary signals are present, it is typically necessary to estimate the instantaneous frequency of the signals [60]. Time–frequency distributions (TFDs) are widely used for IF estimation based on peak detection techniques [61, 62, 63]. The most frequently TFD used for linear chirps is the Wigner–Ville distribution (WVD) due to its ideal representation for such signals. However, in the case of multi–component signals, Wigner–Ville distribution does not perform well because of the presence of extraneous cross–terms.

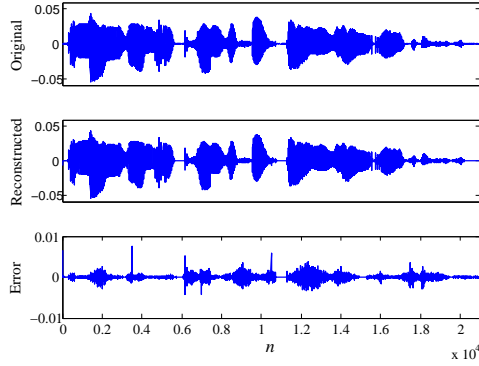
The work of [64] in multi–component signal IF estimation requires to have a TFD that has high resolution and is free of cross–terms. In [65] an iterative method is proposed for IF estimation using the evolutionary spectrum. In general, the instantaneous frequency estimation requires signal separation, for multi–component signals, and high resolution time–frequency distributions.

In this section we develop an algorithm that combines the DLCT with the Wigner–Ville distribution (WVD) to obtain a time–frequency representation with high resolution. Locally the DLCT approximates the signal as a sum of linear chirps, for each of which the WVD

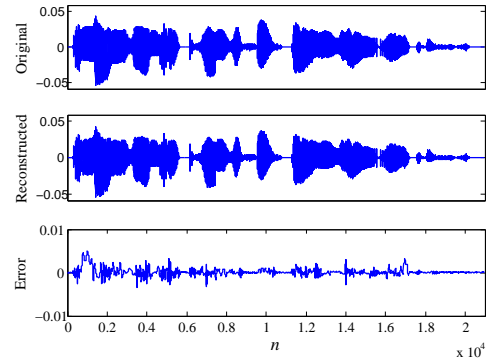


(a)

(b)



(c)



(d)

Figure 23: (a) Decomposition of the speech segment and their corresponding spectra using DLCT; (b) The synthesized IMFs of the speech segment using EMD; (c) Original and reconstructed speech segments, and error signal $e(t)$; (d) Original speech signal, reconstructed signal, and error signal $r(t)$.

provides optimal representations. Superposing these WVDs we obtain a time–frequency representation of the whole signal without interfering cross–terms. The proposed algorithm is shown in Fig. 24.

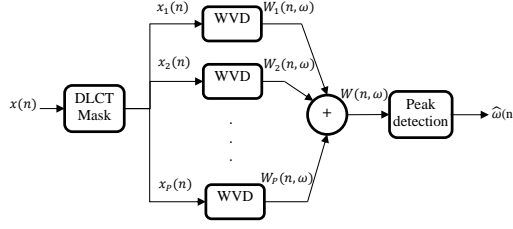


Figure 24: Time–frequency representation algorithm and instantaneous frequency estimator.

The energy of the signal can be found in the joint chirp–rate frequency domain using the DLCT. Using equation (2.8) we obtain the following Parseval relation between the energy in the two domains:

$$\begin{aligned} \sum_{n,m} |x_m(n)|^2 &= \sum_{m,k,s} \frac{X(k,m)X^*(s,m)}{N^2} \times \sum_n \exp\left(j\frac{2\pi}{N}n(s-k)\right) \\ &= \sum_{m,k} \frac{|X(k,m)|^2}{N^2} \end{aligned}$$

and since $x_m(n) = x(n)$ then

$$\begin{aligned} \sum_{n,m} |x_m(n)|^2 &= \sum_n L|x(n)|^2 \quad \text{so that} \\ \sum_n |x(n)|^2 &= \frac{1}{LN^2} \sum_{m,k} |X(k,m)|^2. \end{aligned} \quad (4.4)$$

The energy concentration is thus indicated by the peak values of $|X(k,m)|^2$ as a function of k and m . Considering the region in the joint chirp–rate frequency plane where these peak values occur, we are able to find the values of the chirp–rates and frequencies that can be used to approximate the given signal locally as a sum of linear chirp components

$$x(n) = \sum_{i=1}^P x_i(n). \quad (4.5)$$

The instantaneous frequency of each of these components can be parametrically represented by the chirp–rates and frequencies. Corresponding to the peaks, the determination

of the range of chirp-rates and frequencies where the energy of the signal is the most significant is analogous to masking. A better way to display the instantaneous frequencies of the signal components is to use the Wigner–Ville distribution which for a linear chirp concentrates the energy exactly along the instantaneous frequency in an optimal way. Indeed, for $x(t) = \exp(j(\gamma t^2/2 + \Omega_0 t))$ with instantaneous frequency $IF(t) = \gamma t + \Omega_0$, its Wigner–Ville distribution [2] gives

$$\begin{aligned} W(t, \Omega) &= \frac{1}{2\pi} \int x^* \left(t - \frac{\tau}{2} \right) x \left(t - \frac{\tau}{2} \right) e^{-j\tau\Omega} d\tau \\ &= \delta(\Omega - [\gamma t + \Omega_0]), \end{aligned}$$

i.e., a line in the time–frequency plane that coincides with the $IF(t)$ of the linear chirp. However, for multi–component signals cross–terms appear. Using the DLCT filter or mask however the time–frequency representation of the signal $x(n)$ in (4.5) would be

$$W(n, \omega) = \sum_{i=1}^P W_i(n, \omega)$$

where $W_i(n, \omega)$ is the Wigner–Ville distribution of the linear chirp components $x_i(n)$. Since the Wigner–Ville distribution concentrates the energy along the instantaneous frequency, the IF is estimated by

$$\hat{\omega}(n) = \arg \left[\max_{\omega} \sum_{i=1}^P W_i(n, \omega) \right] \quad (4.6)$$

As indicated above, the instantaneous frequency is approximated locally by linear chirps. Thus the signal in general is windowed before applying the above procedure locally. The estimated IF $\hat{\omega}(n)$ is obtained from the peak detection approach for the high resolution time–frequency distribution which is a result of combining the DLCT with the WVD. The accuracy of the estimation is measured by the mean square error

$$MSE = \langle \{\omega(n) - \hat{\omega}(n)\}^2 \rangle \quad (4.7)$$

where $\langle \cdot \rangle$ is the average.

The DLCT mask is time–varying mask that can be used to filter non–stationary signals in the frequency chirp–rate space. As shown in Fig. 25, by selecting the frequency band

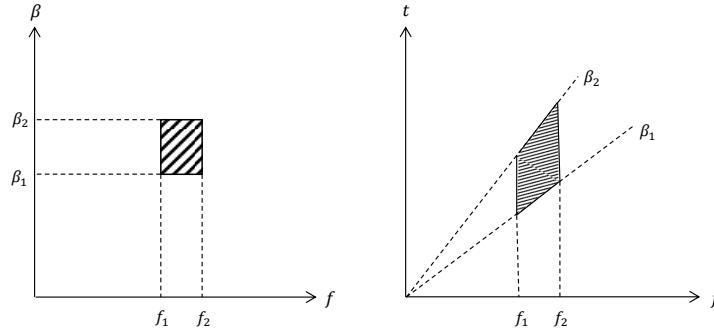


Figure 25: Joint chirp-rate frequency filtering in chirp-rate frequency plane and in time-frequency plane.

$[f_1, f_2]$ and the chirp-rate range $[\beta_1, \beta_2]$ one can select the components of $x(t)$ having a DLCT with joint chirp-rate and frequencies in the chirp-rate and frequency band.

This is equivalent to masking in the time-frequency plane using a time-varying mask with the desired frequency band $[f_1, f_2]$ but the slope determined by the chirp-rate range $[\beta_1, \beta_2]$ (See Fig. 25). Notice that the frequency response of the mask changes with time.

To evaluate the performance of the proposed instantaneous frequency estimation method, we consider multi-component signals with linear, quadratic, and sinusoidal instantaneous frequencies. Also, we add noise to the signals and test our procedure for several signal to noise ratios (SNRs) values.

Table 1: Comparison of mean square error (MSE) for different time-frequency distributions with four different SNRs.

Time-frequency Distribution	SNR (dB)			
	-5	0	5	100
Synthesized WVD	-36.2 dB	-40.01 dB	-41.78 dB	-43.06 dB
STFT	-5.96 dB	-34.42 dB	-38.79 dB	-42.01 dB
WVD	-3.93 dB	-5.47 dB	-6.72 dB	-6.95 dB

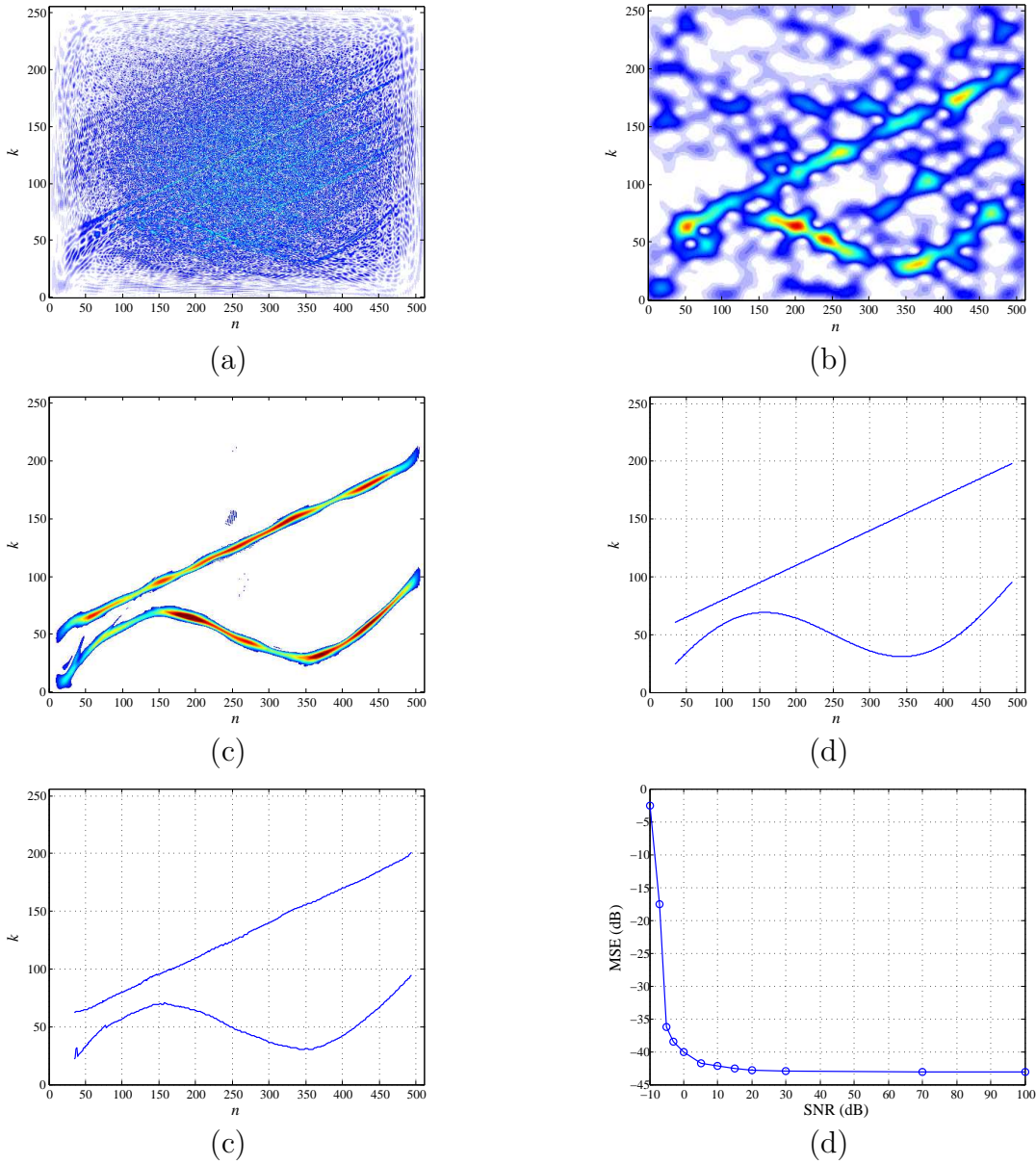


Figure 26: Example 1, $x_1(n)$ with SNR = -5 dB: (a) Wigner-Ville distribution of $x_1(n)$; (b) STFT with Hamming window of length 64; (c) Synthesized Wigner-Ville distribution; (d) Original IF; (e) Estimated IF; (f) Mean square error.

Consider the multi-component signal $x_1(n)$

$$\begin{aligned}
 x_1(n) = & \exp\left(j\frac{\pi}{256}(0.15n^2 + 50n)\right) \\
 & + \exp\left(j\left(\frac{\pi n^2}{2560} - 40\cos\left(\frac{\pi}{500}n\right)\right)\right) + \eta(n)
 \end{aligned}$$

where $\eta(n)$ is a complex white gaussian noise with a total of variance σ^2 is added to the signal. Figures 26(a) and (b) display the WVD and the short time Fourier transform (STFT) of $x_1(n)$ for a SNR= -5 dB while Fig. 26(c) shows the superposition of the WVDs of the chirp components (synthesized WVD). Notice that the WVD does not clearly display the chirps due to cross-components and the smearing of the noise over the time-frequency space and the STFT is not robust against noise. The estimated and the original instantaneous frequencies of the signal $x_1(n)$ at SNR= -5 dB are given in Figs. 26(d) and (e). The mean square error (MSE) for the instantaneous frequency is shown in Fig. 26(f). It shows that, the estimated IF using the proposed method matches well the original IF even at low SNRs. Let the signal $x_2(n)$ be a multi-component signal which has two intersected components in the time-frequency plane. The considered signal is embedded in noise as

$$x_2(n) = \exp\left(j\frac{\pi}{256}(\xi(n-256)^3 + 10n)\right) + \exp\left(j\frac{\pi}{256}(\xi(n-256)^3 - 246n)\right) + \eta(n)$$

where $\xi = 4 \times 10^{-4}$. The WVD, STFT, and synthesized WVD of the signal $x_2(n)$ with SNR= 0 dB are shown in Figs. 27(a), (b), and (c). Figures 27(d) and (e) illustrate the original ($\omega(n)$) as well as its estimate ($\hat{\omega}(n)$). The MSE error as a function of SNR is given in Fig. 27(f).

Tables 1 and 2 summarize the MSE measured in dB for the estimated IFs using synthesized WVD, STFT, and WVD under the effect of noise. It is shown, the synthesized WVD is more robust against noise attack and gives better IF estimation than the other time-frequency distributions. On the other hand, the WVD presents poor IF estimate even for high SNRs because it suffers from the cross-terms interference. The STFT shows good results for high SNRs but it gives poor IF estimate for low SNRs.

Finally, we apply our algorithm to the bat signal shown in Fig. 13(a). The STFT of this signal is given in Fig. 28(a), where the signal components are smoothed as expected. The Wigner-Ville distribution is shown in Fig. 28(b). The WVD has interference cross-terms which make it difficult to recognize the signal components.

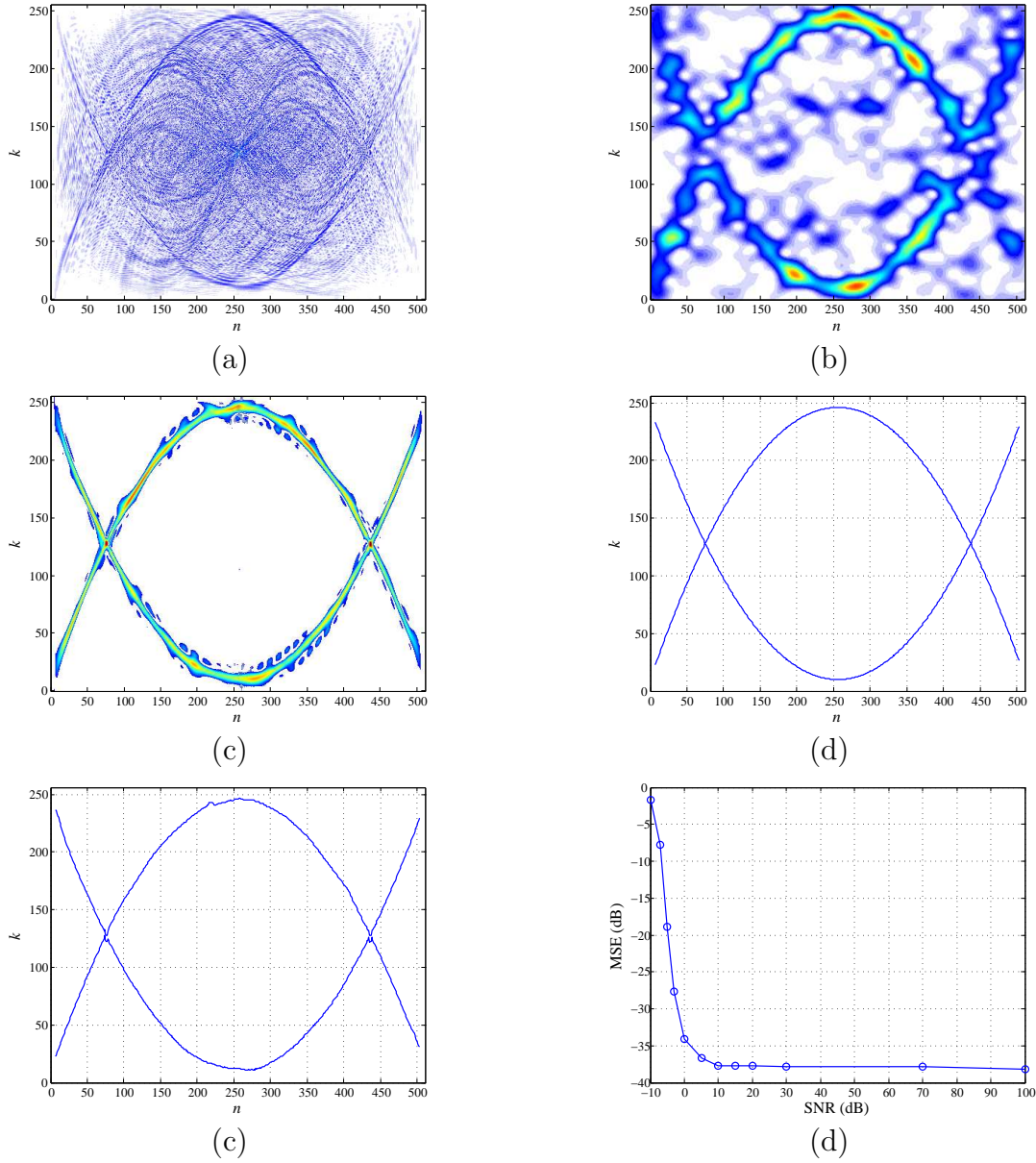


Figure 27: Example 2, $x_2(n)$ with SNR = 0 dB: (a) Wigner–Ville distribution of $x_2(n)$; (b) STFT with Hamming window of length 64; (c) Synthesized Wigner–Ville distribution; (d) Original IF; (e) Estimated IF; (f) Mean square error.

Figure 28(c) depicts the time–frequency distribution which is computed by the proposed algorithm. The estimated IF of the bat signal is illustrated in Fig. 28(d) from which we can observe that the bat signal has five components.

Table 2: Comparison of mean square error (MSE) for different time–frequency distributions with four different SNRs.

Time-frequency Distribution	SNR (dB)			
	-5	0	5	100
Synthesized WVD	-18.85 dB	-31.56 dB	-34.96 dB	-38.14 dB
STFT	-4.12 dB	-13.26 dB	-20.22 dB	-23.28 dB
WVD	-0.74 dB	-0.91 dB	-1.36 dB	-1.88 dB

The results of the proposed algorithm for the bat signal are interesting. A new fifth component is obtained. In the past publication some of them are shown two components [40], three components [20, 21, 22], or four components [28, 66] for the same bat signal. In addition, as we can see from Fig. 28(d), the bat signal is suffering from some aliasing as shown in the third and forth components. Therefore, the sampling frequency of the bat signal, which originally is sampled at 0.4 MHz [67], should be sampled at higher sampling frequency rate to avoid the aliasing that occurs at the third and forth components.

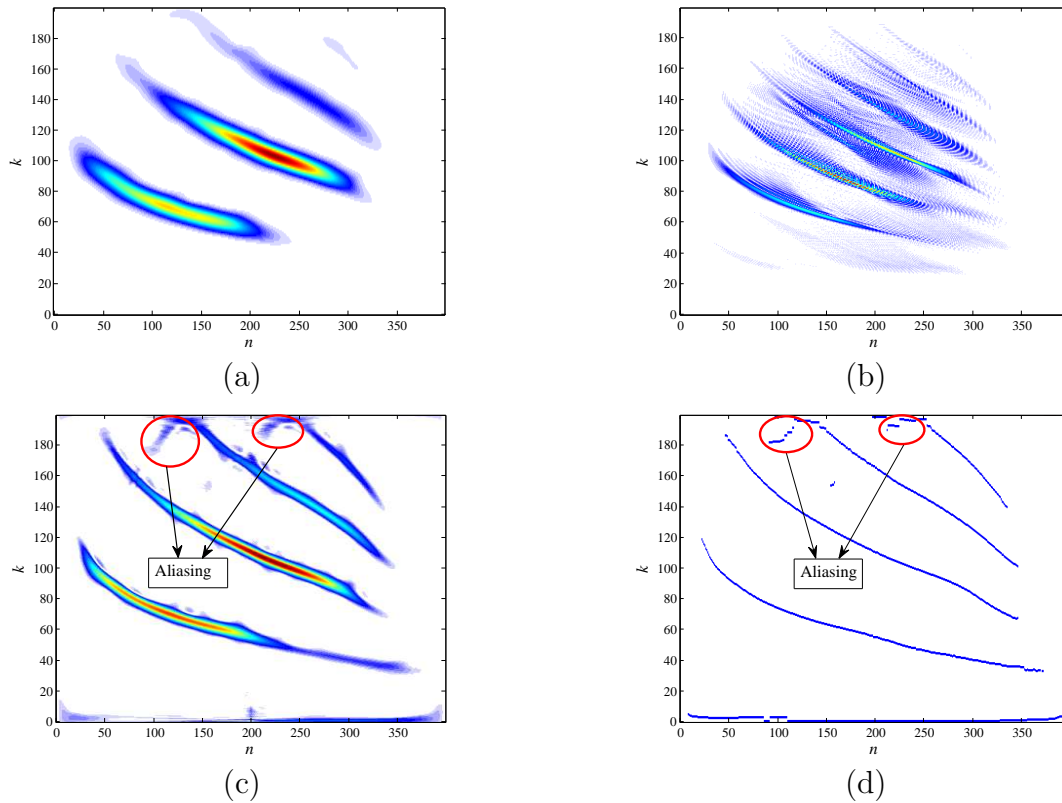


Figure 28: Example 3: (a) The bat signal in the time domain; (b) Wigner-Ville distribution of the bat signal; (c) STFT with Hamming window of length 64; (d) Synthesized Wigner-Ville distribution; (e) Estimated IF.

5.0 HIGH DATA RATE AND HIGH CAPACITY COMMUNICATION SYSTEMS

The rapid growth, marketing, and applications of wireless communications has increased research interest in looking for an alternative digital communications that can adapt to the increasing demand of the limited bandwidth. The desired properties for an ideal digital communication system would be low transmission power, high bit transmission rate, and less bandwidth. As one can feel, such system is not possible and often, as in most engineering applications, we trade-off one quantity for the other. This leads to choosing different modulation schemes that have different characteristics like “power-efficient schemes”, “bandwidth-efficient schemes” [68].

In the last few years, wireless communications have shown enormous growth in the market and technology. Researchers have focused their attention on the next generation of wireless communication systems to send large volumes of data and to provide users with a wide range of services such as voice, video, text messages, and high speed internet. The challenge for achieving these goals is to have a communication system that can transmit data with high data speed transmission and has high capacity (i.e. can handle as many users as possible) without increasing the bandwidth which is often limited by the cost of the radio spectrum required or by the international telecommunication union (ITU) spectrum allocation [69].

5.1 DIGITAL COMMUNICATIONS BASED ON LINEAR CHIRP CARRIERS

Chirp signals have been extensively used in radar and sonar systems to determine distance, velocity, and object detection [70]. The use of chirp signals for digital communication was first proposed by Winkler [71]. The advantage of using chirp signal carriers compared to FSK and PSK for various channels was discussed in [72, 73, 74, 75]. Among several applications for chirp modulations is high frequency data transmission [76].

The work on digital modulation using chirp waveforms has not received much consideration. In this section, we propose five different digital modulation schemes based on linear chirp carriers and their performance are investigated for coherent receivers with matched filter detection. We optimize the parameters of the chirp carriers such that they maximize the transmitted difference signal energy. Moreover, we use the continuous linear chirp transform (CLCT) in the context of time-varying filter. The CLCT can be used to filter the pass band signals in the frequency chirp-rate plane. Therefore, we can eliminate the impact of the chirp rate on bandwidth. Consequently, preservation of bandwidth occupancy is achieved.

5.1.1 Bit error rate calculation

The probability of error for the output signal is the performance measure of a digital system. To derive a general form for the bit error rate (BER) of a detected binary signal, let the transmitted signal over a bit interval $0 < t \leq T_b$ be

$$s(t) = \begin{cases} s_1(t), & 0 < t \leq T_b, & \text{for binary 1} \\ s_2(t), & 0 < t \leq T_b, & \text{for binary 0} \end{cases}$$

The general expression of $s_1(t)$ and $s_2(t)$ for linear chirp carriers can be written as

$$s_1(t) = A \cos(\Omega_1 t + \gamma_1 t^2) \tag{5.1}$$

and

$$s_2(t) = A \cos(\Omega_2 t + \gamma_2 t^2) \tag{5.2}$$

The transmitted signal $s(t)$ is usually corrupted by an additive noise $\eta(t)$. Thus, the received signal $r(t)$ is given by

$$r(t) = s(t) + \eta(t)$$

Following the procedure given in [77] for calculating the BER of binary signalling corrupted by additive white Gaussian noise, coherent detection, matched filter reception, and by using the optimum threshold setting, the BER is

$$P_e = Q\left(\sqrt{\frac{E_d}{2N_0}}\right) \quad (5.3)$$

where $Q(x) = \frac{1}{\sqrt{2\pi}} \int_x^\infty e^{-t^2/2} dt$, $N_0/2$ is the power spectral density of the noise, and E_d is the transmitted difference signal energy defined as

$$E_d = \int_0^{T_b} [s_1(t) - s_2(t)]^2 dt \quad (5.4)$$

To minimize P_e , we need to maximize E_d . The transmitted difference signal energy E_d can be maximized by choosing the parameters $\{\Omega_1, \Omega_2, \gamma_1, \gamma_2\}$ of the chirp carriers appropriately. The optimized parameters can be found by solving an optimization problem with inequality constraints as

$$\begin{aligned} & \max_{\Omega_1, \Omega_2, \gamma_1, \gamma_2} E_d \\ & \text{subject to } \Omega_1, \Omega_2 \geq 2\pi/T_b \end{aligned} \quad (5.5)$$

If we define the bit energy by $E_b = A^2 T_b$, then the optimal solution for E_d would be

$$E_d = \lambda E_b \quad (5.6)$$

where λ is a real positive number and it depends on the type of modulation scheme used and the bit interval (bit rate). We can think of (5.5) as an upper bound for E_d (lower bound for P_e). The lower bound for E_d can be achieved by minimizing E_d in (5.5) after imposing the following constraints: $|\Omega_1 - \Omega_2| \geq \epsilon_\Omega$ or $|\gamma_1 - \gamma_2| \geq \epsilon_\gamma$ to avoid the trivial solution which

is $s_1(t) = s_2(t)$. If we represent the lower bound by μ_1 and the upper bound by μ_2 where μ_1 and μ_2 are real positive numbers, then we can rewrite (5.6) as

$$E_d = \lambda E_b, \quad \mu_1 \leq \lambda \leq \mu_2 \quad (5.7)$$

Substituting (5.7) into (5.3), we acquire the general bit error rate formula for matched filter coherent detection digital modulation

$$P_e = Q \left(\sqrt{\frac{\lambda E_b}{2 N_0}} \right), \quad \mu_1 \leq \lambda \leq \mu_2 \quad (5.8)$$

P_e forms a lower bound when $\lambda = \mu_2$.

It is difficult to solve (5.5) for a closed form solution since the evaluation of E_d requires to deal with integrals of the form

$$\begin{aligned} \int_0^{T_b} \cos(a t + b t^2) dt &= \sqrt{\frac{\pi}{2b}} \times [\cos(\theta_1^2) \left\{ C_F(\theta_2) - C_F \left(\sqrt{\frac{2}{\pi}} \theta_1 \right) \right\} \\ &\quad + \sin(\theta_1^2) \left\{ S_F(\theta_2) - S_F \left(\sqrt{\frac{2}{\pi}} \theta_1 \right) \right\}] \end{aligned}$$

where $C_F(u)$ and $S_F(u)$ are Fresnel functions defined as

$$C_F(u) = \int_0^u \cos \left(\frac{\pi}{2} z^2 \right) dz ,$$

$$S_F(u) = \int_0^u \sin \left(\frac{\pi}{2} z^2 \right) dz$$

$$\theta_1 = \frac{a}{2\sqrt{b}}, \quad \text{and} \quad \theta_2 = \sqrt{\left(\frac{2b}{\pi} \right)} \left(T_b + \frac{a}{2b} \right)$$

Therefore, we will solve (5.5) numerically for different digital modulation schemes.

5.1.2 Digital modulation schemes

- **Chirp on-off keying (C-OOK)**

The C-OOK is an amplitude modulation operating on a unipolar digital data $m(t)$ and it is represented by

$$s_1(t) = A \cos(\Omega t + \gamma t^2), \quad 0 < t \leq T_b \quad (\text{binary 1})$$

and,

$$s_2(t) = 0, \quad 0 < t \leq T_b \quad (\text{binary 0})$$

For coherent detection, the demodulation process is illustrated in Fig. 29. The performance of this match filter receiver for C-OOK scheme is obtained using (5.8) where $0.267 \leq \lambda \leq 0.695$ for $T_b/T_s = 32$ and T_s is the sampling period. Figure 30(a) shows the

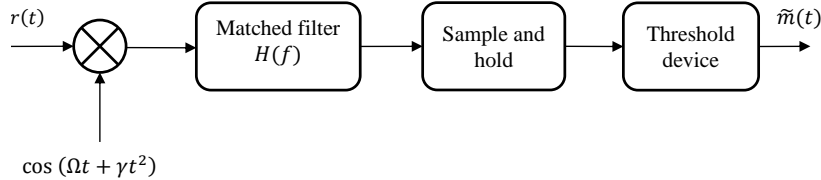


Figure 29: Coherent detection of C-OOK or C-PSK schemes.

BER of the conventional OOK ($\lambda = 0.5$) [77] and the BER of the C-OOK with $\lambda = 0.695$ where the frequency and the chirp rate of the carrier are set to $12.57/T_b$ and $10.66/T_b^2$, respectively. The C-OOK can perform better than the OOK if we choose the parameters of the chirp carrier so that $\lambda > 0.5$. As we mentioned before, the constant λ depends on the modulation scheme and the bit rate ($R_b = 1/T_b$). The effect of the bit rate on λ for C-OOK scheme is given in Fig. 30(b) for the lower and the upper bounds. The bandwidth of the transmitted C-OOK signal is $12.57/T_b$, twice the bit rate.

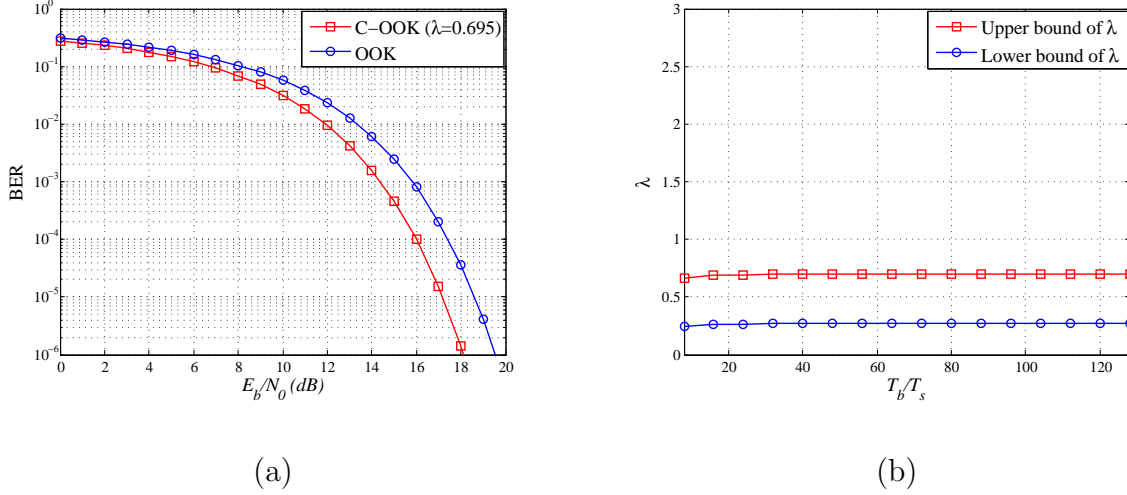


Figure 30: (a) BER of C-OOK and OOK; (b) Effect of bit rate on λ_{max} and λ_{min} .

• Chirp phase shift keying (C-PSK)

Refereing to (5.1) and (5.2), we can represent the transmitted data as

$$s_1(t) = A \cos(\Omega t + \gamma t^2), \quad 0 < t \leq T_b \quad (\text{binary 1})$$

and,

$$s_2(t) = -A \cos(\Omega t + \gamma t^2), \quad 0 < t \leq T_b \quad (\text{binary 0})$$

The receiver of the C-PSK is shown in Fig. 29. We explore the performance of the C-PSK for coherent detection. For the bit interval $T_b/T_s = 32$, $1.07 \leq \lambda \leq 2.782$. The upper bound $\lambda = 2.782$ is determined by choosing the following carrier parameters $\Omega = 12.57/T_b$ and $\gamma = 10.66/T_b^2$. The corresponding BER for the upper bound of λ is presented in Fig. 31(a) with a comparison to the conventional PSK digital modulation scheme [77]. The λ_{max} and λ_{min} as a function of the bit interval T_b/T_s is illustrated in Fig. 31(b). The bandwidth between first nulls around the carrier is $2\Omega_b$.

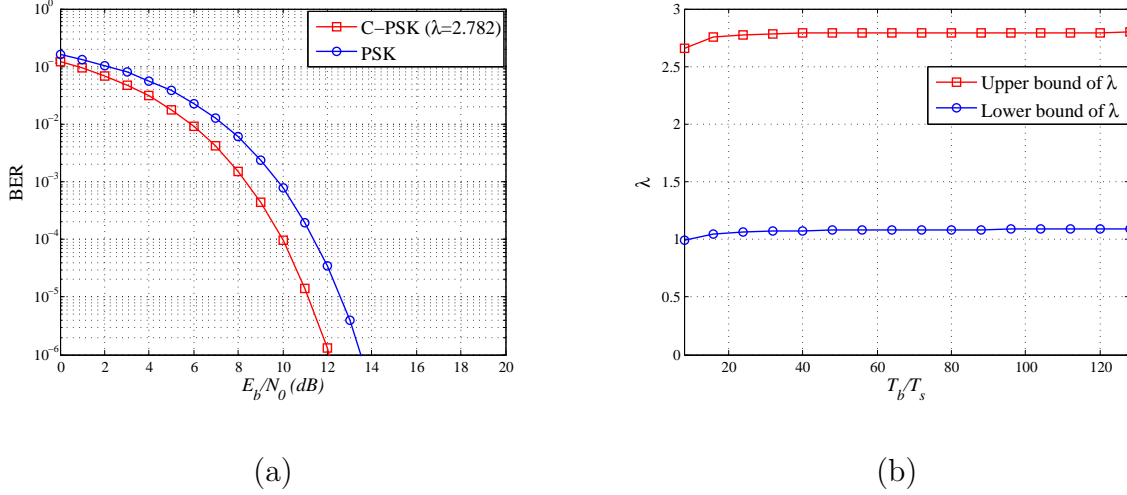


Figure 31: (a) BER of C-PSK and PSK; (b) Effect of bit rate on λ_{max} and λ_{min} .

• Chirp frequency shift keying (C-FSK)

In binary chirp frequency shift keying (C-FSK), the binary data $m(t)$ can be transmitted using the following carriers

$$s_1(t) = A \cos(\Omega_1 t + \gamma t^2), \quad 0 < t \leq T_b \quad (\text{binary 1})$$

and,

$$s_2(t) = -A \cos(\Omega_2 t + \gamma t^2), \quad 0 < t \leq T_b \quad (\text{binary 0})$$

We can demodulate C-FSK signals using a receiver as shown in Fig. 32. The carrier frequency $\Omega = (\Omega_1 + \Omega_2)/2$ and $\Delta\Omega = \Omega_2 - \Omega_1$.

The BER versus E_b/N_0 for C-FSK and FSK [77] with $T_b/T_s = 32$ is shown in Fig. 33(a). We find the frequencies $\Omega_1 = 12.57/T_b$, $\Omega_2 = 16.99/T_b$, and the chirp rate $\gamma = -10.86/T_b^2$ maximizes the difference signal energy E_d and gives $\lambda = 1.999$. In this scheme, $0.299 \leq \lambda \leq 1.999$ where the lower bound is evaluated when $\epsilon_\Omega = 6.03/T_b$. The impact of bit

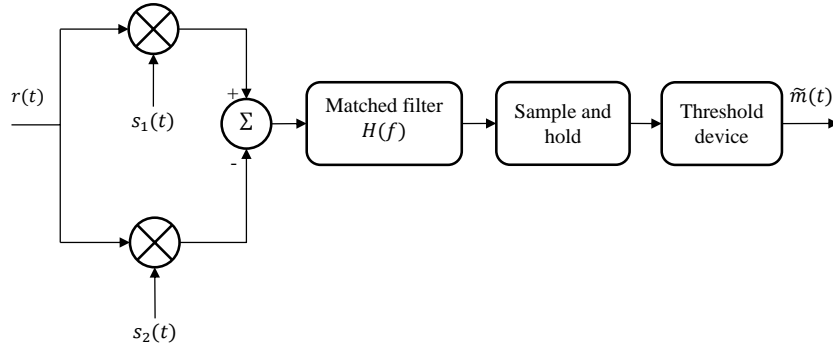


Figure 32: Coherent detection of C-FSK, CRSK, and CRFSK digital modulation schemes.

rate on λ is depicted in Fig. 33(b). We can determine the channel bandwidth of C-FSK as

$$B_T = (\Delta\Omega + 4\pi/T_b) \quad (5.9)$$

Since $\Delta\Omega = 4.42/T_b$, the bandwidth of the C-FSK channel would be $B_T = 16.99/T_b$.

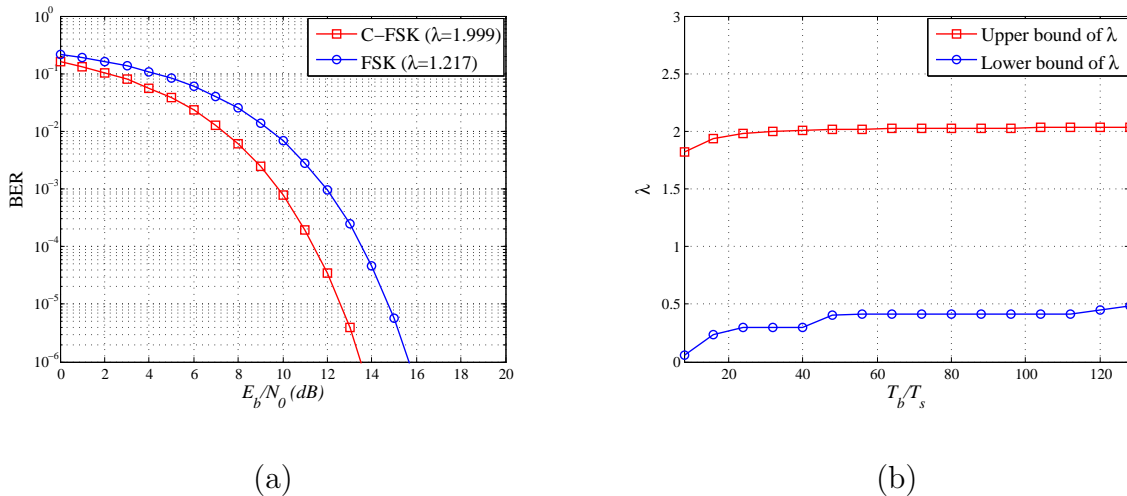


Figure 33: (a) BER of C-FSK and FSK; (b) Effect of bit rate on λ_{max} and λ_{min} .

- **Chirp rate shift keying (CRSK)**

Chirp rate shift keying (CRSK) represents digital data ones and zeros by carrier pulses with two distinct chirp rates, γ_1 and γ_2 as

$$s_1(t) = A \cos(\Omega t + \gamma_1 t^2), \quad 0 < t \leq T_b \quad (\text{binary 1})$$

and,

$$s_2(t) = -A \cos(\Omega t + \gamma_2 t^2), \quad 0 < t \leq T_b \quad (\text{binary 0})$$

Figure 32 shows the proposed receiver structure labeled with the relevant signals for the interval under consideration. We can achieve the upper bound of λ if we use $\gamma_1 = -11.86/T_b^2$, $\gamma_2 = -6.74/T_b^2$, and $\Omega = 13.47/T_b$. The lower bound of λ depends on the constraint ϵ_γ . For $\epsilon_\gamma = 12.06/T_b^2$, the parameter λ can take the values in the range $0.18 \leq \lambda \leq 1.49$ when $T_b/T_s = 32$. The BER of the CRSK is given in Fig. 34(a). Figure 34(b) explains how the bit rate can affect the upper and the lower values of λ . The bandwidth of CRSK channel is $12.57/T_b$.

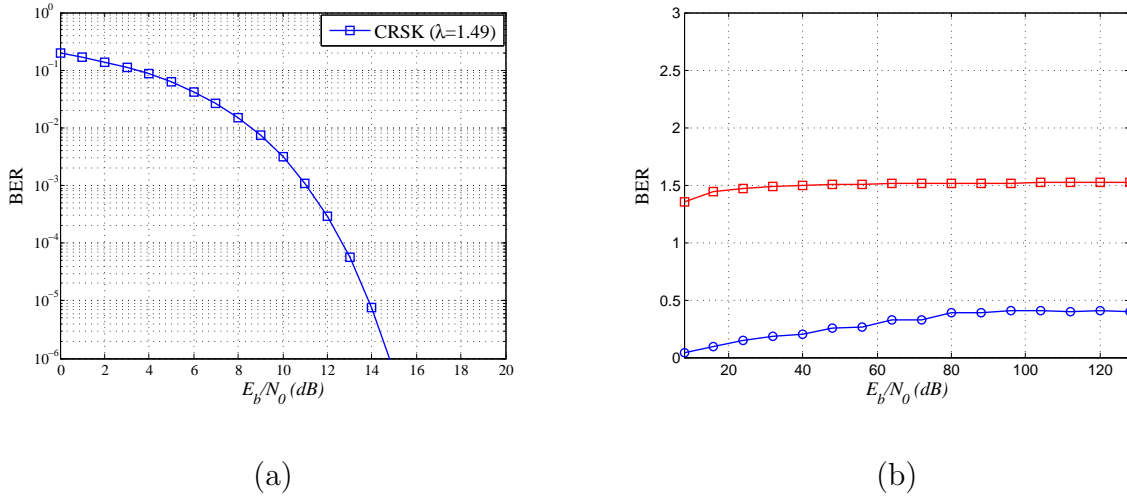


Figure 34: (a) BER of CRSK for $T_b/T_s = 32$; (b) Effect of bit rate on λ_{max} and λ_{min} .

- **Chirp rate frequency shift keying (CRFSK)**

Binary chirp rate frequency shift keying (CRFSK) impresses baseband information onto a carrier by changing the carrier's frequency and chirp rate in sympathy with the baseband digital data as

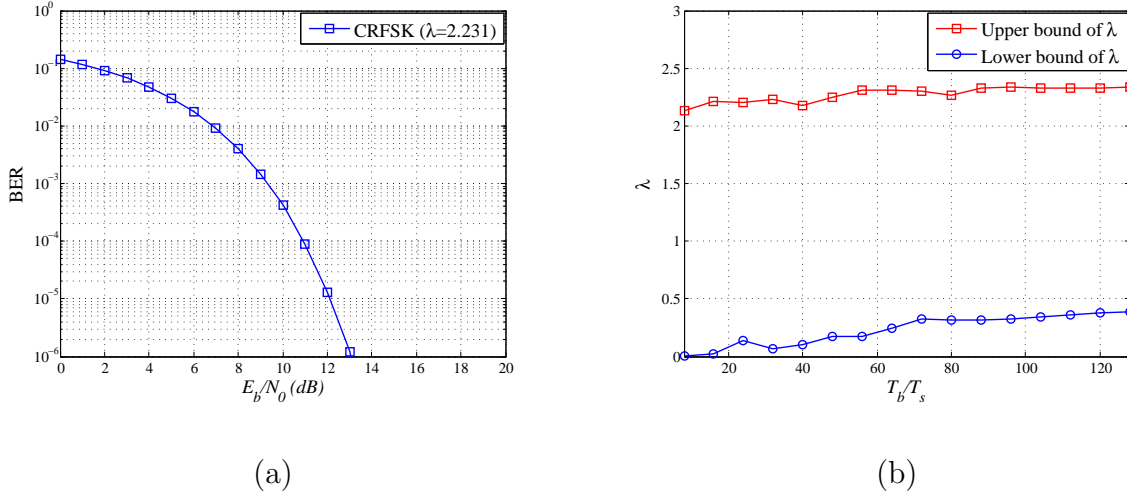


Figure 35: (a) BER of CRFSK for $T_b/T_s = 32$; (b) Effect of bit rate on λ_{max} and λ_{min} .

$$s_1(t) = A \cos(\Omega_1 t + \gamma_1 t^2), \quad 0 < t \leq T_b \quad (\text{binary 1})$$

and,

$$s_2(t) = -A \cos(\Omega_2 t + \gamma_2 t^2), \quad 0 < t \leq T_b \quad (\text{binary 0})$$

The modulated signal will be switched between these two chirps depending on the message and separated in the frequency and chirp rate plane by $\Delta\Omega$ and $\Delta\gamma$ where $\Delta\Omega = \Omega_2 - \Omega_1$ and $\Delta\gamma = \gamma_2 - \gamma_1$.

The transmitted data can be detected by the receiver shown in Fig. 32. The performance of CRFSK with $T_b/T_s = 32$ for $\lambda = 2.231$ is shown in Fig. 35(a). We can attain the upper bound of λ by setting the parameters of the carriers to $\Omega_1 = 14.58/T_b$, $\gamma_1 = -8.04/T_b^2$, $\Omega_2 = 26.64/T_b$, and $\gamma_2 = -18.1/T_b^2$. The lower bound is a function of ϵ_Ω and ϵ_γ where they

are set to $6.03/T_b$ and $12.06/T_b^2$, respectively, to acquire the lower bound $\lambda = 0.063$. Thus, $0.063 \leq \lambda \leq 2.231$. The upper and the lower bounds of λ versus the bit period T_b/T_s is illustrated in Fig. 35(b). We can measure the bandwidth of CRFSK channel by (5.9). If the frequency deviation $\Delta\Omega = 12.06/T_b$, then the bandwidth of CRFSK channel is given by

$$B_T = \Delta\Omega + 4\pi/T_b = 24.63/T_b$$

Plots of the BERs for all proposed digital modulation schemes with the upper bound of λ and bit period $T_b/T_s = 32$ are shown in Fig. 36. To compare performance of various proposed systems and to serve as a convenient reference, the channel bandwidth required and the E_b/N_0 that we need to obtain an average bit error rate of 10^{-4} for each system are summarized in Table 3.

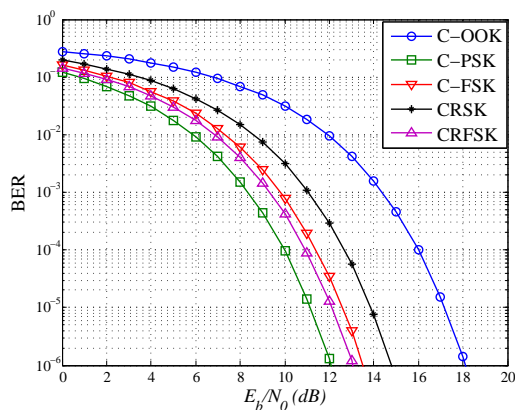


Figure 36: Comparison of proposed binary digital modulation schemes performance.

Table 3: Comparison of different digital modulation schemes in terms of power and channel bandwidth with $P_e = 10^{-4}$.

Modulation	¹ Nominal bandwidth (Hz/sec)	E_b/N_0 (dB)
OOK	$2R_b$	17.43
PSK	$2R_b$	11.41
FSK	$2.715R_b$	13.57
C-OOK	$2R_b$	16
C-PSK	$2R_b$	9.98
C-FSK	$2.704R_b$	11.41
CRSK	$2R_b$	12.69
CRFSK	$3.92R_b$	10.93

5.2 COUPLED OFDM COMMUNICATION SYSTEM

A better approach for securing a transmission system with high capacity and high speed transmission is how we can exploit the allocated spectrum more efficiently. To achieve this, a resource management scheme is required. Time division multiplexing (TDM), frequency division multiplexing (FDM), code division multiplexing (CDM), orthogonal frequency division multiplexing (OFDM), and space division multiplexing are well-known techniques for resource management based on the principle of time sharing, frequency sharing, code sharing, and space sharing [78, 79, 80]. Among these existing resource management techniques, orthogonal frequency division multiplexing (OFDM) [81, 82, 84, 83] has shown a number of advantages and has attracted substantial interest. The main merit of OFDM is that the radio channel is divided into many narrow band, low rate, frequency subchannels or subcarriers, so that multiple symbols can be transmitted in parallel, while maintaining a high spectral efficiency. Each subcarrier may also deliver information for a different user, resulting in a simple multiple access scheme known as orthogonal frequency division multiple access

¹Nominal bandwidth is the null to null bandwidth and it is equal to two times the minimum bandwidth.

(OFDMA) [85, 86]. The OFDM have already been used in the market for applications such as digital video broadcasting, wireless LAN networks, forth generation cellular network, and WiMAX [87].

The use of linear chirps for resource management technique is reported in [88, 89, 90]. It has been shown that, this modulation technique has an inherent capability to mitigate the effects of channel Doppler shifts and multi-path fading due to a moving receiver [10].

This section introduces the concept of coupled OFDM (C-OFDM) system and investigates its suitability for broadband applications in additive white Gaussian channel. Three different scenarios for operating the C-OFDM based on the application and the needs of service provider are proposed. In the first scenario, we can use all the coupled OFDM system channels to transmit the input serial data with the highest transmission speed of the C-OFDM. If a conventional single carrier modulation technique can send data with a data rate R_b , then the same data can be transmitted with a data rate of up to NMR_b using the C-OFDM transmission system. In the second scenario, the maximum capacity of the system can be achieved if we dedicate one channel for each user. Thus, the system can handle $N \times M$ users simultaneously with a transmission rate of R_b . In the third scenario, a trade-off approach can be used to trade capacity with transmission rate. We can assign one OFDM system to each user. As a result, the system can be utilized by M users with a transmission rate of NR_b for each user. The performance of the developed system is explored in the presence of additive white Gaussian noise. Simulation results show the effectiveness of the proposed system for handling a large amount of data with an acceptable bet error rate.

5.2.1 Coupled OFDM system (C-OFDM)

A block diagram of the general coupled OFDM communication system appears in Fig. 37. We consider the transmission of digital data pulses over additive Gaussian noise channel.

- **System model**

Let the transmitted data pulses $X_k(t)$ for $k = 0, 1, \dots, N - 1$ represented as

$$X_k(t) = \begin{cases} d_k, & 0 \leq t \leq T_b \\ 0, & \text{otherwise} \end{cases}$$

where d_k are the transmitted symbols. In case of BPSK modulation, $d_k = +1$ or -1 . Also, define the coupled functions $g_\ell(t)$ as

$$g_\ell(t) = \begin{cases} \exp(j\gamma_\ell t^2), & 0 \leq t \leq T_b \\ 0, & \text{otherwise} \end{cases}$$

where $\ell = 0, 1, \dots, M-1$. Performing the inverse discrete Fourier transform (DFT) on $X_{k\ell}(t)$ and multiplying each parallel OFDM path by the corresponding coupled linear chirp $g_\ell(t)$, the transmitted signal $y_n(t)$ can be expressed as

$$y_n(t) = \sum_{\ell=0}^{M-1} \sum_{k=0}^{N-1} X_{k\ell}(t) g_\ell(t) \exp\left(j\frac{2\pi}{N}kn\right) + \eta_n(t) \quad (5.10)$$

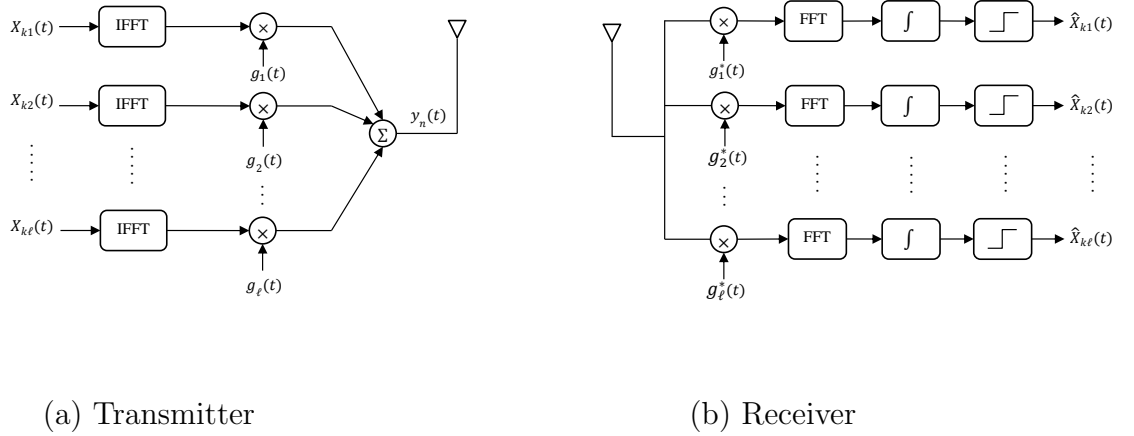


Figure 37: The proposed coupled OFDM communication system.

The received signal after the matched filter can be expressed as follows

$$\hat{Z}_{kr}(t) = T_b X_{kr}(t) + T_b \sum_{\ell=0, \ell \neq r}^{M-1} X_{k\ell}(t) \rho_{\ell r} + T_b W_{kr} \quad (5.11)$$

where,

$$\rho_{\ell r} = \frac{1}{T_b} \int_0^{T_b} g_\ell(t) g_r^*(t) dt \quad \text{and} \quad W_{kr} = \frac{1}{T_b} \int_0^{T_b} \eta_k(t) g_r^*(t) dt$$

The symbol “*” stands for complex conjugate. It is clear from (5.11), in addition to the channel noise effect W_{kr} , the system suffers from a multiple access interference $\rho_{\ell r}$ which can further degrade the system performance. We can reduce the effect of the noise by increasing the signal to noise (SNR) ratio, but the effect of the multiple access interference can only be mitigated by reducing the cross-correlation coefficient $\rho_{\ell r}$.

- **Capacity analysis of C-OFDM**

Consider the C-OFDM system with N used carriers with carrier spacing Δf and M parallel paths. The decision variable \hat{Z}_{kr} can be rewritten as

$$\begin{aligned}\hat{Z}_{kr} &= T_b X_{kr} + U_{kr} + T_b W_{kr} \\ &= T_b X_{kr} + \eta_{kr}\end{aligned}\tag{5.12}$$

where

$$U_{kr} = T_b \sum_{\ell=0, \ell \neq r}^{M-1} X_{k\ell} \rho_{\ell r}$$

If the transmitted symbols X_{kr} are assumed to be uncorrelated circularly symmetric complex Gaussian random variables with zero mean and variance E/M where E is the total power available for transmission and noise W_{kr} is circularly symmetric complex Gaussian with zero mean and variance σ_w^2 , then η_{kr} and \hat{Z}_{kr} are also circularly symmetric complex Gaussian with zero mean and variances $\sigma_{\eta_{kr}}^2$ and $\sigma_{\hat{Z}_{kr}}^2$ given as

$$\sigma_{\eta_{kr}}^2 = T_b^2 \frac{E}{M} \sum_{\ell=0, \ell \neq r}^{M-1} |\rho_{\ell r}|^2 + T_b^2 \sigma_w^2$$

and

$$\sigma_{\hat{Z}_{kr}}^2 = T_b^2 \frac{E}{M} + T_b^2 E_b \sum_{\ell=0, \ell \neq r}^{M-1} |\rho_{\ell r}|^2 + T_b^2 \sigma_w^2$$

The capacity C_{kr} can be defined as

$$C_{kr} = \max_{p(X_{kr})} I(X_{kr}; R_{kr})$$

where $p(X_{kr})$ is the probability density function of the input symbols and $I(X_{kr}; R_{kr})$ is the mutual information defined in [91] as

$$I(X_{kr}; R_{kr}) = \mathcal{H}(R_{kr}) - \mathcal{H}(\eta_{kr})$$

where $\mathcal{H}(\cdot)$ is the differential entropy. Since the interference-plus-noise in (5.12) η_{kr} and \hat{Z}_{kr} are random variables with circularly symmetric complex Gaussian distributions, then the mutual information is given by

$$\begin{aligned} I(X; R) &\leq \sum_k \sum_r I(X_{kr}; R_{kr}) \\ &\leq \sum_k \sum_r \log_2(2\pi e \sigma_{\hat{z}_{kr}}^2) \\ &\quad - \log_2(2\pi e (\sigma_{\eta_{kr}}^2)) \end{aligned} \quad (5.13)$$

Hence, the capacity of C-OFDM system is

$$C = N \sum_{r=0}^{M-1} \log_2 \left(1 + \frac{E/M}{2 \frac{E}{M} \sum_{\substack{\ell=0 \\ \ell \neq r}}^{M-1} |\rho_{\ell r}|^2 + \sigma_w^2} \right) \quad (5.14)$$

If $M = 1$, then (5.14) reduces to the capacity of the conventional OFDM system [80].

• Linear chirp design

To maximize performance and capacity of the C-OFDM system, we need to minimize the cross-correlation coefficient $\rho_{\ell r}$, that is

$$\min_{\gamma_\ell, \gamma_r, r \neq \ell} |\rho_{\ell r}| \quad (5.15)$$

We can find the function of $\rho_{\ell r}$ by evaluating the following integral

$$\rho_{\ell r} = \frac{1}{T_b} \int_0^{T_b} \exp(j(\gamma_\ell - \gamma_r)t^2) dt$$

Hence,

$$|\rho_{\ell r}| = \frac{1}{\xi} \sqrt{C_F(\xi)^2 + S_F(\xi)^2}$$

where $C_F(\xi)$ and $S_F(\xi)$ are Fresnel functions defined as

$$C_F(\xi) = \int_0^\xi \cos\left(\frac{\pi}{2}z^2\right) dz ,$$

$$S_F(\xi) = \int_0^\xi \sin\left(\frac{\pi}{2}z^2\right) dz$$

and,

$$\xi = T_b \sqrt{\frac{2}{\pi}(\gamma_\ell - \gamma_r)}$$

In case of $\gamma_\ell - \gamma_r = \Delta\gamma$, we can plot $|\rho|$ as a function of $\Delta\gamma$ as shown in Fig. 38. It is clear that $\rho \rightarrow 0$ as $\Delta\gamma \rightarrow \infty$. Thus, we can minimize the cross-correlation error by choosing large value for $\Delta\gamma$.

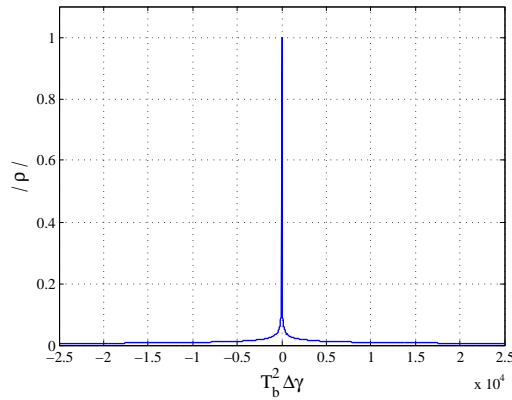


Figure 38: The cross-correlation as a function of $\Delta\gamma$

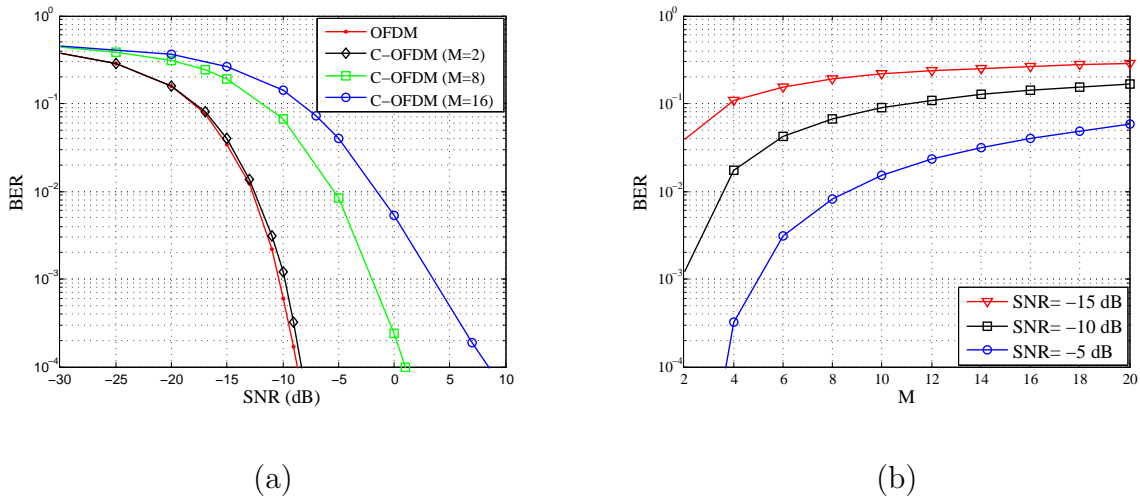


Figure 39: (a) Performance comparison of OFDM and C-OFDM with different values of M ; (b) Impact of increasing parallel paths M on BER for different values of SNRs.

5.2.2 Simulation and numerical analysis

The proposed C-OFDM system is simulated to evaluate and compare its performance with the conventional OFDM system as shown in Fig. 39(a). The performance of the C-OFDM system degrades as M increases. This result coincides with the theoretical analysis since the multiple access interference increases as M increases. Figure 39(b) shows the bit error rate as a function of parallel paths M for SNR = -15 dB, -10 dB, and -5 dB. Again, for certain SNR, the bit error rate increases as M increases.

We also study the capacity of the C-OFDM system. The capacity C (bit/sec/Hz) as a function of SNR for different values of M is given in Fig. 40. We can see that capacity indeed increases for increasing M . We can furthermore observe that for large number of M , system capacity can be increased slightly because of the effect of cross-correlation interference.

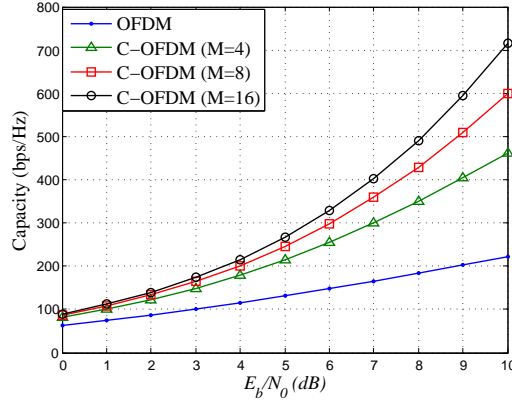


Figure 40: Capacity (in bps/Hz) as a function of E_b/N_0 for various values of M where $E_b/N_0 = E/\sigma_w^2$

5.2.3 Implementation scenarios

This section provides three scenarios that illustrate usage of the C-OFDM system. Service provider can operate the coupled OFDM system in three different ways depending on the type of application and providing good quality of service. In general, C-OFDM system has $N \times M$ channels with a coming in digital data rate R_b where $R_b = 1/T_b$. Clearly, there are many possibilities of assigning these channels with different transmission data rates.

- **Scenario I**

In this scenario, each channel is dedicated to one user. Thus, we can have $N \times M$ users who can use the system at the same time as show in Fig. 41(a). Thus, we increase system capacity by M compared to the conventional OFDM system, but with the same transmission rate R_b .

- **Scenario II**

Figure 41(b) shows transmitting the digital input data with a transmission rate of NMR_b instead of R_b . We operate the C-OFDM system as a one channel. The conventional OFDM can send the same information with a transmission data rate NR_b .

• **Scenario III**

Some applications require high transmission rates and high capacity. Figure 41(c) provides a solution for such applications. In this case, we have M channels and each channel can serve a user with a transmission rate NR_b .

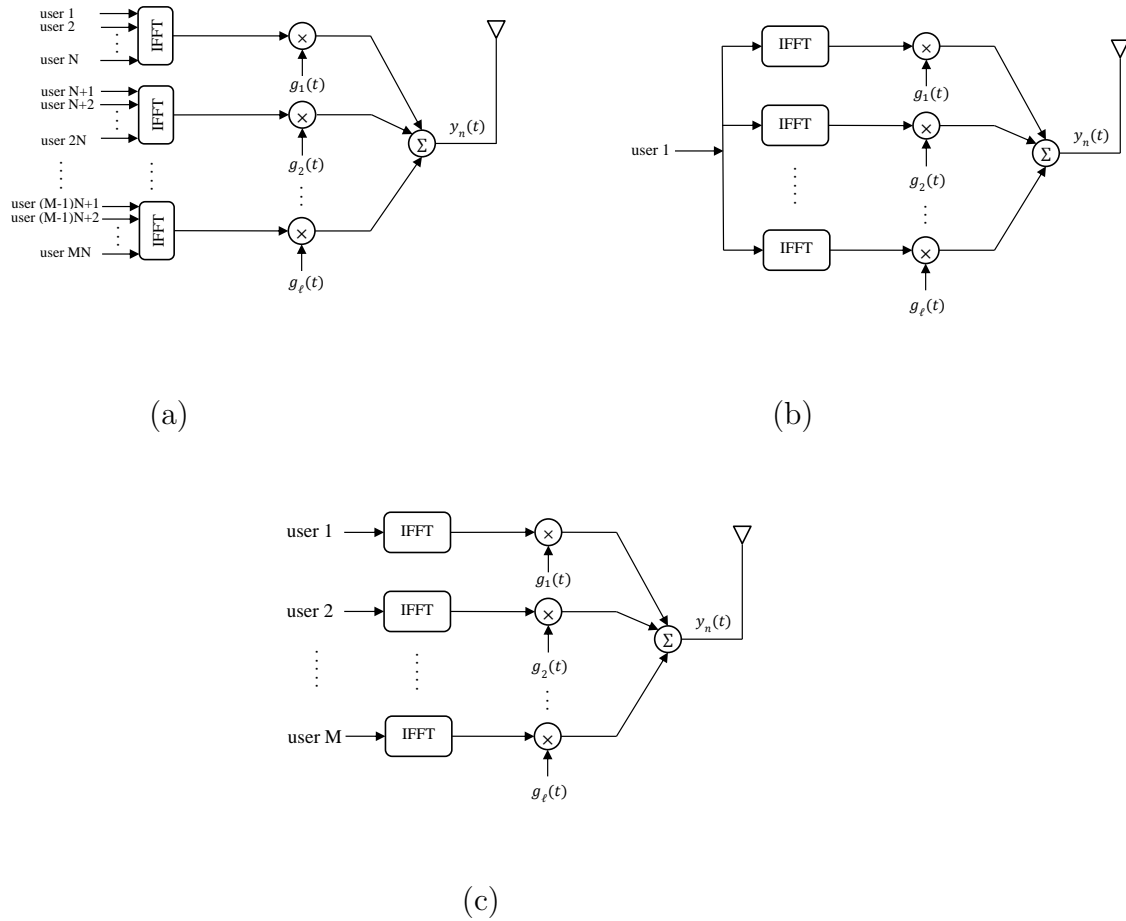


Figure 41: Implementation scenarios: (a) scenario I; (b) scenario II; (c) scenario III.

6.0 CONCLUSIONS AND FUTURE WORK

6.1 SUMMARY

Stationary signals can be analyzed and studied using discrete Fourier transform (DFT). Unfortunately, most of signals that arise in real-life applications are non-stationary. Thus, the DFT would not be suitable to deal with such signals. In this dissertation, we propose chirp transforms using linear chirps. Based on the type of the linear chirp— continuous or discrete, real or complex— three definitions of linear chirp transforms are introduced.

The continuous linear chirp transform (CLCT) uses continuous linear chirp bases. We can reconstruct the signal using the inverse continuous linear chirp transform. The CLCT can be used to filter transmitted signals that have been sent using chirp modulation systems. Thus, we can eliminate the effect of the chirp rate on the bandwidth. Furthermore, we can use the CLCT to detect the transmitted signals if we intent to use non-coherent receivers.

The discrete linear chirp transform (DLCT) is based on discrete complex linear chirps. It is not a time-frequency transformation, but rather a frequency chirp-rate transformation that generalizes the discrete Fourier transform and can be implemented with the fast Fourier transform algorithm. The parameters of a chirp or combination of chirps can be clearly determined with this transform. It also provides a modulation property that allows shifting of chirps into other chirps or sinusoids. The representation of impulses or functions of impulses is possible via a duality property of the transform. An interesting application of the DLCT is the chirp parameter estimation of multi-component signals embedded in noise. We compare the results of the DLCT with the discrete chirp-Fourier transform (DCFT). Unlike the DCFT which can only estimate integer chirp rates, the DLCT can estimate all values of chirp rates. In addition, we analyze and compare the results of the discrete linear

chirp transform (DLCT) with the discrete fractional Fourier transform (DFrFT) in terms of sparsity, computation time, resolution, and peak location. Simulation results show that the DLCT outperforms the DFrFT over all these important aspects. We show that the DLCT gives higher sparsity, lower consume time, higher resolution, and better peak localization than the DFrFT.

The discrete cosine chirp transform (DCCT) depends on discrete cosine linear chirp bases. It is a generalization of the discrete cosine transform. Thus, the DCCT can be used to convert signals into sparse signals in time or frequency by considering locally the DCCT and by appropriately rotating the instantaneous frequencies so that we obtain sinusoidal representations.

In chapter 3, we present a new algorithm for signal compression based on the discrete linear chirp transform (DLCT) and its dual. The extracted coefficients can be arranged in the developed data structure. The simulation results show the effectiveness of the proposed method over the compressive sensing (CS) method. The improvement in the compression ratio depends on the nature of the signal. The effect of chirp rate on the performance of the direct and dual paths is also investigated. It turns out the compression ratio depends on the minimum chirp rate of the linear chirps that forms the signal. The value of $\beta = 0.5$ is the decision maker. If $\beta_{min} \leq 0.5$ we use direct path, otherwise dual path is used. We, also, use the discrete cosine chirp transform (DCCT) to compressive sensing application. Our approach for CS based on the decomposition of a signal using real linear chirps basis and then rotate each one of them with the corresponding chirp rate such that all the chirps become sinusoids. Hence, the compressed signal has two parts— the measurement signal and the extracted chirp rates. Simulation results show CS with the DCCT gives better results than CS with the DCT. Furthermore, we compare the compression performance of using the DCCT which is based on real chirps instead of using a transform that depends on complex chirps such as the DLCT. As can be seen from the results, using real chirps in application such as compressive sensing achieves high quality performance than using complex chirps.

In chapter 4, we compare the DLCT and the EMD methods for the processing of non-stationary signals. Different from the EMD, the basis used in the DLCT are orthogonal and optimal in a mean-square sense. The DLCT uses linear chirps as the IMFs. The

DLCT provides a parametric estimation of the instantaneous frequency of the signal components, which is not affected by the closeness of the frequency of the components. Applying the Hilbert transform to each of the components in the DLCT or the EMD provides the corresponding instantaneous frequencies. The DLCT provides a joint frequency chirp–rate filtering that permits us to separate the signal according to the magnitude of the DLCT— or time–varying filtering. The advantage of the DLCT over the EMD is illustrated using instantaneous–frequency estimation and the decomposition of speech.

Also, In this chapter, a time–frequency algorithm has been proposed to characterize the underlying time–frequency feature of the signal based on the DLCT which decomposes the signal in terms of linear chirps. The proposed time–frequency representation provides a compact, clear, and readable picture of the time–frequency energy content of the signal structure. It has been shown through simulation that the proposed algorithm can efficiently describe the time–frequency content of the signal with high resolution. Therefore, it can be used for instantaneous frequency estimation of multi–component signals.

In chapter 5, we have introduced different digital modulation schemes which are based on time–varying carriers such as linear chirps. The performance of the proposed digital systems has been explored, in particular, we have investigated the bit error rate of these systems. The carrier parameters are chosen such that they maximize the transmitted difference signal energy. The performance of the presented schemes are compared with the conventional digital schemes from the perspective of the transmitted power and the channel bandwidth. Results show the effectiveness of the proposed digital schemes.

In addition, we have introduced the idea of combining M OFDM systems with linear chirps which are more suitable for multi–carrier transmission over rapidly time–varying channels with respect to the traditional frequency–invariant carriers. The performance of the system and its capacity is explored. Simulation results show the effectiveness of the proposed communication system for providing high capacity and high data transmission rates compared to the conventional OFDM communication system.

6.2 FUTURE WORK

The idea of linear chirp transforms can be extended to higher order chirps. However, the case become more challenging since the signal is going to be viewed in more than three dimensions. Thus, looking for a fast algorithm to extract the optimal parameters from the multi-dimensional plane is a good research topic.

In image processing, the DLCT decomposition can be used to analyze images. Hence, we can apply image watermarking to the analyzed images, explore its robustness against attacks, and compare its performance with similar existed techniques such an EMD and wavelet.

The general concept of time-varying filter is to have filters that can follow the individual instantaneous frequencies of multi-component signals. So far, we have used the DLCT to this task by approximating a signal locally with linear chirps. It might be an interesting point for research to design time-varying filters with high polynomial chirps.

To have more efficient use of bandwidth, we need to extend binary linear chirp digital modulations to M-array digital modulation. The performance of such systems needs to be explored in the static as well as fading channels.

The performance of any digital modulation system is dependent on synchronization. In the C-OFDM, when we analyze its performance, we assume having perfect synchronization. However, this assumption is unrealistic. So another possible future research area would concentrate on determining the degradation of the system performance due to synchronization errors.

It is well known the performance of OFDM systems is sensitive to the carrier frequency offset (CFO) and the OFDM receiver must estimate and compensate the CFO effectively to maintain good performance. So, it is an interesting point for research to find out how the performance of the coupled OFDM degrades under these circumstances.

Since the coupled OFDM uses linear chirp carriers, we should also consider linear chirp offset and evaluate the system performance degradation under this condition.

Time-varying channels degrade performance of communication systems. Channel estimation is required to reduce the effect of such channels. As a future work, we need to

investigate perhaps new channel estimation methods that can provide better performance for coupled OFDM under the effect of time-varying channels.

The performance of communication systems can also be improved if we use diversity techniques. In coupled OFDM system, we can assign some of the OFDM channels to carry same information like others and transmit them with different antenna. Thus, we will have space-chirp diversity method which trades capacity for power. It is motivating to see how the advantages of this technique play on trading capacity with power.

BIBLIOGRAPHY

- [1] W. D. Mark, "Spectral analysis of the convolution and filtering of non-stationary stochastic process," *Journal of Sound and Vibration*, vol. 11, no. 1, pp. 19-63, Jan. 1970.
- [2] L. Cohen, *Time-frequency analysis*, Englewood Cliffs, NJ: Prentice-Hall, 1995.
- [3] S. Qazi, A. Georgakis, L. Stergioulas, and M. Shikh-Bahaei, "Interference suppression in the Wigner distribution using fractional Fourier transformation and signal synthesis," *IEEE Transactions on Signal Processing*, vol. 55, no. 6, pp. 3150-3154, Jun. 2007.
- [4] O. A. Alkishriwo, L. F. Chaparro, and A. Akan, "Signal separation in the Wigner distribution using fractional Fourier transform," *European Signal Processing Conference, EUSIPCO*, Barcelona, Spain, Sep. 2011, pp. 1879-1883.
- [5] V. Namias, "The fractional order Fourier transform and its application to quantum mechanics," *IMA Journal of Applied Mathematics*, vol. 25, , no. 3, pp. 241-265, Apr. 1980.
- [6] H. M. Ozaktas, B. Barshan, D. Mendlovic, and L. Onural, "Convolution, filtering, and multiplexing in fractional Fourier domains and their relation to chirp and wavelet transforms," *Journal of Optical Society of America A*, vol. 11, no. 2, pp. 547-559, Feb. 1994.
- [7] L. B. Almeida, "The fractional Fourier transform and time-frequency representations," *IEEE Transactions on Signal Processing*, vol. 42, no. 11, pp. 3084-3091, Nov. 1994.
- [8] H. M. Ozaktas, Z. Zalevsky, and M. A. Kutay, *The Fractional Fourier Transform with Applications in Optics and Signal Processing*, John Wiley, New York, USA, 2001.
- [9] I. Djurovic, S. Stankovic, and I. Pitas, "Digital watermarking in the fractional Fourier transformation domain," *Journal of Network and Computer Applications*, vol 24, no. 2, pp. 167-173, Apr. 2001.

- [10] M. Martone, "A multicarrier system based on the fractional Fourier transform for time-frequency-selective channels," *IEEE Transactions on Communications*, vol. 49, no. 6, pp. 1011-1020, Jun. 2001.
- [11] E. Sejdic, I. Djurovic, and L. Stankovic, "Fractional Fourier transform as a signal processing tool: an overview of recent developments," *Signal Processing*, vol. 91, no. 6, pp. 1351-1369, Jun. 2011.
- [12] S. Peleg and B. Friedlander, "The discrete polynomial-phase transform," *IEEE Transactions on Signal Processing*, vol. 43, no. 8, pp. 1901-1914, Aug. 1995.
- [13] M. Z. Ikram, K. Abed-Meraim, and Y. Hua, "Fast quadratic phase transform for estimating the parameters of multicomponent chirp signals," *Digital Signal Processing*, vol. 7, no. 2, pp. 127-135, Apr. 1997.
- [14] X.-G. Xia, "Discrete chirp-Fourier transform and its application to chirp rate estimation," *IEEE Transactions on Signal Processing*, vol. 48, no. 11, pp. 3122-3133, Nov. 2000.
- [15] Y. Li, H. Fu, and P. Y. Kam, "Improved, approximate, time-domain ML estimators of chirp signal parameters and their performance analysis," *IEEE Transactions on Signal Processing*, vol. 57, no. 4, pp. 1260-1272, May 2009.
- [16] S. Qian, D. Chen, and K. Chen, "Signal approximation via data-adaptive normalized Gaussian functions and its application for speech processing," in *Proc. of IEEE ICASSP-92*, San Francisco, CA, USA, Mar. 1992, pp. 141-144.
- [17] S. Mallat and Z. Zhang, "Matching pursuit with time-frequency dictionaries," *IEEE Transactions on Signal Processing*, vol. 41, no. 12, pp. 3397-3415, Dec. 1993.
- [18] S. Mann and S. Haykin, "The chirplet transform: Physical considerations," *IEEE Transactions on Signal Processing*, vol. 43, no. 11, pp. 2745-2761, Nov. 1995.
- [19] S. Qian, D. Chen, and Q. Yin, "Adaptive chirplet based signal approximation," in *Proc. of IEEE International Conference on Acoustic, Speech, and Signal Processing*, May 1998, pp. 1781-1784.
- [20] A. Bultan, "A four-parameter atomic decomposition of chirplets," *IEEE Transactions on Signal Processing*, vol. 47, no. 3, pp. 731-745, Mar. 1999.
- [21] Q. Yin, S. Qian, and A. Fing, "A fast refinement for adaptive Gaussian chirplet decomposition," *IEEE Transactions on Signal Processing*, vol. 50, no. 6, pp. 1298-1306, Jun. 2002.
- [22] Y. Lu, R. Demirli, G. Cardoso, and J. Saniie, "A successive parameter estimation algorithm for chirplet signal decomposition," *IEEE Transactions on Signal Processing*, vol. 53, no. 11, pp. 2121-2131, Nov. 2006.

- [23] Z. K. Peng, G. Meng, F. L. Chu, Z. Q. Lang, W. M. Zhang, and Y. Yang, "Polynomial chirplet transform with application to instantaneous frequency estimation," *IEEE Transactions on Instrumentation and Measurement*, vol. 60, no. 9, pp. 3222-3229, Sep. 2011.
- [24] H. M. Ozaktas, O. Arikan, M. A. Kutay, and G. Bozdagi, "Digital computation of the fractional Fourier transform," *IEEE Transactions on Signal Processing*, vol. 44, no. 9, pp. 2141-2150, Sep. 1996.
- [25] C. Candan, M. Kutay, and H. Ozaktas, "The discrete fractional Fourier transform," *IEEE Trans. on Signal Processing*, vol. 48, no. 5, pp. 1329-1337, May 2000.
- [26] S. C. Pei and M. H. Yeh, "Improved discrete fractional Fourier transform," *Optics Letters*, vol. 22, no. 14, pp. 1047-1049, Jul. 1997.
- [27] S. C. Pei, C. C. Tseng, M. H. Yeh, and J. J. Shyu, "Discrete fractional Hartley and Fourier transforms," *IEEE Transactions on Circuits and Systems II: Analog and Digital Signal Processing*, vol. 45, no. 6, pp. 665-675, Jun. 1998.
- [28] C. Capus, Y. Rzhanov, and L. Linnett, "The analysis of multiple linear chirp signals," in Proc. of IEE Seminar on Time-scale and Time-Frequency Analysis and Applications, Feb. 2000, pp. 4/1-4/7.
- [29] L. Durak and O. Arikan, "Short-time Fourier transform: Two fundamental properties and an optimal implementation," *IEEE Transactions on Signal Processing*, vol. 51, no. 5, pp. 1231-1242, May 2003.
- [30] C. Capus and K. Brown, "Short-time fractional Fourier methods for the time-frequency representation of chirp signals," *Journal of Acoustical Society of America*, vol. 113, no. 6, pp. 3253-3263, Jun. 2003.
- [31] D. Cowell and S. Freear, "Separation of overlapping linear frequency modulated (LFM) signals using the fractional Fourier transform," *IEEE Transactions on Ultrasonics, Ferroelectrics, and Frequency Control*, vol. 57, no. 10, pp. 2324-2333, Oct. 2010.
- [32] J. Starck, F. Murtagh, and J. Fadili, *Sparse Image and Signal Processing*, Cambridge University Press, 2010.
- [33] N. Ahmed, T. Natarajan, and K. R. Rao, "Discrete cosine transform," *IEEE Transactions on Computers*, vol. C-23, no. 1, pp. 90-93, Jan. 1974.
- [34] L. Claude and P. Vilbe, "On the uncertainty principle in discrete signals," *IEEE Transactions on Circuits and Systems-II: Analog and Digital Signal Processing*, vol. 39, no. 6, pp. 394-395, Jun. 1992.

- [35] W. El Kaakour, M. Guglielmi, J. M. Piasco, and Le Carpentier, "Two identification methods of chirp parameters using state space models," in *Proc. of IEEE International Conference on Digital Signal Processing*, Greece, vol. 2, Jul. 1997, pp. 903-906.
- [36] M. Adjrad, A. Belouchrani, and A. Ouldali, "Estimation of chirp signal parameters using state space modelization by incorporating spatial information," in *Proc. of IEEE Seventh International Symposium on Signal Processing and Its Applications*, France, vol. 2, Jul. 2003, pp. 531-534.
- [37] H. Li and P. M. Djuric, "MMSE estimation of nonlinear parameters of multiple linear/quadratic chirps," *IEEE Transactions on Signal Processing*, vol. 46, no. 3, pp. 796-800, Mar. 1998.
- [38] H. Li and P. M. Djuric, "An iterative MMSE procedure for parameter estimation of damped sinusoidal signals," *Signal Processing*, vol. 51, no. 2, pp. 105-120, Jun. 1996.
- [39] R. M. Liang and K. S. Arun, "Parameter estimation for superimposed chirp signals," in *Proc. of IEEE International Conference Acoustic , Speech, and Signal Processing*, San Francisco, CA, USA, vol. 5, Mar. 1992, pp. 273-276.
- [40] S. Qian and D. Chen, "Adaptive Chirplet based signal approximation," in *Proc. of IEEE International Conference on Acoustics, Speech, and Signal Processing, ICASSP*, vol. 3, pp. 1781-1784, May 1998.
- [41] P. Mowlae, H. Saber, and A. Amid, "Chirplet representation for audio signals based on model order selection criteria," in *Proc. of IEEE/ACS International Conference on Computer Systems and Applications*, May 2009, pp. 927-934.
- [42] A. Gersho, "Advances in speech and audio compression," in *Proc. of IEEE*, vol. 82, no. 6, pp. 900-918, Jun. 1994.
- [43] J. D. Gibson, "Speech coding methods, standards, and applications," *IEEE Circuits and Systems Magazine*, vol. 5, no. 4, pp. 30-49, Fourth Quarter 2005.
- [44] R. G. Baraniuk, "Compressive sensing," *IEEE Signal Processing Magazine*, vol. 24, no. 4, pp. 118-121, Jul. 2007.
- [45] E. J. Candes and J. Romberg, *Toolbox-MAGIC*, California Inst. Of Technology, Pasadena, CA, (<http://www.acm.caltech.edu/l1magic/>).
- [46] E. J. Candes, "Compressive sampling," in *Proc. of the International Congress of Mathematicians*, Madrid, Spain, 2006, pp. 1-20.
- [47] G. Peyre, "Best basis compressed sensing," *IEEE Transactions on Signal Processing*, vol. 58, no. 5, pp. 2613-2622, May 2010.
- [48] H. Ozaktas, Z. Zalevsky, and M. Kutay, *The Fractional Fourier Transform: with Applications in Optics and Signal Processing*, John Wiley & Sons, 2001.

- [49] S. Senay, L. F. Chaparro, and L. Durak, "Reconstruction of nonuniformly sampled time-limited signals using prolate spheroidal wave functions," *Signal Processing*, pp. 2585-2595, 2009.
- [50] D. Donoho, "Compressed sensing," *IEEE Transactions on Information Theory*, vol. 52, no. 4, pp. 1289-1306, Apr. 2006.
- [51] E. Candes, J. Romberg, and T. Tao, "Stable signal recovery from incomplete and inaccurate measurements," *Communications on Pure and Applied Mathematics*, vol. 59, no. 8, pp. 1207-1223, Aug. 2006.
- [52] N. E. Huang, Z. Shen, S. R. Long, M. L. Wu, H. H. Shih, Q. Zheng, N. C. Yen, C. C. Tung, and H. H. Liu, "The empirical mode decomposition and hilbert spectrum for nonlinear and non-stationary time series analysis," *Proc. R. Soc. London A*, vol. 454, 1998, pp. 903-995.
- [53] P. Flandrin, G. Rilling, and P. Goncalves, "Emperical mode decomposition as a filter bank," *IEEE Signal Processing Letter*, vol. 11, no. 2, pp. 112-114, Feb. 2004.
- [54] M. Molla and K. Hirose, "Single-mixture audio source separation by subspace decomposition of Hilbert spectrum," *IEEE Transactions on Audio, Speech, and Language Processing*, vol. 15, no. 3, pp. 893-900, Mar. 2007.
- [55] M. Molla, M. A. Shaikh, and K. Hirose, "Time-frequency representation of audio signals using Hilbert spectrum with effective frequency scaling," in *Proc. of the IEEE International conference on Computer and Iformation Technology*, Khulna, Bangladesh, Dec. 2008, pp. 335-340.
- [56] X Li, C Bao, and M. Jia, "A sinusoidal audio and speech analysis/synthesis model based on improved EMD by adding pure tone," in *Proc. of the IEEE International Workshop on Machine Learning for signal processing*, Beijing, China, Sep. 2011, pp. 1-5.
- [57] C. Park, D. Looney, P. Kidmose, M. Ungstrup, and D. P. Mandic, "Time-Frequency analysis of EEG asymmetry using bivariate empirical mode decomposition," *IEEE Transactions on Neural Systems and Rehabilitation Engineering*, vol. 19, no. 4, pp. 366-373, Aug. 2011.
- [58] H. Li, S. Kwong, L. Yang, D. Huang, and D. Xiao, "Hilbert-Huang transform for analysis of heart rate variability in cardiac health," *IEEE/ACM Transactions on Computational Biology and Bioinformatics*, vol. 8, no. 6, pp. 1557-1567, Dec. 2011.
- [59] T. Huang, C Chou, W. Fang, A. Li, Y. Chang, B. Huang, and Y. Shau, "Time-frequency analysis of heart sound signals based on Hilbert-Huang transformation," in *Proc. of the IEEE International Symposium on Consumer Electronics*, Harrisburg, PA,USA, Jun. 2012, pp. 1-3.

- [60] B. Boashash, "Estimating and interpreting the instantaneous frequency of a signal— Part 2: algorithms and applications," in *Proc. of IEEE*, vol. 8, pp. 520-568, Apr. 1992.
- [61] E. Sejdic, L. Stankovic, M. Dakovic, and J. Jiang, "Instantaneous frequency estimation using S-transform," *IEEE Signal Processing Letters*, vol. 15, pp. 309-312, Feb. 2008.
- [62] L. Stankovic, I. Djurovic, and R. Lakovic, "Instantaneous frequency estimation by using the Wigner distribution and linear interpolation," *Signal Processing*, vol. 83, no. 3, pp. 483-491, Mar. 2003.
- [63] I. Djurovic, "Viterbi algorithm for chirp-rate and instantaneous frequency estimation," *Signal Processing*, vol. 91, no. 5, pp. 1308-1314, May 2011.
- [64] Z. Hussain and B. Boashash, "Adaptive instantaneous frequency estimation of multicomponent signals using quadratic time-frequency distributions," *IEEE Trans. on Signal Processing*, vol. 50, no. 8, pp. 1866-1876, Aug. 2002.
- [65] A. Akan, M. Yalcin, and L. F. Chaparro, "An iterative method for instantaneous frequency estimation," in *Proc. of the IEEE Intl. Conf. Electronics Circuits, and Systems*, Malta, vol. 3, pp. 1335-1338, Sep. 2001.
- [66] J. Lerga, V. Sucic, and B. Boashash, "An efficient algorithm for instantaneous frequency estimation of nonstationary multicomponent signals in low SNR," *EURASIP Journal on Advances in Signal Processing*, vol. 2011, pp. 1-16, Jan 2011.
- [67] C. Condon, K. White, and A. Feng. (2009) Bat echolocation chirp. [Online]. Available: <http://dsp.rice.edu/software/bat-echolocation-chirp>.
- [68] J. G. Proakis, *Digital communications*, 4th edition, McGraw-Hill, New York, 2001.
- [69] M. Jiang and L. Hanzo, "Multiuser MIMO-OFDM for next-generation wireless systems," *Proceeding of the IEEE*, vol. 95, no. 7, pp. 1430-1469, Jul. 2007.
- [70] J. R. Klauder, A. C. Price, S. Darlington, and W. J. Albersheim, "The theory and design of chirp radars," *Journal of Bell System Technical*, vol. 39, no. 4, pp. 745-808, Jul. 1960.
- [71] M. R. Winkler, "Chirp signals for communications," in *IEEE WESCON Convension Record*, pp. 14-17, 1962.
- [72] A. J. Berni and W. D. Gregg, "On the utility of chirp modulation for digital signaling", *IEEE Transactions on Communications*, vol. 21, no. 6, pp. 748-751, Jun. 1973.
- [73] W. Hirt and S. Pasupathy, "Continuous phase chirp (CPC) signals for binary data communication-Part I: Coherent detection," *IEEE Transactions on Communications*, vol. COM-29, no. 6, pp. 836-847, Jun. 1981.

- [74] W. Hirt and S. Pasupathy, "Continuous phase chirp (CPC) signals for binary data communication-Part II: Noncoherent detection," *IEEE Transactions on Communications*, vol. COM-29, no. 6, pp. 848-858, Jun. 1981.
- [75] R. Dutta, A. Kokkeler, R. Zee, and M. Bentum, "Performance of chirped-FSK and chirped-PSK in the presence of partial-band interference," in *Proceeding of the IEEE Symposium on Communications and Vehicular Technology in the Benelux*, Ghent, Belgium, Nov. 2011, pp. 1-6.
- [76] G. F. Gott and J. P. Newsome, "H.F. data transmission using chirp signals," in *Proceeding of the IEE*, vol. 118, no. 9, pp. 1162-1166, Sep. 1971.
- [77] L. W. Couch, *Digital and analog communication systems*, Seventh Edition, Pearson Prentice Hall, New Jersey, 2007.
- [78] L. Hanzo, M. Munster, B. J. Choi, and T. Keller, *OFDM and MC-CDMA for Broadband Multi-User Communications WLANs and Broadcasting*, Piscataway, NJ: IEEE Press/Wiley, 2003.
- [79] H. Schulze and C. Luders, *Theory and Applications of OFDM and CDMA*, John Wiley and Sons Ltd, 2005.
- [80] Y. Cho, J. Kim, W. Yang, and C. Kang, *MIMO-OFDM Wireless Communications with MATLAB*, John Wiley and Sons (Asia) Pte Ltd, 2010.
- [81] B. R. Salzberg, "Performance of an efficient parallel data transmission system," *IEEE Transactions on Communication Technology*, vol. COM-15, pp. 805-811, Dec. 1967.
- [82] S. B. Weinstein and P. M. Ebert, "Data transmission by frequency division multiplexing using the discrete Fourier transform," *IEEE Transactions on Communication Technology*, vol. COM-19, no. 5, pp. 628-634, Oct. 1971.
- [83] G. J. Foschini and M. J. Gans, "On limits of wireless communications in a fading environment when using multiple antennas," *Wireless Personal Communications*, vol. 6, pp. 311-335, 1998.
- [84] H. Bolcskei, D. Gesbert, and A. J. Paulraj, "On the capacity of OFDM-based spatial multiplexing systems," *IEEE Transactions on Communications*, vol. 50, no. 2, pp. 225-234, Feb. 2002.
- [85] I. Koffman and V. Roman, "Broadband wireless access solutions based on OFDM access in IEEE 802.16," *IEEE Communication Magazine*, vol. 40, no. 4, pp. 96-103, Apr. 2002.
- [86] P. Xia, S. Zhou, and G. B. Giannakis, "Bandwidth- and power-efficient multicarrier multiple access," *IEEE Transactions on Communications*, vol. 51, no. 11, pp. 1828-1837, Nov. 2003.

- [87] L. J. Cimini, "Analysis and simulation of a digital mobile channel using orthogonal frequency division multiplexing," *IEEE Transactions on Communications*, vol. COM-33, no. 7, pp. 665-675, Jul. 1985.
- [88] C. E. Cook, "Linear FM signal formats for beacon and communication systems," *IEEE Transactions on Aerospace and Electronic Systems*, vol. AES-10, no. 4, pp. 471-478, Jul. 1974.
- [89] M. Kowatsch and J. T. Lafferl, "A spread-spectrum concept combining chirp modulation and pseudonoise coding," *IEEE Transactions on Communications*, vol. COM-31, no. 10, pp. 1133-1142, Oct. 1983.
- [90] S. E. El-Khamy, S. E. Shaaban, and E. A. Tabet, "Efficient multiple-access communications using multi-user chirp modulation signals," in *Proceeding of the IEEE 4th International Symposium on Spread Spectrum Techniques and Applications*, vol. 3, pp. 1209-1213, Sep. 1996.
- [91] I. E. Telatar, "Capacity of Multi-Antenna Gaussian Channels," *AT & T Bell Laboratories*, BL0112170-950615-07TM, 1995.